CHARACTERIZATION OF NUCLEOBINDIN2/NESFATIN-1 IN THE LUNG AND NEUTROPHILS

A Thesis Submitted to the College of

Graduate and Postdoctoral Studies

In Partial Fulfillment of the Requirements

For the Degree of Master of Science

In the Department of Veterinary Biomedical Sciences

University of Saskatchewan

Saskatoon

By

JASMINE HUI

© Copyright Jasmine Hui, March, 2018. All rights reserved.

PERMISSION TO USE

In presenting this thesis in partial fulfilment of the requirements for a Postgraduate degree from the University of Saskatchewan, I agree that the Libraries of this University may make it freely available for inspection. I further agree that permission for copying of this thesis in any manner, in whole or in part, for scholarly purposes may be granted by the professor or professors who supervised my thesis work or, in their absence, by the Head of the Department or the Dean of the College in which my thesis work was done. It is understood that any copying or publication or use of this thesis or parts thereof for financial gain shall not be allowed without my written permission. It is also understood that due recognition shall be given to me and to the University of Saskatchewan in any scholarly use which may be made of any material in my thesis.

Requests for permission to copy or to make other use of material in this thesis in whole or part should be addressed to:

Head of the Department of Veterinary Biomedical Sciences
Western College of Veterinary Medicine, University of Saskatchewan
Saskatoon, Saskatchewan S7N 5B4
Canada

Or

Dean of College of Graduate and Postdoctoral Studies
University of Saskatchewan
116 Thorvaldson Building, 110 Science Place
Saskatoon, Saskatchewan S7N 5C9
Canada

ABSTRACT

Neutrophil-mediated pulmonary inflammatory conditions such as chronic obstructive pulmonary disease and acute lung injury/adult respiratory distress syndrome are all associated with high mortality rates. While they have been studied extensively, effective treatments remain to be found, suggesting a need to further understand the underlying mechanisms. Nucleobindin 2(NUCB2)/nesfatin-1 is a multifunctional protein originally found to have a role in satiety regulation; it has since been implicated in many other biological processes including inflammation. Studies have shown expression of NUCB2/nesfatin-1 in mouse lungs, and through animal studies, researchers have also suggested it to play an anti-inflammatory and anti-apoptotic role in traumatic brain injury and subarachnoid hemorrhage-induced oxidative brain damage in rats. Cell culture studies, on the other hand, found the addition of nesfatin-1 to chondrocytes to be pro-inflammatory. In addition, cultured chondrocytes and adipocytes showed that NUCB2/nesfatin-1 is upregulated following inflammatory stimulation. Thus far, no studies have characterized the expression of NUCB2/nesfatin-1 in lungs or neutrophils or its role in acute lung inflammation. Hence, the objective of my study was to determine the localization of NUCB2/nesfatin-1 in normal and inflamed lungs and neutrophils, then examine the role it plays following inflammatory stimulus.

In our first study, immunohistochemistry and immune-gold electron microscopy was used to locate NUCB2/nesfatin-1 in normal and inflamed human and mouse lungs and neutrophils. We found that NUCB2/nesfatin-1 localizes in the bronchiolar epithelium, alveolar septa, vascular endothelium, immune cells and red blood cells of normal and inflamed human and mouse lungs; subcellularly, the protein is present in both the nucleus and cytoplasm. Furthermore, localization does not change with inflammatory status. Studies of NUCB2/nesfatin-1 distribution within human neutrophils stimulated with LPS revealed that the protein accumulates within 0.5μm of the plasma membrane after 90mins of stimulation. NUCB2/nesfatin-1 was consistently at higher concentrations in the euchromatin compared to heterochromatin, and cytoplasm compared to nucleus.

Following the localization studies, we performed mechanistic studies into the role of NUCB2/nesfatin-1 during LPS-induced acute lung injury by using wild type (WT) and NUCB2 knock-out mice (NKO) mice. Acute lung injury was accessed through histological evidence of

injury, changes in vascular permeability and inflammatory response. Results revealed that NKO lungs had higher adherent neutrophil accumulation, and inflammatory cytokine concentration than WT; vascular permeability was not significantly different between NKO and WT. Further, examining bone marrow-derived mouse neutrophils stimulated with LPS suggested that NKO neutrophils may secrete less inflammatory cytokines compared to WT.

Lastly, we determined that LPS-stimulation does not change NUCB2/nesfatin-1 mRNA or protein expression in mouse lungs. Protein expression of NUCB2/nesfatin-1 in mouse neutrophils were similarly unchanged following LPS treatment.

Taken together, our results suggest that NUCB2/nesfatin-1 is a constitutively expressed protein in WT mice and plays an anti-inflammatory role during acute lung inflammation by inhibiting adherent neutrophil accumulation and inflammatory cytokine expression. Its presence in epithelial, endothelial and immune cells may enable it to inhibit neutrophil infiltration and adhesion, whereas its presence in neutrophilic euchromatin and its apparent ability to regulate inflammatory cytokine expression suggest it may play a role in regulating cytokine transcription.

ACKNOWLEDGEMENTS

I would first like to acknowledge Dr. Baljit Singh, my supervisor, for the immense support he has given to my research. He has been an excellent teacher who has given me a lot of freedom with my research while providing guidance through an abundance of feedback and experience in the field. I owe much of my success to his leadership. Furthermore, I'm grateful for his commitment to his students, even as he found his new position at the Faculty of Veterinary Medicine in Calgary, that he remained available for discussions whenever I needed and allowed me to continue my degree.

Secondly, I would like to acknowledge Dr. Gurpreet Aulakh, my co-supervisor, for all her encouragement throughout the course of my project. Moreover, her being available for discussions with technical and theoretical aspects of my research despite her busy schedule has been most helpful to its success. She has shown a great amount of patience and commitment during this time and I will be ever grateful for her kind support.

I would like to thank my committee members, Dr. Suraj Unniappan and Dr. Vikram Misra for their insight, guidance and perspective into my project, the committee chair, Dr. Ali Honaramooz, for his encouragement and support in facilitating our meetings, and the external examiner, Dr. Heather Wilson, for her review of my research and constructive comments.

During the course of my project, I have also received technical support from several people in the college, without whom my experiments would have been a great deal more difficult. I would like to express my gratitude to Kim Tran for her assistance with human blood collections, Eiko Kawamura for her guidance with confocal microscopy, Larhonda Sobchishin for her technical assistance in immunoelectron microscopy, and Karen Yuen for her assistance with tissue processing. The animal facility staff of both the Laboratory Animal Services Unit and Animal Care Unit has also provided an abundance of support in their dedication to animal care and facilitating my work in their facilities; I would like to give special thanks to Michele Moroz for providing insight into the management of animal facilities and lab animals which helped orient me to my CREATE program externship for Animal Care Services in the University of British Columbia. Thank you to the administrative staff, Cindy Pollard, Paula Nordick and Cheryl Hack as well for facilitating my work in the department.

I would also like to thank, Brent Bobick, John Ching, Jim Gibbons, Rhonda Shewfelt and Dr. Jaswant Singh, for being my mentors during my time as a teaching assistant for Veterinary Microscopic Anatomy and Veterinary Anatomy; they have provided a wealth of knowledge and the opportunity to teach as I learn.

Lastly, I would like to thank my family, friends and lab mates for their encouragement and support throughout this journey. They have been a great source of comfort and motivation during tough times, and also an important factor in making the whole process enjoyable. Thank you for being there for me!

TABLE OF CONTENTS

LIST OF FIGURES

LIST OF TABLES

LIST OF ABBREVIATIONS

ALI	Acute lung injury
ARDS	Acute respiratory distress syndrome
BALF	Broncho-alveolar lavage fluid
IEM	Immunoelectron microscopy
IFM	Immunofluorescence microscopy
IHC	Immunohistochemistry
LPS	Lipopolysaccharide
MHC	Major histocompatibility complex
MPO	Myeloperoxidase
NET	Neutrophil extracellular trap
NKO	NUCB2 knock-out
NUCB2	Nucleobindin2
TNFα	Tumor necrosis factor alpha
vWF	von Willebrand Factor
WBC	White blood cell
WT	Wild type

CHAPTER 1. REVIEW OF LITERATURE

1.1 Introduction

The average adult breathes around 9,000 litres of air per day, continuously exposing their respiratory system to a large array of pathogens, and organic and inorganic particulates (American Medical Association, 1890). Adapted for efficient gas exchange, a human lung has the estimated total surface area of 24-69 square meters, making it the largest surface of the body to come in contact with the external environment (Hasleton *et al.*, 1972). While the upper respiratory tract may come in contact with larger particulates, only those smaller than 1μm are typically capable of entering the alveolar space (Martin & Frevert, 2005).

Mechanical and innate immune responses provide an important line of defense against exogenous materials carried in during inhalation. Mechanical defenses include the mucociliary system where particles sediment onto the mucus layer and are removed through the upward propulsive force of ciliated epithelium; the innate immune system consists of humoral components such as antibodies and collectins that recognize and bind to the surface of pathogens to promote elimination, and cellular components such as neutrophils and alveolar macrophages that phagocytose, release cytokines and mediate the transition from innate to adaptive immunity (Martin & Frevert, 2005). Innate immune responses are immediate and have relatively broad specificities; should they fail to resolve infection, cytokines and growth factors produced by macrophages and dendritic cells would subsequently facilitate the transition to adaptive immunity where responses are highly specific. As part of the adaptive immune response, regulatory, helper and cytotoxic T cells and B cells have specificities conferred by antigen-presenting MHCI and MHCII molecules (Curtis, 2005). Their main roles include resolving of T cell immunity, facilitating immunological processes, destruction of infected cells, and production of high-affinity antibodies against antigens to facilitate their neutralization or destruction respectively (Curtis, 2005). Lastly, acquired immunity is conferred with the formation of memory T and B cells. This enables stronger and more rapid host responses in future encounters (Curtis, 2005). Collectively, innate and adaptive responses of the lung allow it to counteract the invasion of exogenous materials.

Amongst these defense mechanisms is acute pulmonary inflammation, a self-limited innate response characterized by rapid influx of inflammatory cells - predominantly neutrophils - through vasodilation, increased vascular permeability and recruitment of monocytes (Levy & Serhan, 2014). The goal of acute pulmonary inflammation is the capture and elimination of infectious agents, whereupon resolution, apoptotic inflammatory cells would be removed by macrophages to facilitate recovery by specialized proresolving mediators (Levy & Serhan, 2014). However, in conditions such as acute lung injury (ALI) and acute respiratory distress syndrome (ARDS), inflammation persists and is amplified to affect the entire organ. Furthermore, these conditions may convert to chronic obstructive pulmonary disease (COPD) (Levy and Serhan, 2014). These three conditions are prominently characterized by neutrophilic accumulation. Although neutrophil-mediated lung inflammation is an extensively studied subject, these conditions remain associated with high mortality rates where no effective treatment is available, pointing towards the necessity to further investigate the underlying mechanisms of neutrophilic immune regulation (World Health Organization, 2017).

Nucleobindin2 (NUCB2)/nesfatin-1 is a recently discovered multi-functional protein that, amongst its many roles, has been implicated in inflammatory responses. However, its function as a pro- or anti-inflammatory protein is yet to be defined. In 2014, Leivo-Korpela *et al.* discovered that human patients with COPD had levels of NUCB2/nesfatin-1 in the circulating plasma which correlated positively with levels of inflammatory cytokines: IL-6, IL-8 and TNF-α. Scotece *et al.* (2014) showed increased pro-inflammatory mRNA of IL-6 and MIP-1α, and IL-6 and protein expression of IL-8, COX-2 and MIP-1α when a murine chondrogenic cell line and primary human chondrocytes were incubated with 1μM nesfatin-1. In contrast, rats with subarachnoid haemorrhage treated intraperitoneally with 10 μg/kg nesfatin-1 showed decreased pro-inflammatory protein expression of IL-6, IL-1β and TNF-α (Ozsavci *et al.*, 2011). These conflicting results may indicate that the role of nesfatin-1 in inflammation is tissue-specific.

My work builds upon preliminary data generated by Yadu Balachandran in our laboratory and aims to characterize the expression and role of NUCB2/nesfatin-1 in lung inflammation.

1.2 Neutrophils and Inflammation

1.2.1 Life cycle of neutrophils

Neutrophils are polymorphonuclear leukocytes that originate from myeloid precursors in the bone marrow where they reach maturation through a process termed granulopoiesis. Thereafter, the life cycle of mature neutrophils consists of bone marrow storage and release, circulation, intravascular margination, clearance and destruction (Summers *et al.*, 2010).

1.2.1.1 Granulopoiesis and storage

During granulopoiesis, haematopoietic stem cells that have committed to becoming granulocytic progenitor cells chronologically proliferate and differentiate into myoblasts, promyelocytes, and myelocytes. Cell division ceases as they differentiate into metamyelocytes, band neutrophils and finally mature into polymorphonuclear neutrophils. After maturation, the bone marrow acts as a reserve where neutrophils can be stored for 4-6days and rapidly mobilized during inflammatory events (Rice and Teruya, 2016). Under basal conditions, only mature neutrophils, as opposed to its precursors, are released in significant numbers (Farlex and Partners, 2013).

Neutrophil production can be stimulated by hemopoietins such as IL-3 and G-CSF (Rice and Teruya, 2016). In particular, G-CSF is able to reduce the average transit time through granulocytic compartments and expand the mitotic pool, stimulating proliferation and accelerating neutrophil release into circulation (Price *et al*., 1996). G-CSF production in macrophages, endothelial cells and other immune cells is up-regulated by inflammatory cytokines such as IL-1β and TNF-α or pathogenic toxins such as LPS (Demetri and Griffin, 1991).

1.2.1.2 Neutrophil circulation and recruitment

Upon release into circulation, conservative estimates of neutrophil half-life are approximately 1.5 and 8 hours in mice and humans, respectively (Suratt *et al.*, 2001; Dancey *et al.*, 1976); neutrophil longevity can be extended several folds upon tissue infiltration or activation (Colotta *et al.*, 1992). Neutrophils make up 50-70% of circulating leukocytes in humans, whereas in mice, they only make up 10-25% of the population (Mestas and Hughes, 2004; Doeing *et al.*, 2003).

Free circulating neutrophils can be recruited through activated endothelial cells where the increased expression of selectins on endothelial surfaces allows for tethering (Kolackowska and Kubes, 2013). As tethered neutrophils roll slowly along the endothelial surface, they encounter chemokines that result in subsequent activation (Kolackowska and Kubes, 2013). Conformational changes upon activation allow neutrophil integrins to initiate adhesion with endothelial cells; neutrophils then proceed to crawl along the chemokine gradient until they reach preferential sites of transmigration (Kolackowska and Kubes, 2013).

While selectins and integrins play an important role in neutrophil recruitment, there are exceptions within the lung. In pulmonary circulation, capillaries - as opposed to postcapillary venules in other organs - are the main site of neutrophil sequestration where mechanisms can be selectin-independent, and CD11/CD18 integrin-independent based on activating stimulus (Zarbock and Ley, 2009; Looney and Bhattacharya, 2014; Doerschuk, 2001). It is proposed that as neutrophils (6-8 μm in diameter) pass through pulmonary capillaries (2-15 μm in diameter), spatial constraints, low perfusion pressure and limited cellular flexibility increases their transit time, facilitates sequestration and subsequent transmigration (Doerschuk, 1993; Greene K.E. and Parsons P.E.; Looney and Bhattacharya, 2014).

1.2.1.3 Neutrophil margination

Margination occurs when neutrophils transiently form intravascular pools in organs such as the spleen, liver and lungs (Doerschuk *et al.*, 1987; Summers *et al.*, 2010). In a recent study by Yipp *et al.* (2017), it was found that these neutrophils tethered, crawled or firmly adhered within capillaries of the lung under basal conditions. Upon stimulation with LPS, neutrophils were immediately triggered to the crawling stage of the recruitment cascade, showing that marginated neutrophils present a defense mechanism in the lung that could be activated in minutes independent of mononuclear phagocyte recruitment (Yipp *et al.*, 2017). These observations built upon previous findings where neutrophils showed no delay in arterioles or venules but could spend more than 20mins to transit pulmonary capillaries to form transient margination pools (Lien *et al.*, 1987).

1.2.1.4 Neutrophil clearance and destruction

To balance out the continuous production and release of neutrophils, a corresponding amount in circulation are removed and destroyed by the liver, bone marrow and spleen to

maintain homeostasis (Summers *et al.*, 2010; Suratt *et al.*, 2001). Apoptotic neutrophils display recognition structures that promote removal either by directing them to specific organs or phagocytic cells (Kolaczkowska and Kubes, 2013). There are a number of pathways for neutrophil cell death; depending on the pathway, neutrophils could exert a pro- or anti-inflammatory effect on surrounding cells (Bratton and Henson, 2011). Some of common processes, in order from most to least pro-inflammatory, include necrosis, NETosis and apoptosis (Bratton and Henson, 2011). Clearance following apoptosis has little to no inflammatory effects as they are quickly phagocytized by macrophages; however, failure to do so leads to secondary necrosis and an increased inflammatory burden with cell rupture (Rydell-Tormanen *et al.*, 2006).

While it is commonly recognized that apoptotic neutrophils are cleared by macrophages after an inflammatory response, there is also evidence for reverse transmigration where activated neutrophils re-enter the vasculature (Mathias *et al.*, 2006; Buckley *et al.*, 2006). The biological function and mechanism of this phenomenon remains unclear; however, it suggests a mechanism through which inflammation could disseminate into other organs (Kolaczkowska and Kubes, 2013).

1.2.2 Neutrophil structure

Neutrophils are easily distinguishable from other white blood cell types by the multilobed (3-5 lobes) structure of their nucleus (Mescher, 2016). In circulation, they have an average diameter of 8 µm. Visualization methods are known to change their apparent sizes: blood smears tend to make neutrophils appear larger (15 µm), whereas chemical processing (e.g. during IEM, IFM) often reduces their size (6 µm).

There are 3 main types of cytoplasmic granules present in neutrophils: azurophilic primary granules, specific secondary granules and small storage tertiary granules. The first are large vesicles densely packed with proteases and anti-bacterial proteins such as lysozyme and myeloperoxidase (MPO). Secondary granules are smaller, but more numerous and less dense; they contain complement activators as well as enzymes such as collagenases. Finally, tertiary granules are the smallest and least dense of all 3; they contain enzymes that promote neutrophil

transmigration such as cathepsin, and are known to be released at the leading front of neutrophils during chemotaxis (Murphy, 2008).

1.2.3 Role of neutrophils in inflammation

The primary function of neutrophils during inflammation is the clearance of pathogens to resolve infection in tissues. Upon infiltrating the site of infection, neutrophils are able to recognize various pathogens through pattern recognition receptors (PRRs) that have affinities for evolutionarily conserved structures (e.g. LPS, flagellin or dsRNA) collectively referred to as pathogen-associated molecular patterns (PAMPs) (Mogensen, 2009). There are 3 killing mechanisms that neutrophils are known to employ upon such encounters: phagocytosis, degranulation and release of neutrophil extracellular traps (NETs).

Phagocytosis occurs when neutrophils engulf pathogens to form phagosomes. Reactive oxygen species and hydrolytic enzymes are then secreted from surrounding neutrophil granules into the phagosomes to eliminate intracellular pathogens. Degranulation, on the other hand, allows neutrophils to eliminate extracellular pathogens by secreting their granules into the extracellular space.

Finally, the release of NETs into the extracellular space allows highly activated neutrophils to immobilize pathogens through a process termed NETosis. During this process, neutrophilic components such as chromatin, DNA-associated proteins (e.g. histones) and various enzymes (e.g. MPO) facilitate the trapping, phagocytosis and direct elimination of pathogens. Studies have shown that NETs remain anchored to neutrophils that released them (Yipp *et al.*, 2012). Furthermore, neutrophils are able to continue phagocytosis and chemotaxis without lysis after releasing NETs (Yipp *et al.*, 2012). Aside from bacterial infection, several conditions known to cause NET formation include atherosclerosis, a chronic inflammatory disease, and transfusion-related acute lung injury (Megens *et al.*, 2012; Caudrillier *et al.*, 2012).

1.2.4 Neutrophil-mediated respiratory diseases

While critical in defending the host against pathogen invasion, neutrophil-mediated inflammation also causes direct and indirect damage to lung tissues. Adverse effects induced by neutrophil infiltration are associated with several respiratory diseases including neutrophilic

asthma, acute lung injury, chronic obstructive pulmonary disease, infectious pneumonia and many more (Liu *et al.*, 2017).

Details on the role of neutrophils in various respiratory diseases is beyond the scope of this review, however acute lung injury/acute respiratory distress syndrome (ALI/ARDS) and chronic obstructive pulmonary disease (COPD) will be discussed briefly to provide understanding of the models used during the course of experiments. Both conditions are primarily neutrophil-mediated and associated with high mortality rates where only supportive treatment is available (World Health Organization, 2017), hence highlighting the importance of further exploring mediators and mechanisms behind neutrophilic inflammation.

1.2.4.1 Acute lung injury/acute respiratory distress syndrome (ALI/ARDS)

ALI/ARDS is characterized by the rapid onset of pulmonary inflammation where large numbers of neutrophils infiltrate the lung in a diffuse manner causing injury to both vascular endothelium and alveolar epithelium (Bernard *et al.*, 1994). Cellular characteristics include compromised alveolar-capillary membrane integrity, excessive neutrophil infiltration, and release of pro-inflammatory, cytotoxic mediators (Matthay and Zimmerman, 2005). In particular, excessive activation of neutrophils is known to damage basement membranes and increase alveolar-capillary permeability through mechanical enlargement of paracellular migratory paths (Zemans *et al.*, 2009). Pro-inflammatory mediators released also perpetuate damage by creating ulcerating lesions (Zemans *et al.*, 2009). However, studies have also shown that ALI can develop in neutropenic patients, implicating the existence of alternate clinical pathways (Laufe *et al.*, 1986).

The causes of this condition are heterogeneous with inherent differences in innate immune pathway activation, and hence also mortality-predictive cytokine concentrations (e.g. IL-6, IL-8, TNF-α) in BAL fluid (Park *et al.*, 2001). Mortality risk varies according to the underlying clinical disorder with sepsis presenting a higher risk compared to major trauma (43% vs 11% mortality rate) (Eisner *et al.*, 2001); mortality risk further increases with age where 60% are patients older than 85 (Rubenfeld *et al.*, 2005).

1.2.4.2 Experimental model for ALI/ARDS

Since clinical ALI/ARDS is a complex condition, there are no animal models that can completely recapitulate all complex components. However, several features were established by the American Thoracic Society to be most relevant in assessing the development of experimental lung injury: histological evidence of tissue injury, changes in alveolar-capillary barrier, inflammatory response and physiological evidence of dysfunction; at least 3 of the 4 features must be present to demonstrate that ALI has occurred (Matute-Bello *et al*., 2010). Mouse models of ALI, in particular, have been extensively studied, and also carry the advantage of genetic model availability in mice. It should be noted that apart from anatomical differences with humans, mice have much fewer circulating neutrophils (10-25% compared to 50-70% in humans), and also do not produce IL-8 (Matute-Bello *et al*., 2010). The lack of genetic variability in inbred mice, though effective in decreasing sample size required, also limits the range of possible outcomes (Altemeier *et al.*, 2017).

Various methods are available for the induction of ALI in mice. For the purpose of this thesis, we have chosen to induce direct injury through intra-nasal injection of O55:B5 LPS. This method has been shown to allow for reproducible sterile lung inflammation to occur via Toll-like receptor (TLR) pathways (Takuma *et al.*, 2005; Altemeier *et al.*, 2017). Briefly describing the mechanism of action, LPS induces activation of TLR4 and TLR2 receptors which signal the production of pro-inflammatory cytokines through a MyD88-dependent pathway (Takuma *et al.*, 2005). These receptors are highly expressed in macrophages and neutrophils, and, to a lesser extent, in other leukocytes, endothelial and epithelial cells (Muzio *et al.*, 2000).

1.2.4.3 Chronic obstructive pulmonary disease

Similar to ALI/ARDS, COPD is a pulmonary inflammatory disease characterized by neutrophil infiltration. Neutrophils are hypothesized to be the primary effector cells of the condition as patients with COPD have increased neutrophil numbers in BALF, sputum and intraepithelial space; neutrophil sequestration in pulmonary vasculature is similarly increased (Selby *et al.*, 1991; Pilette *et al.*, 2007; Sapey and Stockley, 2009). Neutrophil numbers positively correlate with degree of airflow obstruction and decline in FEV_1 (volume exhaled at the end of the first second of forced expiration) (Donaldson *et al.*, 2005; Pilette *et al.*, 2007).

Furthermore, the resolution time of neutrophilic inflammation has been found to coincide with clinical recovery of COPD exacerbations (Gompertz *et al.*, 2001).

Studies implicate increased recruitment of neutrophils in the imbalance of proteinase and anti-proteinase activity observed in COPD, leading to lung proteolysis which is suggested to be responsible for most observed pathological features (Sapey and Stockley, 2009). The specifics on COPD pathology is beyond the scope of this thesis, however it is clear that further understanding mechanisms behind neutrophilic inflammation would aid in the development of treatment against COPD exacerbations.

1.3 Nucleobindin 2/Nesfatin-1

1.3.1 NUCB2/Nesfatin-1 structure

Nucleobindin2 (NUCB2) is a 50 kDa secreted protein initially identified as a satiety regulatory molecule from the brain hypothalamus by Oh-I *et al.* in 2006. Through sequencing of its DNA fragment, Oh-I *et al.* (2006) determined that the protein is composed of 396 amino acids preceded by a signal peptide of 24 amino acids, with a sequence homology of >85% between mice, rats and humans. NUCB2 is a polyprotein, proposed to be cleaved by prohormone convertases (PC) into 3 fragments: nesfatin-1 (residues 1-82), nesfatin-2 (residues 85-163), and nesfatin-3 (residues 166-396); co-localization of nesfatin-1 with prohormone convertase 1/3 (PC1/3) and prohormone convertase 2 (PC2) suggested that these enzymes are responsible for NUCB2's post-translational processing, but this has not been further confirmed (Oh-I *et al.*, 2006). While NUCB2 and nesfatin-1 have been found to be biologically active, the function of nesfatin-2 and 3 remains unknown (Oh-I *et al.*, 2006). With the basic amino acid rich putative DNA-binding domain of NUCB2 being located within nesfatin-2 and 3 segments but no nuclear translocation signal identified, it remains unknown whether NUCB2 localizes within the nucleus (Barnikol-Watanabe *et al.*, 1994). Further, studies have shown that the leucine zipper motif- a three-dimensional structural motif involved with DNA-binding - found in NUCB2 cannot form homodimers; the possibility of heterodimer formation remains valid (Karabinos *et al.*, 1996).

Within the nucleobindin family, NUCB1, a 55 kDa secreted protein, is a highly similar homolog with >60% sequence identity with NUCB2 (Miura *et al.*, 1992). While both proteins are capable of binding Ca^{2+}, and *in vitro* DNA fragments, only NUCB1 has an identified nuclear localization signal (Miura *et al.*, 1992; Barnikol-Watanabe *et al.*, 1994; Karabinos *et al.*, 1996). Unlike NUCB2, leucine zipper domains in NUCB1 causes it to form stable dimers (Miura *et al.*, 1992; Kapoor *et al.*, 2010).

1.3.2 Expression of NUCB2/Nesfatin-1 and its receptors in lungs

Since the characterization of NUCB2/nesfatin-1 in the rat hypothalamus (Oh-I *et al.*, 2006), the protein has also been identified in peripheral tissues such as the gastric mucosa, reproductive system, adipose tissues, and lungs (Stengel *et al.*, 2013; Chung *et al.*, 2013). NUCB2 is also a secreted protein which circulates in the plasma (Kanai *et al.*, 1993; Barnikol-

Watanabe *et al.*, 1994) where its expression is differentially regulated during conditions such as stress, food restriction and pregnancy (Stengel *et al.*, 2009; Garces *et al.*, 2014; Xu *et al.*, 2015). Studies in rats found that serum levels of NUCB2/nesfatin-1 increased with acute stress (Xu *et al.*, 2015), and decreased after fasting for 24 hours (Stengel *et al.*, 2009). Expression changes in pregnant mice depended on the day of gestation (Garces et al., 2014). From 16 days until the end of pregnancy, serum levels of NUCB2/nesfatin-1 was significantly decreased compared to control groups (Garces *et al.*, 2014). Further, pregnant rats with a 30% food restriction showed decreased serum levels of NUCB2/nesfatin-1 on day 12 of gestation compared to those fed *ad libitum* (Garces *et al.*, 2014). Other studies have suggested factors such as body weight, sex hormones, and type 2 diabetes mellitus to alter NUCB2/nesfatin-1 expression, however results have been conflicting due to variability of experimental conditions between studies (Prinz and Stengel, 2016).

In lungs, one study examined NUCB2/nesfatin-1 expression in mice during different developmental stages; fetal mouse lungs (15.5 days post-coitus) were found to express high levels of NUCB2/nesfatin-1 protein, but this expression drastically decreased in both adult males and females (Chung *et al.*, 2013). There did not seem to be a difference between genders. In a follow-up study, Kim *et al.* (2014) displayed the same Western blot data accompanied by RT-qPCR data showing high levels of NUCB2/nesfatin-1 mRNA expression in adult mouse lungs relative to other peripheral organs. In contrast to protein data presented, mRNA findings also showed twice the NUCB2/nesfatin-1 expression in male lungs compared to female samples (Kim *et al.*, 2014).

Little is currently known about NUCB2/nesfatin-1 receptors, hence presenting considerable challenge to identifying potential downstream regulatory pathways. Studies have suggested G-protein receptors to be likely candidates, however these receptors have yet to be isolated and characterized (Garcia-Marcos *et al.*, 2011). In an experiment to determine the localization of nesfatin-1 receptors in peripheral organs, Prinz *et al.* (2016) used ^{125}I-nesfatin-1 to generate autoradiograph signals in rat tissue sections. Receptors were determined to be present, however compared to other peripheral organs, lungs displayed relatively weak labelling intensity (Prinz *et al.*, 2016).

1.3.3 NUCB2/Nesfatin-1 in inflammation

The widespread distribution of NUCB2/nesfatin-1 amongst various tissues also implies diverse functions for the protein and studies suggest its involvement in fetal development, glucose homeostasis, cardiovascular regulation, stress and others (Yosten and Samson, 2009; Garces *et al.*, 2014, Mohan *et al.*, 2014; Xu *et al.*, 2015). However, very few studies have looked into the role of NUCB2/nesfatin-1 in inflammation.

In one study, researchers measured the plasma levels of NUCB2/nesfatin-1 along with inflammatory cytokines, IL-6, IL-8, TNF-α and MMP-9, and found that levels of NUCB2/nesfatin-1 correlated positively with IL-6, IL-8 and TNF-α in male patients with chronic obstructive pulmonary disease (Leivo-Korpela *et al.*, 2014). As macrophages and neutrophils are major sources of IL-6 and TNF-α, and IL-8 respectively, this study implicated their association with NUCB2/nesfatin-1 (Leivo-Korpela *et al.*, 2014). Previously, it was also found that increasing concentrations of IL-6 and TNF-α in adipocytes differentiated from a mouse embryonic fibroblast cell line, 3T3-L1, increased NUCB2/nesfatin-1 protein expression (Ramanjaneya *et al.*, 2010), further supporting the role of NUCB2/nesfatin-1 in inflammatory responses.

In another study, Scotece *et al.* (2014) treated the murine chondrogenic cell line, ATDC-5, and human primary chondrocytes from osteoarthritis patients with pro-inflammatory cytokines, IL-1 or TNF-α. NUCB2 mRNA and protein expression was increased as a result in ATDC-5 cells; increased NUCB2 protein expression was also confirmed in primary human chondrocytes (Scotece *et al.*, 2014). Nesfatin-1 treatment of human primary chondrocytes resulted in significantly increased mRNA expression for IL-8, MIP-1α and IL-6 (Scotece *et al.*, 2014). Further, incubating murine chondrocytes with IL-1 and nesfatin-1 lead to increased mRNA and protein expression of IL-6 and MIP-1α (Scotece *et al.*, 2014). These results from chondrocytes exposed to inflammatory conditions indicate that nesfatin-1 stimulates expression of chemotaxins (IL-8 and MIP-1α) and inflammatory cytokines (IL-6).

While the studies above using cell cultures may suggest NUCB2/nesfatin-1 as a pro-inflammatory cytokine, studies using animal models have suggested the contrary. In a study where rats with subarachnoid hemorrhage-induced oxidative brain damage were treated with nesfatin-1, the protein demonstrated anti-inflammatory and anti-apoptotic properties (Ozsavci *et*

al., 2011). Myeloperoxidase, a protein abundantly expressed in neutrophils, and caspase-3, an apoptotic protease that cleaves many key cellular proteins, were significantly reduced in nesfatin-1 treated samples (Ozsavci *et al*., 2011). This suggesting that nesfatin-1 may not have only inhibited neutrophil infiltration, but also apoptosis. Further support was provided by the demonstration of reduced lipid peroxidation within brain tissues and pro-inflammatory cytokine expression in plasma, both of which are parameters for inflammatory mediator release from neutrophils (Ozsavci *et al*., 2011). Lastly, when basilar arteries of nesfatin-1 treated rats were observed using electron microscopy, morphological changes were observed to be significantly reduced, demonstrating a neuroprotective effect of the protein (Ozsavci *et al*., 2011).

With similar results, a study performed on rats with traumatic brain injury found nesfatin-1 to be anti-inflammatory and anti-apoptotic. In the group treated with 10 or 20 μg/kg nesfatin-1 30 mins after head trauma, mRNA expression of NF-κB, TNF-α, IL-1β and IL6 decreased significantly (Tang *et al.,* 2012). Caspase-3 activity and the number of apoptotic neuronal cells were also significantly reduced (Tang *et al.,* 2012).

Taken together, cell culture studies suggest NUCB2/nesfatin-1 to be upregulated in cells exposed to inflammatory conditions (e.g. IL-1, TNF-α) which, in turn, upregulates expression of chemotaxins and other inflammatory cytokines, and perpetuates inflammatory responses. Animal model studies suggest NUCB2/nesfatin-1 to be an anti-inflammatory and anti-apoptotic protein, inhibiting neutrophil infiltration, apoptotic protein expression, and ultimately reducing tissue damage. Throughout the course of this thesis, we demonstrate by isolated murine and human neutrophils as well as murine lung injury model, the expression and potential role of NUCB2/nesfatin-1 in neutrophil migration and acute lung inflammation.

1.4 Rationale

Since the discovery of NUCB2/nesfatin-1 in the hypothalamus and brainstem in 2006 (Oh-I *et al.*), the protein has been found in many other peripheral tissues including the lung (Kim *et al.*, 2014); its role has also expanded from satiety regulation to many others including inflammation (Scotece *et al.*, 2014). However, there have yet to be any studies to characterize the localization of its expression in lungs, or how the absence of this protein might affect lung inflammation. It also remains unclear whether NUCB2/nesfatin-1 exerts a pro- or anti-inflammatory effect despite recent studies that have characterized it under various conditions (Leivo-Korpela *et al.*, 2014; Scotece *et al.*, 2014; Ozsavci *et al.*, 2011)

Knowing that neutrophil-mediated pulmonary inflammatory conditions such as ALI, ARDS and COPD are currently the leading causes of death globally due to lack of effective treatment (World Health Organization, 2017), characterizing NUCB2/nesfatin-1 in both lungs and neutrophils will lay down important groundwork to understanding the emerging role of NUCB2/nesfatin-1 in these conditions.

1.4.1 Hypothesis

1. NUCB2/nesfatin-1 is differentially expressed in normal and inflamed lungs and neutrophils
2. Knock-out of NUCB2/nesfatin-1 increases lung inflammation
3. NUCB2/nesfatin-1 mRNA and protein expression increase with LPS stimulation

1.4.2 Objectives

My work begins by characterizing the localization of NUCB2/nesfatin-1 in normal and inflamed human and mouse lungs. Then it closely examines the distribution of NUCB2/nesfatin-1 within human neutrophils under normal and activated states. While there have been conflicting reports on the presence of NUCB2/nesfatin-1 expression in leukocytes (Ravussin, 2008; Stengel *et al.*, 2011), its presence is confirmed in neutrophils throughout our studies.

Afterwards, using a murine model of LPS-induced ALI, neutrophil infiltration, vascular permeability, and inflammatory cytokine expression in WT and NUCB2 KO mouse lungs will be compared to discern the potential role of NUCB2/nesfatin-1 in inflammatory regulation.

Peripheral blood counts are performed to identify any potential systemic changes. Lastly, mRNA and protein expression of NUCB2/nesfatin-1 in mouse lungs and neutrophils under normal and inflammatory conditions are examined *in vitro*, and neutrophil supernatant would also be assessed for differences in cytokine expression.

TRANSITION

The following chapter examines my first hypothesis that NUCB2/nesfatin-1 is differentially expressed in normal and inflamed lungs and neutrophils using samples from mice and humans. As previously mentioned, NUCB2/nesfatin-1 expression has only been confirmed in mouse lungs, and inflammatory stimulus has been shown to upregulate NUCB2/nesfatin-1 mRNA and protein expression in cell culture. Our findings indicate that NUCB2/nesfatin-1/nesfatain-3 is constitutively expressed in the nucleus and cytoplasm of pulmonary and immune cells. In neutrophils, the protein accumulates towards the plasma membrane following LPS-stimulation; it is more concentrated in the cytoplasm than the nucleus of neutrophils and is more concentrated in the euchromatin than the heterochromatin of neutrophilic nuclei.

Contributions of co-authors: Yadu Balachandran performed pilot studies on which my localization experiments were based. Dr. Gurpreet Aulakh assisted with data analysis and interpretation, and provided feedback on thesis writing. Dr. Suraj Unniappan provided mice used in experiments, the custom NUCB2/nesfatin-1 antibody (Pacific Immunology, CA, USA) feedback on thesis writing, and shared much of his expertise on NUCB2/nesfatin-1. Larhonda Sobchishin provided technical assistance for immunoelectron microscopy. I designed and conducted experiments, analyzed results and wrote the thesis. Dr. Baljit Singh provided research directions, infrastructure, funding and feedback on thesis writing; he was involved in directing the collection and interpretation of immunohistochemistry and immunoelectron microscopy images.

CHAPTER 2. LOCALIZATION OF NUCLEOBINDIN2/NESFATIN-1/NESFATIN-3 IN NORMAL AND INFLAMED HUMAN AND MOUSE LUNGS, AND HUMAN NEUTROPHILS

2.1 Abstract

While studies have implicated NUCB2/nesfatin-1 in various inflammatory conditions - one in particular showing that the protein expression in human plasma positively correlated to expression of pro-inflammatory cytokines in patients with chronic obstructive pulmonary disease (COPD) - there have yet to be detailed or mechanistic studies on the role of NUCB2/nesfatin-1 in lung inflammation. In this study, we characterize the expression of NUCB2/nesfatin-1/nesfatin-3 in normal and inflamed human and mouse lungs and neutrophils with light and electron microscopic immunocytochemistry. Light microscopy data show that the localization of NUCB2/nesfatin-1 in the pulmonary epithelium, alveolar septa, vascular endothelium and various immune cells does not change with inflammatory status while electron microscopy revealed constitutive localization within the nucleus and cytoplasm of the aforementioned cells. Immuno-gold electron microscopy showed accumulation of the protein within 0.5μm of the plasma membrane in human neutrophils following 90mins of 1ng/mL LPS stimulation. NUCB2/nesfatin-3 was also found to localize in euchromatic portions of neutrophilic nuclei at 5 times the mean concentration compared to heterochromatin, potentially indicating a role in transcriptional regulation. Finally, our results indicate that NUCB2/nesfatin-3 is predominantly cytoplasmic as it localizes at 2 times the concentration in neutrophilic cytoplasm compared to nucleus. Taken together, these are the first data on detailed localization of NUCB2/nesfatin-1/nesfatin-3 in lungs and neutrophils.

2.2 Introduction

In a study by Leivo-Korpela *et al.* (2014), NUCB2/nesfatin-1 was implicated in chronic obstructive lung disease, a neutrophil-meditated inflammatory condition that has maintained a high mortality rate to this day (World Health Organization, 2017). Researchers demonstrated that increased levels of NUCB2/nesfatin-1 in blood plasma correlated positively with IL-6, IL-8 and TNF-α expression (Leivo-Korpela *et al.*, 2014). While there have been no other studies examining the role of NUCB2/nesfatin-1 during pulmonary inflammatory conditions, reports of its involvement in other inflammatory conditions such as traumatic brain injury and subarachnoid hemorrhage-induced brain damage where *in vitro* studies have demonstrated anti-inflammatory and anti-apoptotic effects prompt us to further investigate its expression and role in lung inflammation (Ozsavci *et al*., 2011; Tang *et al.*, 2012).

Study of a protein's localization within the highly compartmentalized eukaryotic system serves to provide information on its function, potential interaction with other molecules and changes during different states of activation. While the nucleotide coding sequences for NUCB2/nesfatin-1 were first cloned from the human lung tumor cell line, SQ-5, and its mRNA and protein are expressed in mouse lungs, studies have yet to determine the localization of this protein in mouse or human lungs (Oh-I *et al.*, 2006; Chung *et al.*, 2013; Kim *et al.*, 2014). While one study has reported that NUCB2 mRNA was not detectable in white blood cells of rats, a recent study by Ravussin (2016) has shown that this does not hold true in mice and demonstrated mRNA expression in macrophages as well as T cells (Stengel *et al.*, 2011). To the best of our knowledge, there are no detailed data on the expression or localization of NUCB2/nesfatin-1 in murine and human neutrophils.

My study aimed to fill in the gap in knowledge by first determining the cellular presence and location of NUCB2/nesfatin-1 in normal and inflamed human and mouse lungs through immunohistochemistry. We then examine the subcellular localization of NUCB2/nesfatin-1 through immunoelectron microscopy in normal and inflamed mouse lungs. NUCB2/nesfatin-3 is further characterized in human neutrophils as we examine its subcellular distribution through immunoelectron microscopy following 0, 60, 90 and 120 mins of LPS stimulation. Finally, NUCB2/nesfatin-3 expression in other blood cell types, which were present as impurities during neutrophil isolation is briefly examined to provide hints for future research.

2.3 Materials and Methods

2.3.1 Animals

Protocols and the use of mice in this experiment were approved by the University Animal Care Committee Animal Research Ethics Board of University of Saskatchewan (Protocol no.: 20150018). C57BL/6-$^{Tyrc\text{-}Brd}$ WT and NUCB2 knockout (NKO) male mice were generously donated by Dr. Suraj Unniappan. NKO mice were specifically engineered by transcriptionally disrupting the NUCB2 gene (Accession Number: NM_016773) through retroviral insertion of a trapping vector (Mohan, 2015). Genotypes of all animals used were confirmed during reverse transcription q-PCR of lung mRNA.

To study the differences between inflamed and normal mouse lungs with or without the presence of nucleobindin-2 (NUCB2)/nesfatin-1, WT and NKO mice, aged 3-5 months, were divided into LPS or PBS treatment groups (n=6 per group; 24 total). Mice were placed under isoflurane anaesthesia and intranasally injected with 50 µL of PBS or 1 mg/mL *E. coli* O55:B5 LPS (L2880; Sigma-Aldrich, MO, USA). After 9 hours, mice were euthanized through anaesthesia, cardiac puncture and exsanguination. Bronchoalveolar lavage fluid (BALF) was collected from the lungs through 3 aspirations of 0.5 mL PBS through the trachea. 1 mL of PBS was then injected into the right ventricle of the heart to flush remaining blood from the lungs. The right main bronchus was then tied off as the left lung was perfused with 0.5 mL 4% paraformaldehyde/ 0.1% glutaraldehyde using a 20 cm H_2O column. When perfusion was complete, the right lung was extracted into a cryovial and stored in liquid nitrogen; the left lung was fixed overnight in 1mL 4% paraformaldehyde/ 0.1% glutaraldehyde at 4°C, and processed for paraffin embedding the next day.

2.3.2 Biomedical research ethics approval for human subjects

Sample acquisition and study of human neutrophils from healthy volunteers was approved by the Biomedical Research Ethics Board of University of Saskatchewan, Saskatoon, Canada (Protocol no.: Bio 16-170). Consent was obtained from all subjects.

2.3.3 Blood donation

Blood was collected from healthy, male volunteers between 20-40 years of age, weighing between 60-80 kg. A health survey was filled out by each volunteer to document that requirements for eligibility were met. Terms were briefly as follows: they could not participate in the study if they had been ill within the week, been diagnosed with HIV, hepatitis or other infectious diseases, had diabetes, or known pre-existing conditions that affected their haematology. K2 EDTA tubes (CABD367841L; BD Diagnostics, ON, Canada) were used by an approved technician to collect 10 mL of blood from the intravenous cannula. Samples were kept at room temperature and processed immediately (no longer than 30 mins) after collection.

2.3.4 Human neutrophil extraction

Human neutrophils were extracted using the EasySep™ Direct Human Neutrophil Isolation Kit (19666; STEMCELL Technologies, BC, Canada), following the supplier's protocol to process 10 mL of blood. Two cytospin slides were produced by spinning ~$5x10^5$ isolated cells each at 500 rpm for 3 mins. Afterwards, 100-150 cells were counted on each slide and determined to contain ≥97% neutrophil purity before proceeding.

2.3.5 Human neutrophil stimulation

Isolated human neutrophils were resuspended to a concentration of 10^6cells/mL in Iscove's Modified Dulbecco's Medium (IMDM) (ATCC) with 10% FBS. Following, 6 well plates were set up to contain $5x10^6$ cells per well. Cells were then stimulated with 1 ng/mL E. coli O55:B5 LPS (L2880; Sigma-Aldrich, MO, USA) for 0, 60, 90 and 120 mins respectively, and incubated at 37°C with 5% CO_2. After stimulation, cells were resuspended through gentle pipetting, collected and washed with PBS twice before downstream processing.

2.3.6 Tissue processing and sectioning

Mouse lung samples in fixative were washed for 2 hours in dH_2O and then transferred into a tissue processor which cycles through 13 changes of reagents for 1 hour each as follows: 70%, 80%, 95% (2x), 100% (3x) ethanol, alcohol-xylene, xylene (2x), and paraplast (3x). Upon completion, samples were taken out and embedded in paraffin wax.

Paraffin-embedded samples were trimmed until at least 5 bronchioles were visible in each lung section. Each slide produced thereafter would contain 4 sequentially sectioned samples, each 5 μm thick, to be used for immunohistochemistry and haematoxylin and eosin staining.

2.3.7 Immunohistochemistry (IHC)

Mouse lung tissues used in this study were taken from the above mentioned *in vivo* experiment (n=6 per group). Human lung samples were acquired from deceased donors with chronic obstructive pulmonary disease (COPD) or healthy lungs (n=3 per group).

Tissue sections were deparaffinized in xylene, rehydrated using decreasing concentrations of ethanol then placed into PBS. Samples were then placed in 0.5% H_2O_2 for 20mins to neutralize endogenous peroxidase. After washing in PBS, antigen retrieval was performed by adding pepsin (2mg/mL in 0.01N HCl) to samples and incubating for 45mins. Samples were then washed in PBS, blocked with 5% BSA for 30mins, and incubated overnight in primary antibody diluted in 5% BSA. To determine the protein's localization in normal and inflamed human and mouse lungs, a custom rabbit NUCB2/nesfatin-1 antibody (1mg/mL; Pacific Immunology, CA, USA) raised against a synthetic peptide, VDKTKVHNTEPVENARIEP-Cys (20 AA) was used at 1:200 and 1:150 dilutions respectively. The next day, samples were washed and incubated in HRP-conjugated anti-rabbit secondary antibody (1:200; P0448; Dako, CA, USA) for 30mins. The samples were washed in PBS and was developed using VECTOR VIP Peroxidase Substrate Kit (VECTOR Laboratories, ON, Canada) for 3-5mins depending on species. Slides were washed in dH_2O and counter-stained in methyl green for 1min, washed in dH_2O and dehydrated using increasing concentrations of ethanol followed by xylene. Lastly, samples were mounted and visualized under a light microscope.

With each set of antibodies used, the corresponding isotype and negative controls were performed. As a positive control, staining with polyclonal anti-human von Willebrand Factor (vWF) antibody (1:500; A0082; Dako, CA, USA), followed by HRP-conjugated anti-rabbit secondary antibody (1:200; P0448; Dako, CA, USA), was also performed in tissues of each species.

2.3.8 Immunoelectron microscopy (IEM)

Immunoelectron microscopy (IEM) was performed on human neutrophils fixed with 2% paraformaldehyde/0.5% glutaraldehyde in 0.1 M sodium cacodylate buffer (pH 7.2) for 3 hours at 4°C. A similar processing procedure was adopted for IEM of mouse lungs. During sample collection, a small section of each right mouse lung was taken and fixed with 2% paraformaldehyde/0.5% glutaraldehyde in 0.1 M sodium cacodylate buffer (pH 7.2) overnight at 4°C. The next day, tissues were washed 3 times with 0.1 M sodium cacodylate buffer and stored at 4°C until they could be processed for immunoelectron microscopy.

All samples were embedded in LR White Resin, sectioned to 90 nm and mounted on grids. Non-specific antibody binding for human neutrophils was blocked with 3% BSA in 1x TBS (pH 7.9) with 0.1% Tween 20 for 30 mins; non-specific antibody binding for mouse lungs was blocked with 5% BSA in 1x TBS (pH 7.9) with 0.1% Tween 20 for 2 hours. Human neutrophil samples were then incubated in rabbit anti-NUCB2/nesfatin-3 antibody (1:20; NBP1-87383, Novus Biologicals, ON, Canada), and mouse lung samples in rabbit anti-NUCB2/nesfatin-1 antibody (1:20; 1mg/mL; Pacific Immunology, CA, USA) for 1 hour at RT. Subsequently, samples were rinsed with TBS, incubated in 15 nm gold-conjugated antibody (1:200; EMGAR-15; BBI International, ND, USA) for 1 hour at RT, rinsed with TBS, and washed in dH_2O. Sample sections were visualized with a TEM-transmission electron microscope (Hitachi HT7700), and images were taken at 80 kV. In the imaging of human neutrophils, 10 per sample were randomly selected upon meeting the criteria that its nucleus was visible and plasma membrane was mostly intact.

2.3.9 Statistical analysis

For the relative quantification of immunolabelling between compartments of different experimental groups using IEM, 10 neutrophils were chosen at random for each group (Control, LPS60, LPS90, and LPS120) with requirement that their nucleus be visible and their plasma membrane mostly intact. Each neutrophil was then divided into 4 regions: 0.5 µM within the plasma membrane (0.5PM), remainder of cytoplasm (RC), euchromatin (Eu) and heterochromatin (Het). The area and number of gold particles within each region were quantified and transformed into concentrations (Conc.) (equation 2.1). The ratios were then used for comparison between different cell compartments (equation 2.2, equation 2.3).

No. of particles/ Total area = Conc. (2.1)

Conc.(0.5PM)/Conc.(RC) = Ratio(Cytoplasm) (2.2)

Conc.(Euchromatin)/ Conc.(Heterochromatin) = Ratio(Nucleus) (2.3)

Means for each group were then obtained by averaging the values for 10 neutrophils, using results from equation 2.2 and 2.3.

Five biological replicates were performed. Repeated measures one-way ANOVA with Geisser-Greenhouse correction was used for the comparison between groups; Dunnett's multiple comparisons test was used to identify groups significantly different from the control group; t-test was used to compare the identified groups of interest. In the case that repeated measures one-way ANOVA was not statistically significant, data was also analyzed for differences in compartmental concentrations throughout time using repeated measures two-way ANOVA followed by Sidak's multiple comparisons test. Only p values ≤ 0.05 were considered statistically significant. Results are presented as Mean±SEM, and GraphPad Prism 7 (Avenida de la Playa, CA, USA) was used for all analysis. For a more detailed explanation of the immunolabelling quantification process, refer to Appendix I.

2.4 Results

2.4.1 NUCB2/nesfatin-1 localizes in epithelium, endothelium, connective tissue and blood cells of normal and inflamed human and mouse lungs

First, we determined the localization of NUCB2/nesfatin-1 within normal and inflamed mouse and human lungs. Controls were implemented to ensure validity of our IHC protocol: negative controls using secondary antibody only, isotype controls corresponding to the host and concentration of primary antibodies, and positive controls staining von Willebrand Factor (vWF) protein only in endothelial cells and blood vessel endothelium of each tissue type (Figure 2.1A).

As shown in Figure 2.1B, IHC performed with the custom NUCB2/nesfatin-1 antibody on normal mouse lungs shows specific staining in immune cells and red blood cells, as well as the alveolar septum, vascular endothelium and bronchiolar epithelium. Similarly, in inflamed lungs of mice (Figure 2.1C), staining can be seen in immune cells and vascular endothelium. Staining in red blood cells, bronchiolar epithelium, and alveolar septum of LPS-treated samples appeared lighter compared to its PBS-treated samples.

Human lungs were similarly stained using the custom NUCB2/nesfatin-1 antibody. In normal lungs, we observed staining in all vascular endothelial layers (Figure 2.1D). In addition, heavy staining was present in the tunica adventitia of arteries as well as throughout the alveolar septum (Figure 2.1Di, ii). Staining was also observed in red blood cells, but only a few immune cells carried any significant staining (Figure 2.1Diii). Inflamed human lungs presented a similar pattern with moderate staining in all endothelial layers and red blood cells, and heavy staining in connective tissues, tunica adventitia and perichondrium (Figure 2.1E). Some immune cells were darkly stained, while others did not appear stained at all (Figure 2.1Eii). Notably, staining was absent in adipose tissues, hyaline cartilage and smooth muscle fibers of the tunica media (Figure 2.1Ei, iv).

2.4.2 NUCB2/nesfatin-1 localizes in the nucleus and cytoplasm of pulmonary cells and blood cells

Next, we examined normal and inflamed mouse lungs further to identify the subcellular localization of NUCB2/nesfatin-1. Similar to our findings with IHC staining, signals for NUCB2/nesfatin-1 localization were not qualitatively different between inflamed and normal lungs (Figure 2.2A-M). In both LPS and PBS-treated lungs, we were able to see staining in both

the nucleus and cytoplasm of type I and type II pneumocytes, endothelial cells, RBC (enucleate) and monocytes (Figure 2.2A, B, C, E, H, I, J, L). Clustering of staining could be observed in the monocyte nucleus (Figure 2.2E, L). Furthermore, images of an alveolar macrophage and neutrophil in an LPS-treated mouse lung revealed staining in the cytoplasm for both cells, with nuclear staining also apparent in the neutrophil (Figure 2.2F, G). Image of an eosinophil captured in a PBS-treated mouse lung also revealed staining in nucleus and cytoplasm (Figure 2.2M). Notably, much of the cytoplasmic staining resides in eosinophil granules.

Figure 2.2N shows a negative control devoid of staining to support the validity of the IEM protocol used. Magnification was lowered to include a more diverse array of cells in this figure.

2.4.3 NUCB2/nesfatin-3 accumulates within 0.5μm of the plasma membrane in neutrophils following 90mins LPS stimulation

To determine whether NUCB2/nesfatin-3 distributions within human neutrophils change with LPS treatment, NUCB2/nesfatin-3 in neutrophils stimulated for 0, 60, 90 and 120mins (Ctrl, LPS60, LPS90 and LPS120) were immune-gold labelled and imaged. Each neutrophil was divided into 4 areas (Appendix I), and the concentration of labelling (gold particles/area) was compared. First, we wanted to examine whether the protein concentrated towards the plasma membrane (PM) with LPS treatment, as supposed to the random distribution observed in control samples. Close proximity was defined as "within 0.5μm of PM" (0.5PM), and the remaining areas excluding the nucleus was defined as "remainder of cytoplasm" (RC).

When the ratios of 0.5PM/RC were compared in a repeated measures one-way ANOVA, results revealed the groups were significantly different ($p=0.010$). Post-hoc analysis using the Dunnett's multiple comparisons test determined that neutrophils stimulated for 90mins had a statistically significant difference in 0.5PM/RC gold particle ratio compared to control samples, presenting a mean NUCB2/nesfatin-3 concentration 1.8 times higher at 0.5PM than RC; the 0.5PM/RC ratio in LPS90 samples were 1.6 times that of control samples ($p=0.017$; Figure2.3A).

To determine which compartment's change in mean NUCB2/nesfatin-3 concentration effected this result, we performed repeated measures one-way ANOVA on 0.5PM and RC compartments separately; neither were statistically significant ($p=0.626$ and 0.187 respectively).

However, we note that NUCB2/nesfatin-3 concentrations remained relatively constant in the 0.5PM compartment, while the Ctrl group in the RC compartment had 1.8 times the mean NUCB2/nesfatin-3 concentration of LPS90. The observation suggests NUCB2/nesfatin-3 is depleted from the RC compartment after 90 mins of LPS stimulation while its concentration in the 0.5PM compartment does not change.

2.4.4 NUCB2/nesfatin-3 is constitutively more concentrated in euchromatin than heterochromatin portions of neutrophilic nuclei

Next, we examined whether the distribution of NUCB2/nesfatin-3 within neutrophilic nuclei changed with LPS treatment. The lighter portion of nuclei was defined as euchromatin (Eu), and the darker portion heterochromatin (Het) (Appendix I, Figure I.III). Repeated measures one-way ANOVA revealed that groups did not significantly differ ($p=0.265$; Figure 2.4A). However, results did show a consistent 5 times higher mean NUCB2/nesfatin-3 concentration in Eu compared to Het throughout LPS stimulation time points.

To determine whether this observation was statistically significant, we performed a repeated measures two-way ANOVA, followed by Sidak's multiple comparisons test. Results from the two-way ANOVA indicated that mean NUCB2/nesfatin-3 concentrations did not significantly differ throughout time ($p=0.467$), but were significantly different between compartments ($p=0.001$). Finally, Sidak's multiple comparisons test used to compare mean NUCB2/nesfatin-3 concentrations between Eu and Het portions across all time points revealed that the 5 times difference observed was statistically significant ($p<0.003$; Figure 2.4B).

2.4.5 NUCB2/nesfatin-3 is consistently more concentrated in neutrophil cytoplasm than nuclei

In our last study of NUCB2/nesfatin-3 distribution with LPS stimulation, we determined whether the protein accumulated in nuclei or cytoplasm differently throughout (Appendix I, Figure I.III). Comparing mean labelling concentrations in the cytoplasm (Cyto) and nuclei (Nu), repeated measures one-way ANOVA revealed no significant difference between groups ($p=0.276$; Figure 2.5A). However, results showed a consistent 2 times higher mean NUCB2/nesfatin-3 concentration in Cyto compared to Nu. To determine whether this observation was statistically significant, a repeated measures two-way ANOVA was performed comparing the two variables: duration of LPS stimulation, and compartment (Cyto or Nu).

Results revealed that while the duration of LPS stimulation was not a significant factor in differences of NUCB2/nesfatin-3 concentration ($p=0.401$), compartmental differences was ($p=0.001$). Sidak's multiple comparisons test revealed that the observed 2 times higher mean NUCB2/nesfatin-1 concentration in Cyto compared to Nu was significant across all time points ($p<0.003$; Figure2.5B).

2.4.6 NUCB2/nesfatin-3 immunogold staining is high in neutrophils and red blood cells, but low in eosinophils, lymphocytes and monocytes

During the course of imaging human neutrophils for NUCB2/nesfatin-3 distribution studies, we also came across other immune cells due to impurities from neutrophil isolation. Figure2.6 shows immune cells of LPS-treated samples, imaged to establish an idea of NUCB2/nesfatin-3 abundance in other blood cell types, complimentary to information of NUCB2/nesfatin-1 localization in mouse lung.

Observed throughout the NUCB2/nesfatin-3 distribution studies of human neutrophils, high levels of staining are present within the nucleus and cytoplasm (Figure2.6A). Similarly, red blood cells displayed high levels of labelling with the additional presence of clusters throughout (Figure2.6B). In contrast, NUCB2/nesfatin-3 staining was scarce in eosinophils and lymphocytes, each cell showing no more than 5 immunogold particle (Figure2.6C, D). Finally, we observe the presence of NUCB2/nesfatin-3 in the nucleus and cytoplasm of monocytes albeit in substantially lower quantities than neutrophils (Figure2.6E).

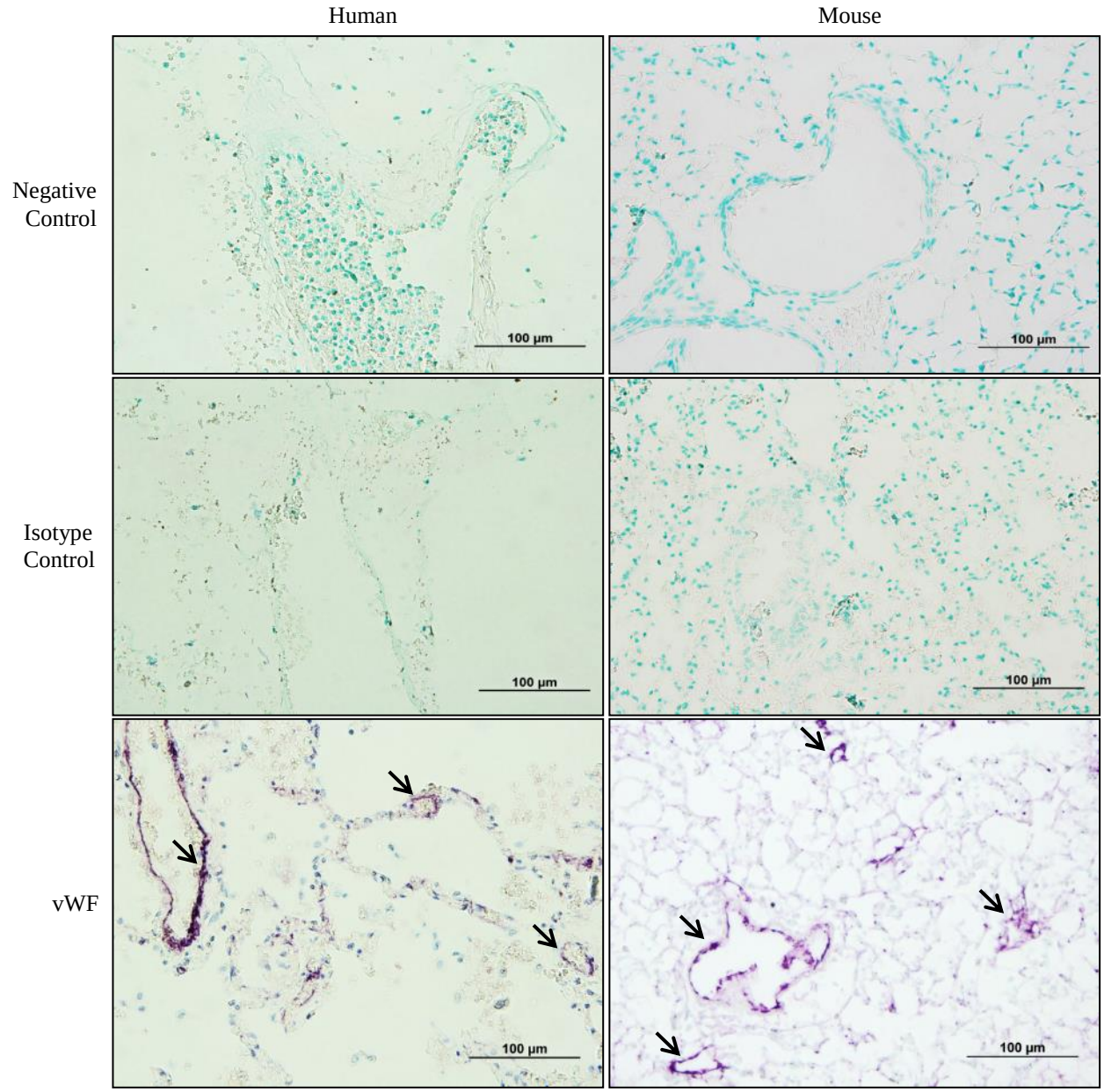

Figure 2.1A: Immunohistochemistry controls.
Lung sections from human and mouse were stained with only secondary antibody (negative control), IgG rabbit antibody (isotype control) and vWF (positive control). Negative and isotype controls were devoid of antibody staining, while vWF strongly stained vascular endothelium (arrows), but not epithelium.

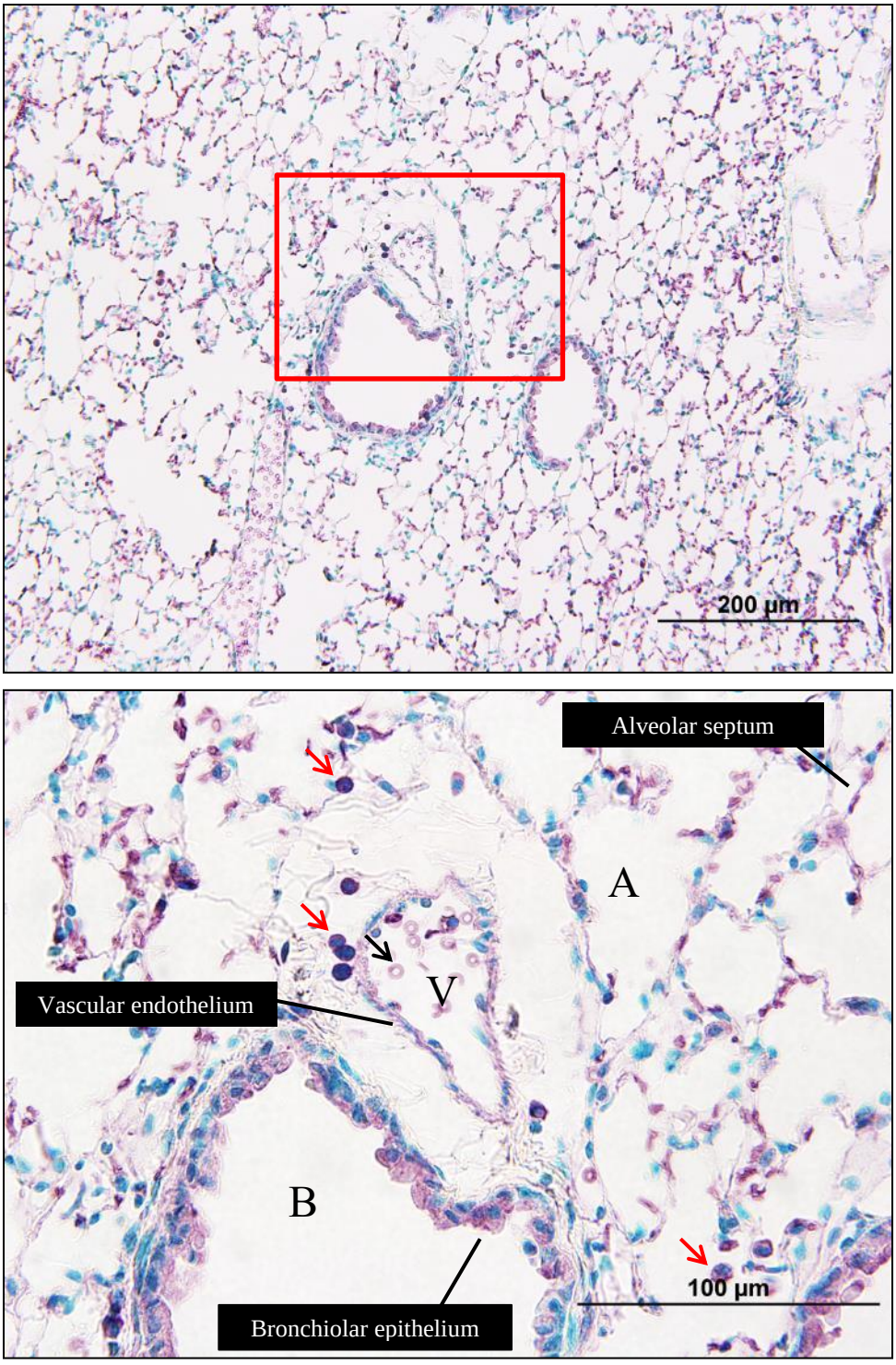

Figure 2.1B: Immunohistochemistry of NUCB2/nesfatin-1 staining in WT PBS-treated mouse lung. Images are representative of NUCB2/nesfatin-1 staining pattern in WT PBS-treated mouse lungs. Image in 20X magnification (above) presents an overview; image in 60X magnification (below) shows specific staining in RBC (black arrow), immune cells (red arrows), alveolar septum, vascular endothelium and bronchiolar epithelium. AS: Alveolar space; V: vein; B: bronchiole.

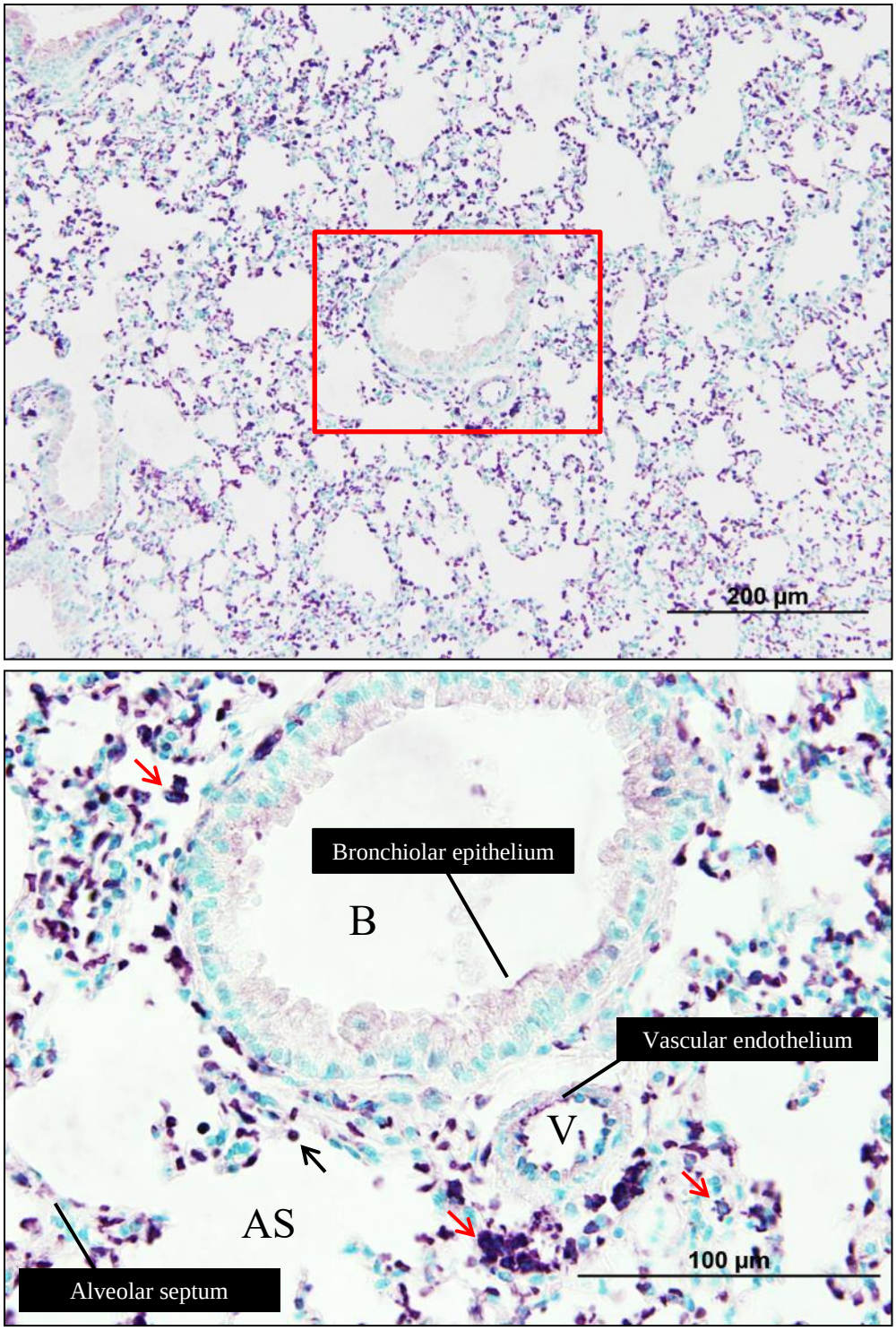

Figure 2.1C: Immunohistochemistry of NUCB2/nesfatin-1 staining in WT LPS-treated mouse lung. Images are representative of NUCB2/nesfatin-1 staining pattern in WT LPS-treated mouse lungs. Image in 20X magnification (above) presents an overview; image in 60X magnification (below) shows specific staining in RBC (black arrow), immune cells (red arrows), alveolar septum, vascular endothelium and bronchiolar epithelium. AS: Alveolar space; V: vein; B: bronchiole.

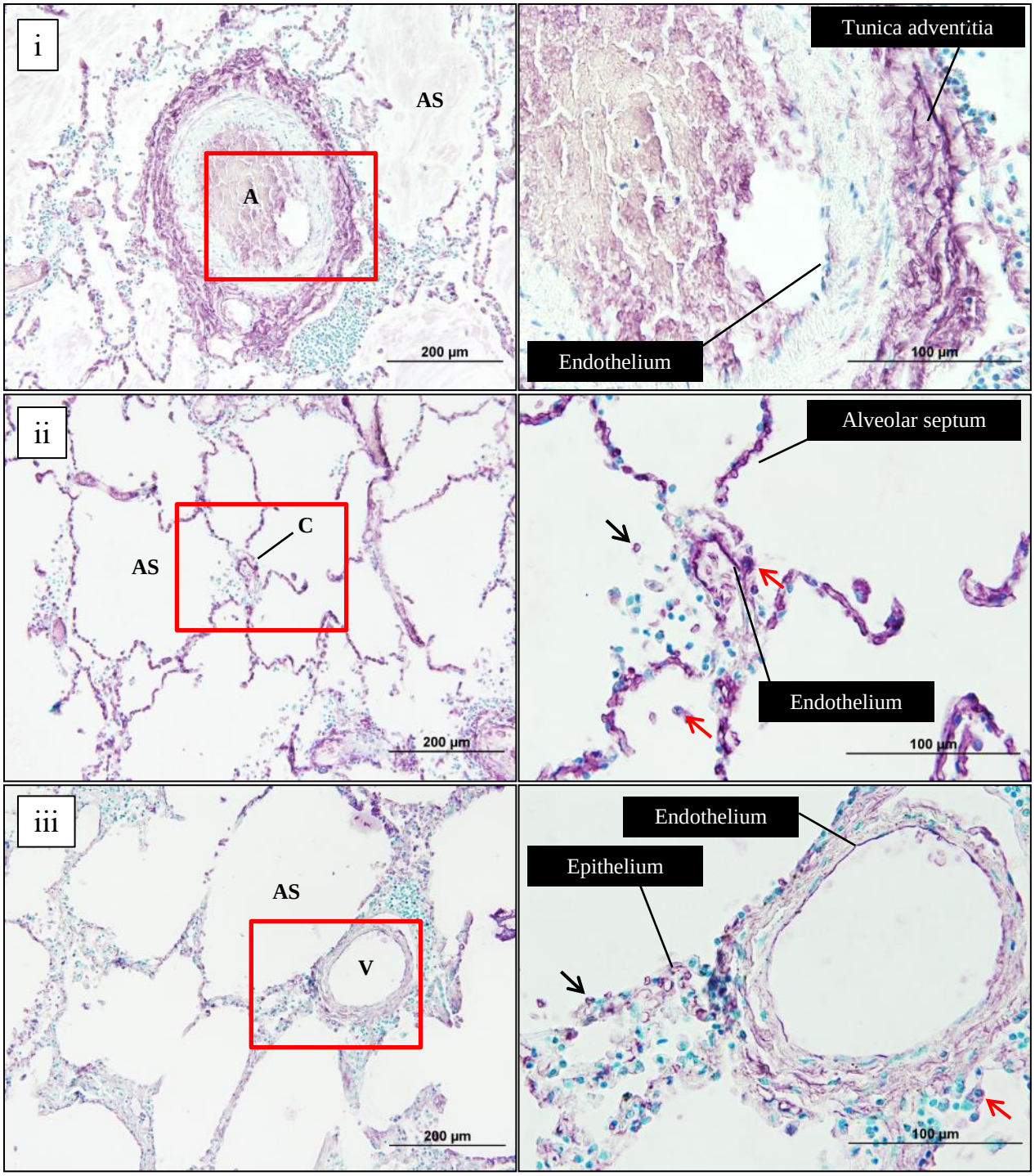

Figure 2.1D: Immunohistochemistry of NUCB2/nesfatin-1 staining in normal human lungs. Images are representative of NUCB2/nesfatin-1 staining pattern in normal human lungs. Images in 20X magnification (left) present an overview; images in 60X magnification (right) show specific staining in RBCs (black arrows), immune cells (red arrows), alveolar septum, endothelium, and artery tunica adventitia. A: Artery; C: capillary; V: vein; AS: Alveolar space.

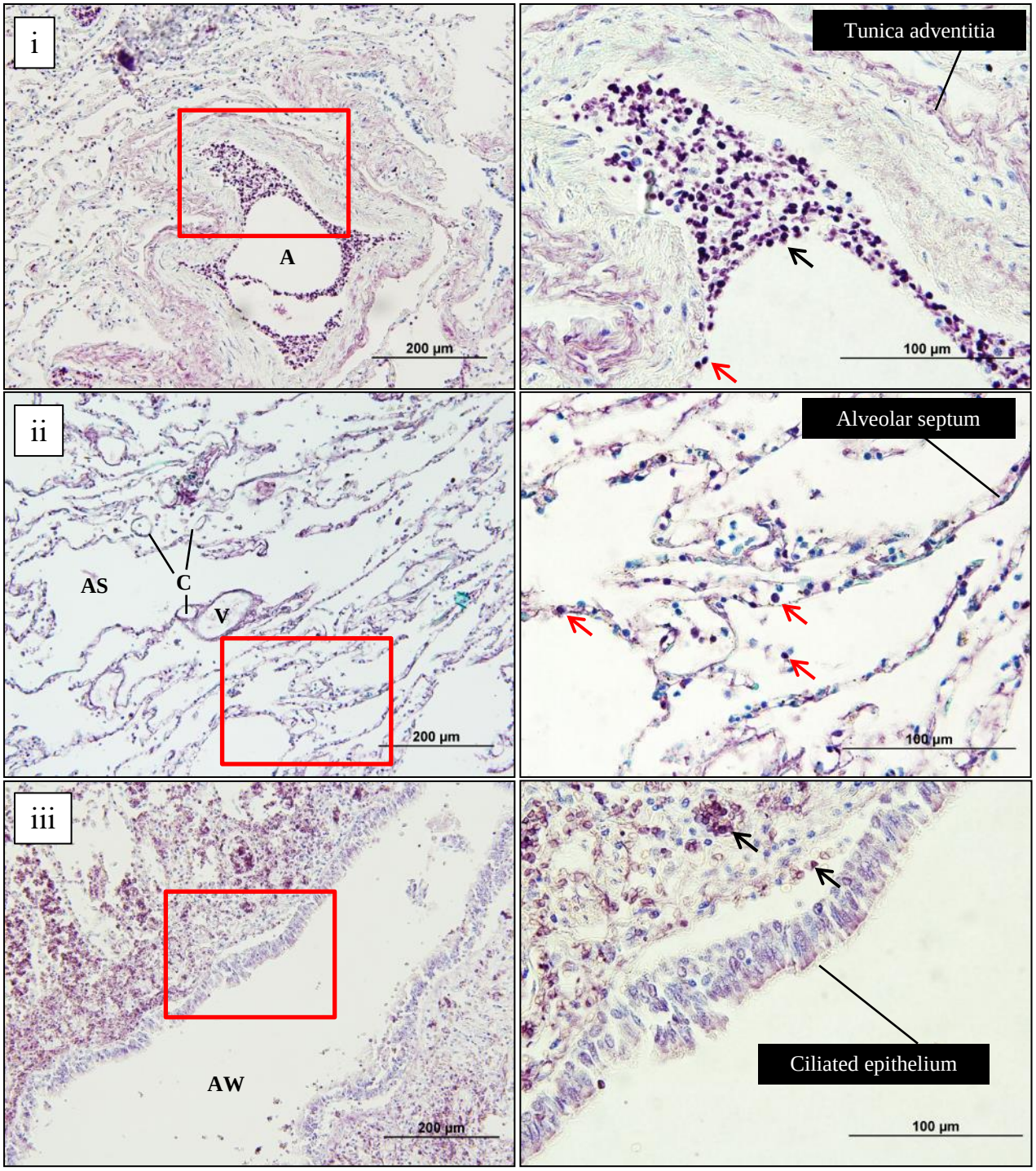
i
A
200 µm
Tunica adventitia
100 µm
ii
AS
C
V
200 µm
Alveolar septum
100 µm
iii
AW
200 µm
Ciliated epithelium
100 µm

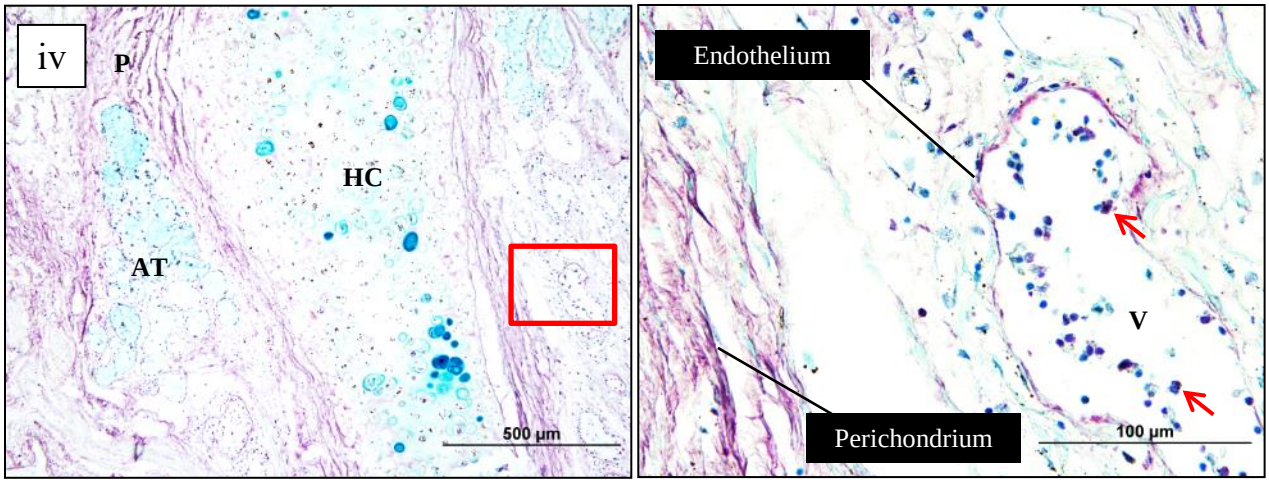

Figure 2.1E: Immunohistochemistry of NUCB2/nesfatin-1 staining in inflamed human lungs. Images are representative of NUCB2/nesfatin-1 staining pattern in inflamed human lungs. Images in 10X/20X magnification (left) present an overview; images in 60X magnification (right) show specific staining in RBCs (black arrows), immune cells (red arrows), endothelium, perichondrium, alveolar septum, ciliated epithelium and artery tunica adventitia. P: Perichondrium; AT: adipose tissue; HC: hyaline cartilage; A: Artery; C: capillary; V: vein; AS: Alveolar space; AW: Airway.

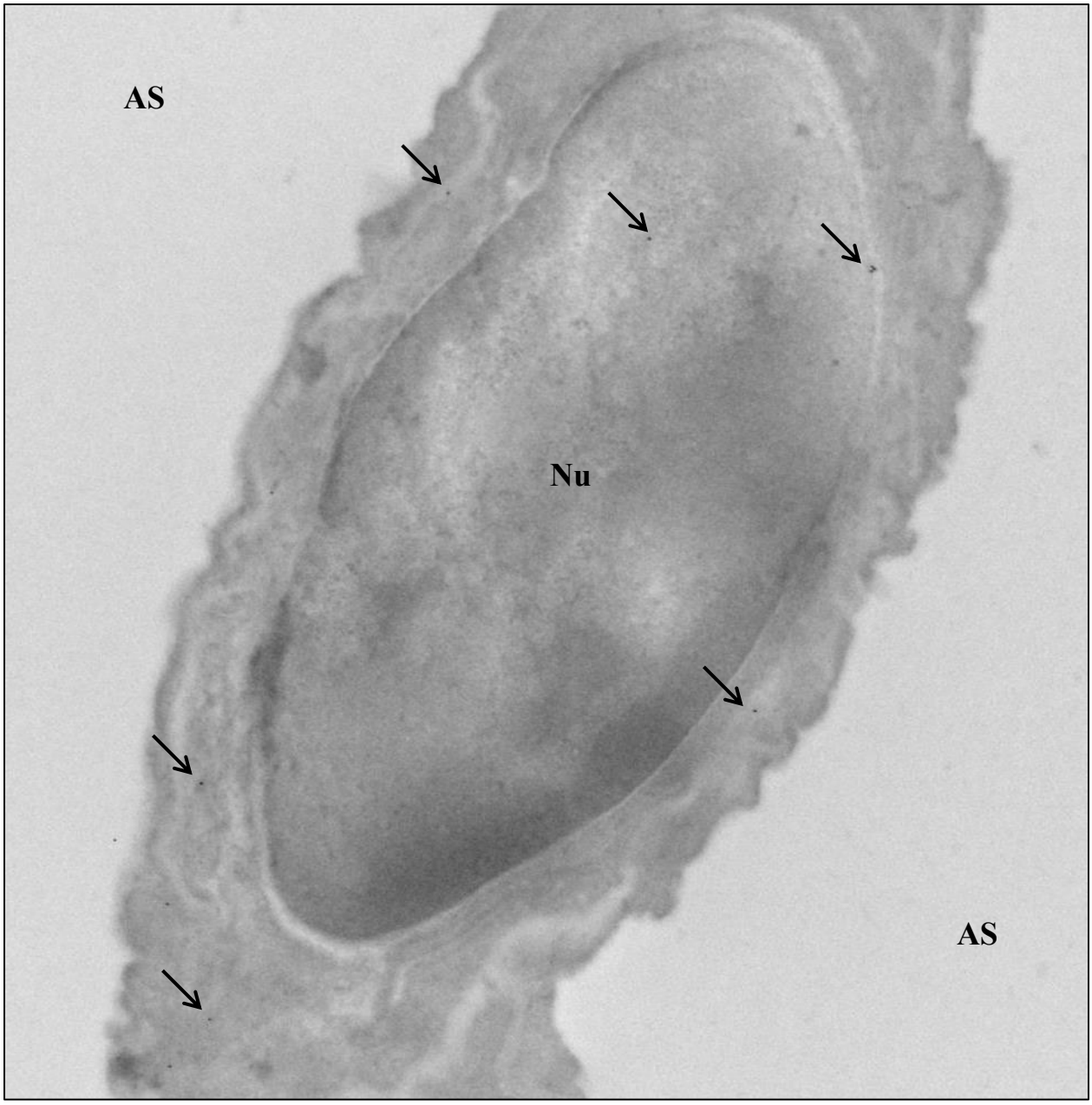

Figure 2.2A: Immuno-gold electron microscopy for NUCB2/nesfatin-1 in LPS-treated mouse lung. Type I pneumocyte of a mouse lung treated with LPS for 9 hours shows NUCB2/nesfatin-1 (arrows) (n=6). Nu: Nucleus; AS: alveolar space. Original magnification: X15,000.

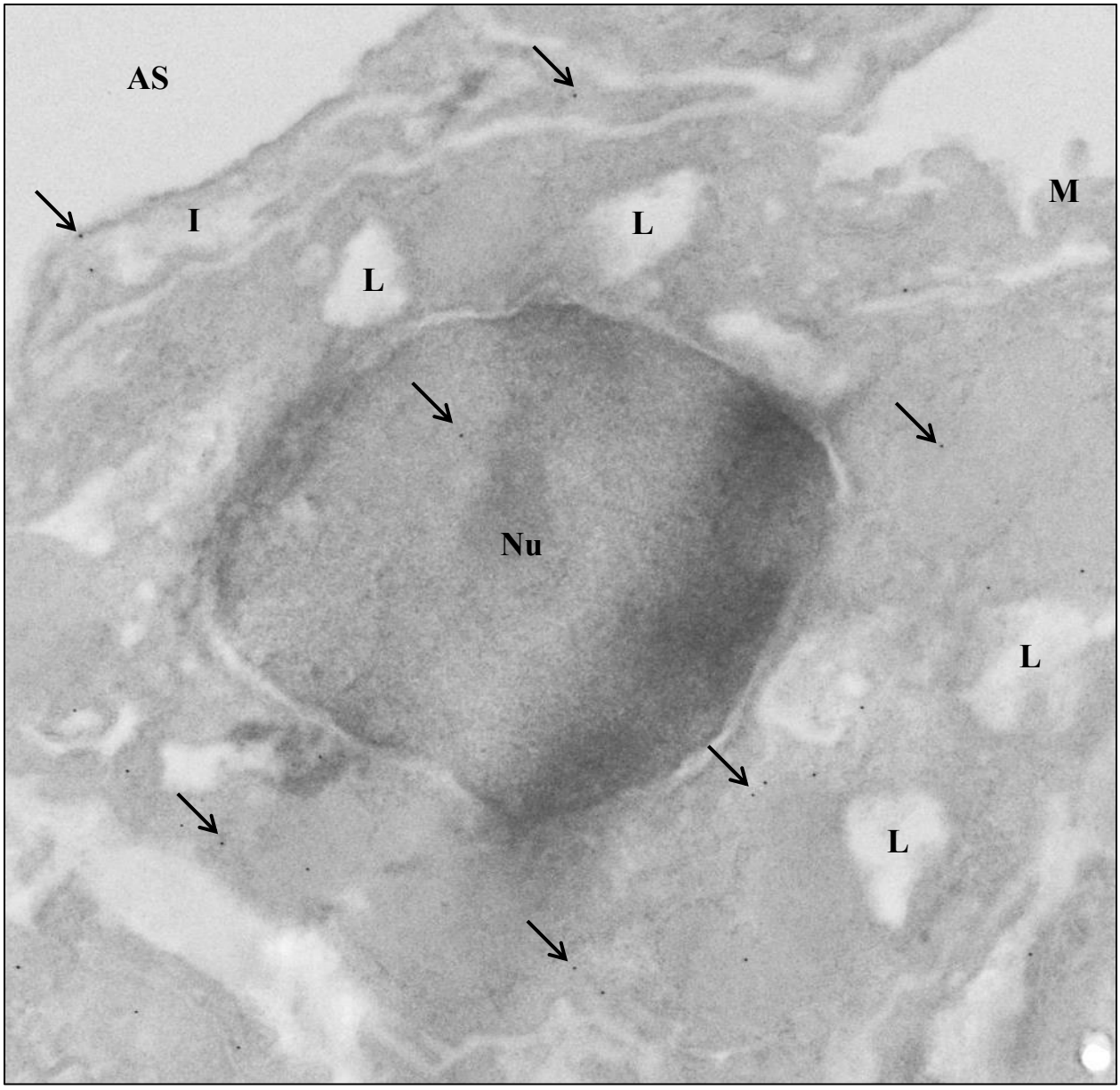

Figure 2.2B: Immuno-gold electron microscopy for NUCB2/nesfatin-1 in LPS-treated mouse lung. Type II pneumocyte of a mouse lung treated with LPS for 9 hours shows NUCB2/nesfatin-1 (arrows) (n=6). Nu: Nucleus; L: lamellar bodies; M: microvilli; AS: alveolar space; I: type I pneumocyte. Original magnification: X15,000.

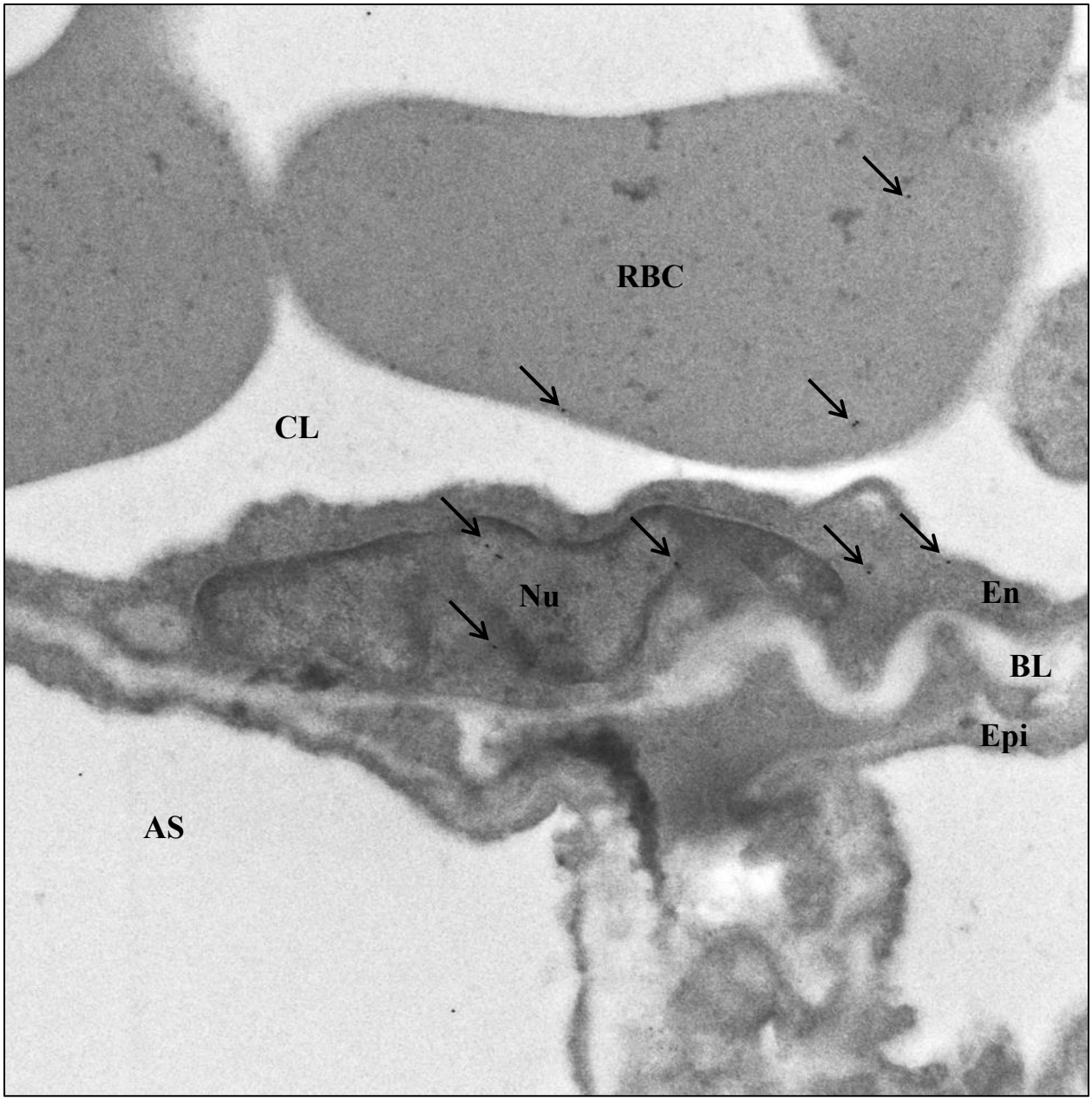

Figure 2.2C: Immuno-gold electron microscopy for NUCB2/nesfatin-1 in LPS-treated mouse lung. Endothelial cell and red blood cells in alveoli of a mouse lung treated with LPS for 9 hours shows NUCB2/nesfatin-1 (arrows) (n=6). Nu: Nucleus; RBC: red blood cell; CL: capillary lumen; En: endothelium; BL: basal lamina; Epi: epithelium; AS: alveolar space. Original magnification: X15,000.

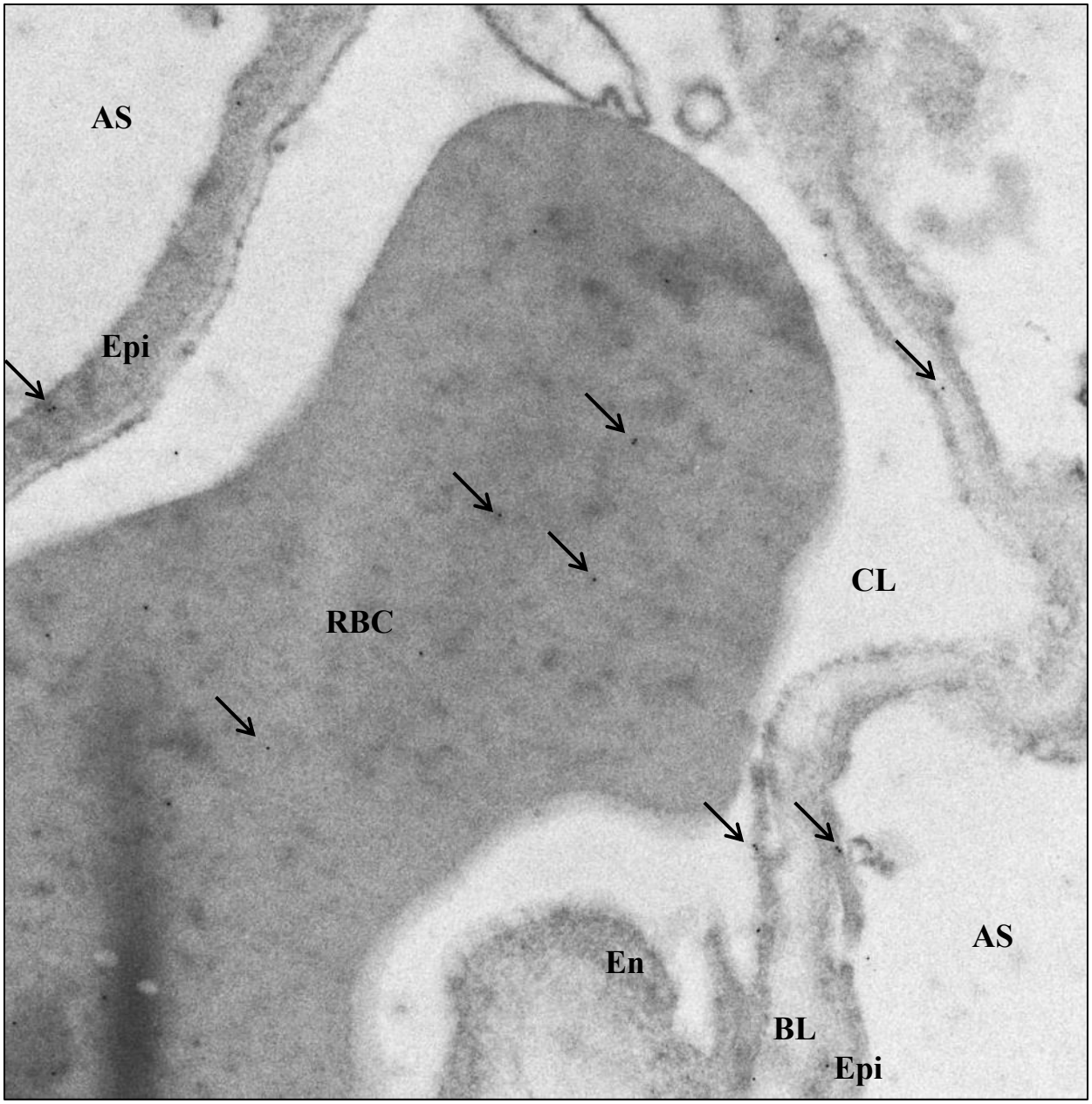

Figure 2.2D: Immuno-gold electron microscopy for NUCB2/nesfatin-1 in LPS-treated mouse lung. Red blood cell and alveolar capillary of a mouse lung treated with LPS for 9 hours shows NUCB2/nesfatin-1 (arrows) (n=6). RBC: Red blood cell; CL: capillary lumen; En: endothelium; BL: basal lamina; Epi: epithelium; AS: alveolar space. Original magnification: X15,000.

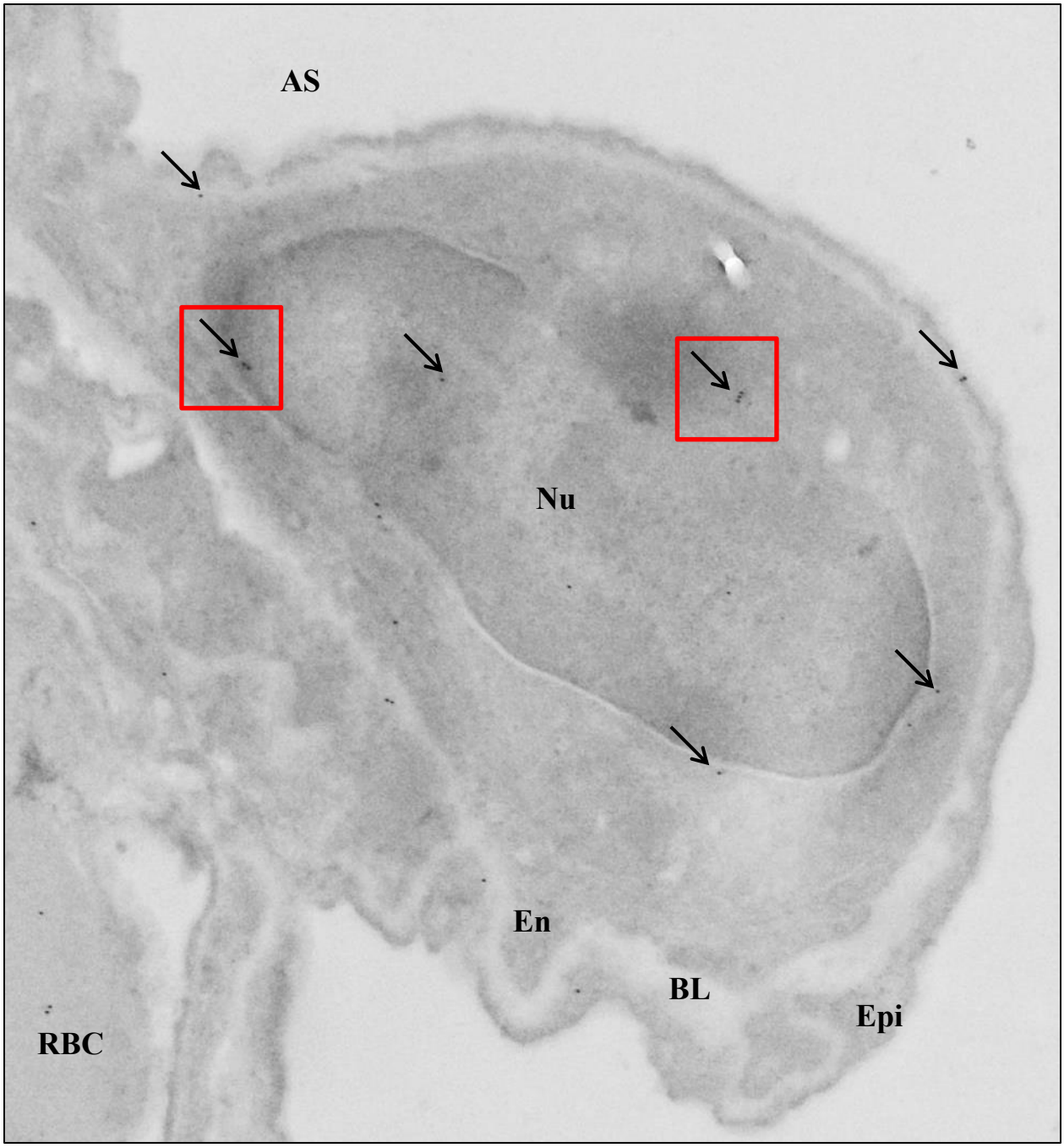

Figure 2.2E: Immuno-gold electron microscopy for NUCB2/nesfatin-1 in LPS-treated mouse lung. Monocyte and alveolar capillary of a mouse lung treated with LPS for 9 hours shows NUCB2/nesfatin-1 (arrows) with staining clustered within monocyte (red box) (n=6). Nu: Nucleus; En: endothelium; BL: basal lamina; Epi: epithelium; AS: alveolar space; RBC: red blood cell. Original magnification: X15,000.

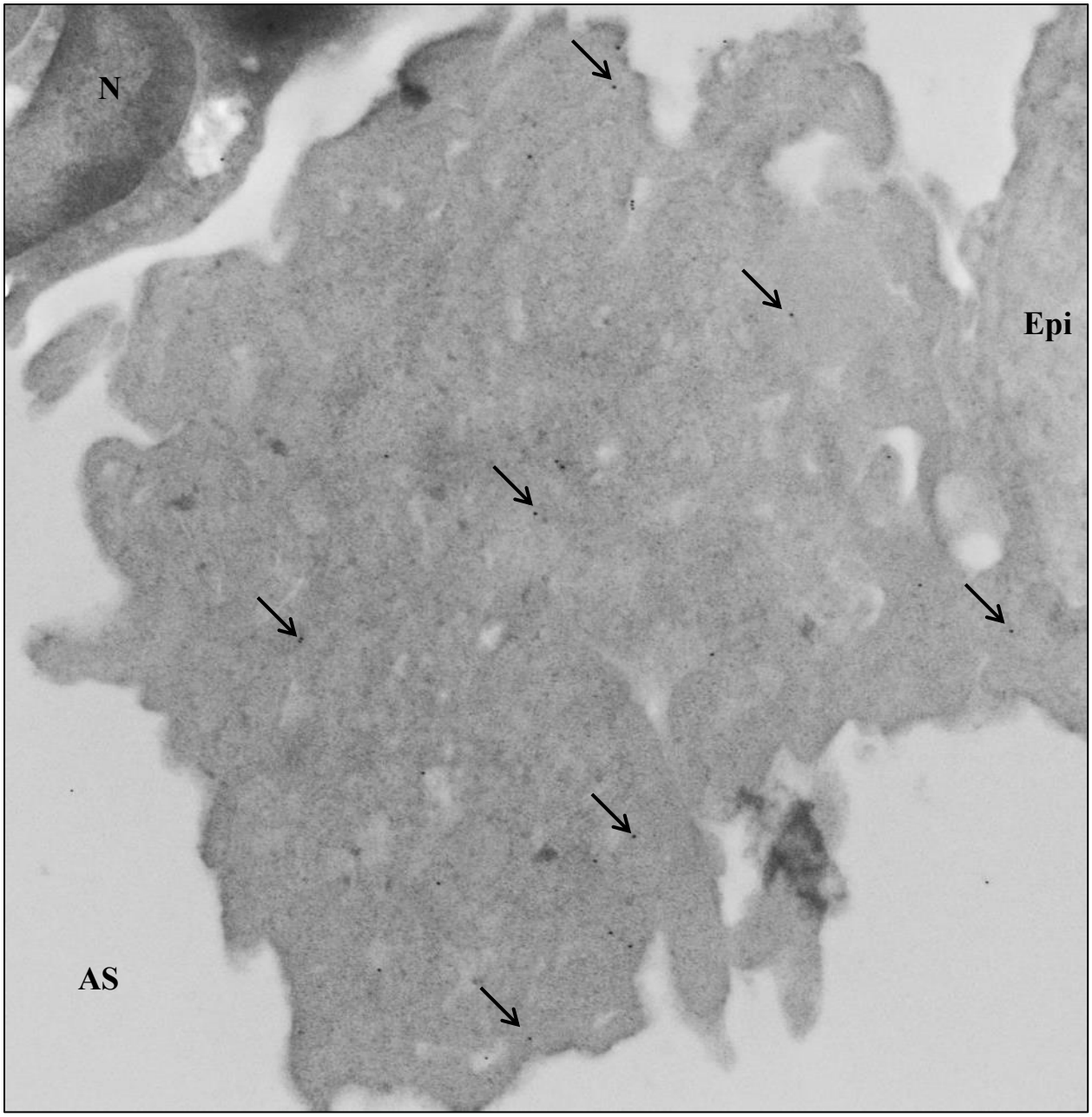

Figure 2.2F: Immuno-gold electron microscopy for NUCB2/nesfatin-1 in LPS-treated mouse lung. Macrophage in a mouse lung treated with LPS for 9 hours shows NUCB2/nesfatin-1 (arrows) (n=6). N: Neutrophil; Epi: epithelial cell; AS: alveolar space. Original magnification: X15,000.

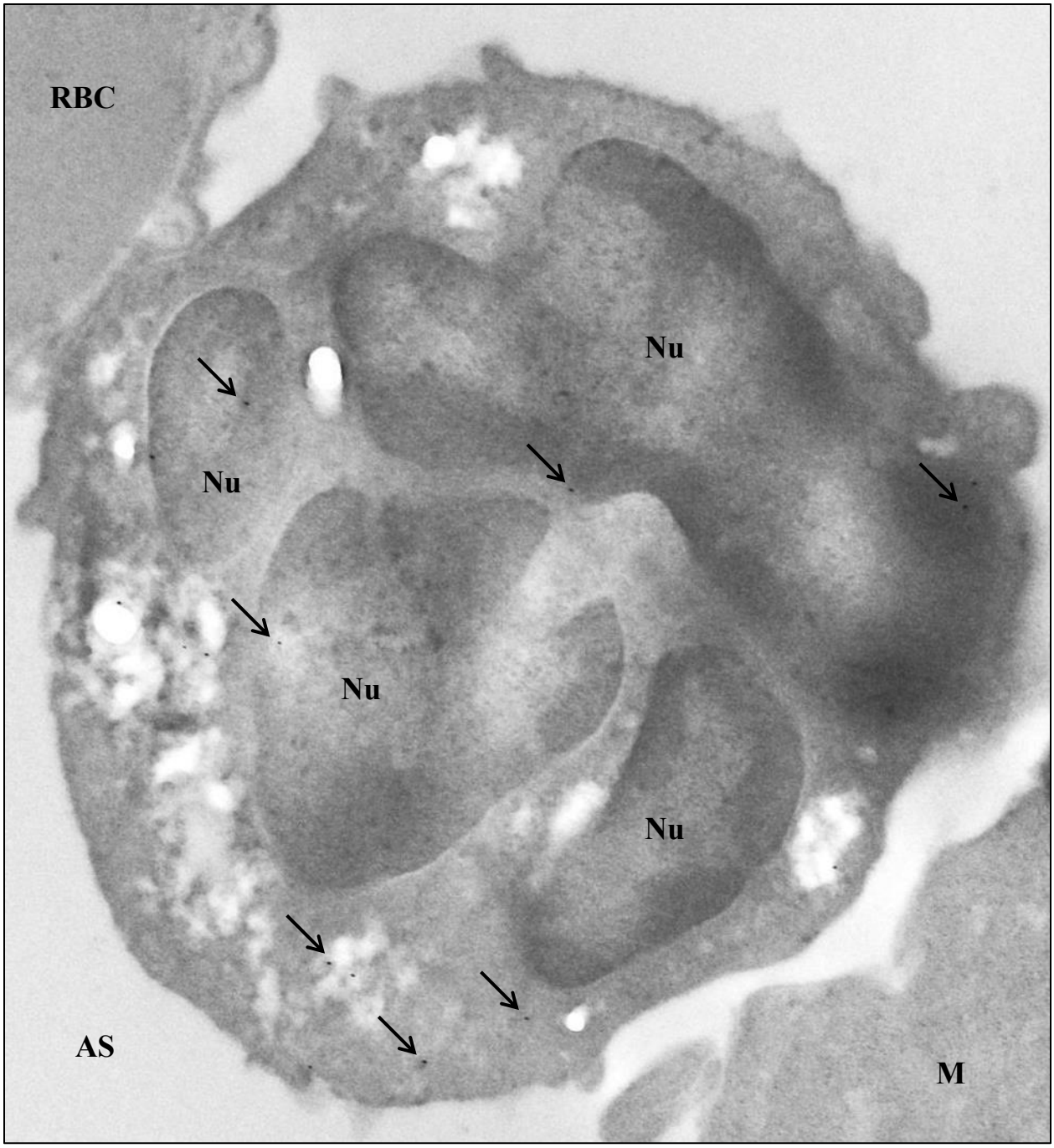

Figure 2.2G: Immuno-gold electron microscopy for NUCB2/nesfatin-1 in LPS-treated mouse lung. Neutrophil in a mouse lung treated with LPS for 9 hours shows NUCB2/nesfatin-1 (arrows) (n=6). Nu: Nuclear; M: macrophage; RBC: red blood cell; AS: alveolar space. Original magnification: X15,000.

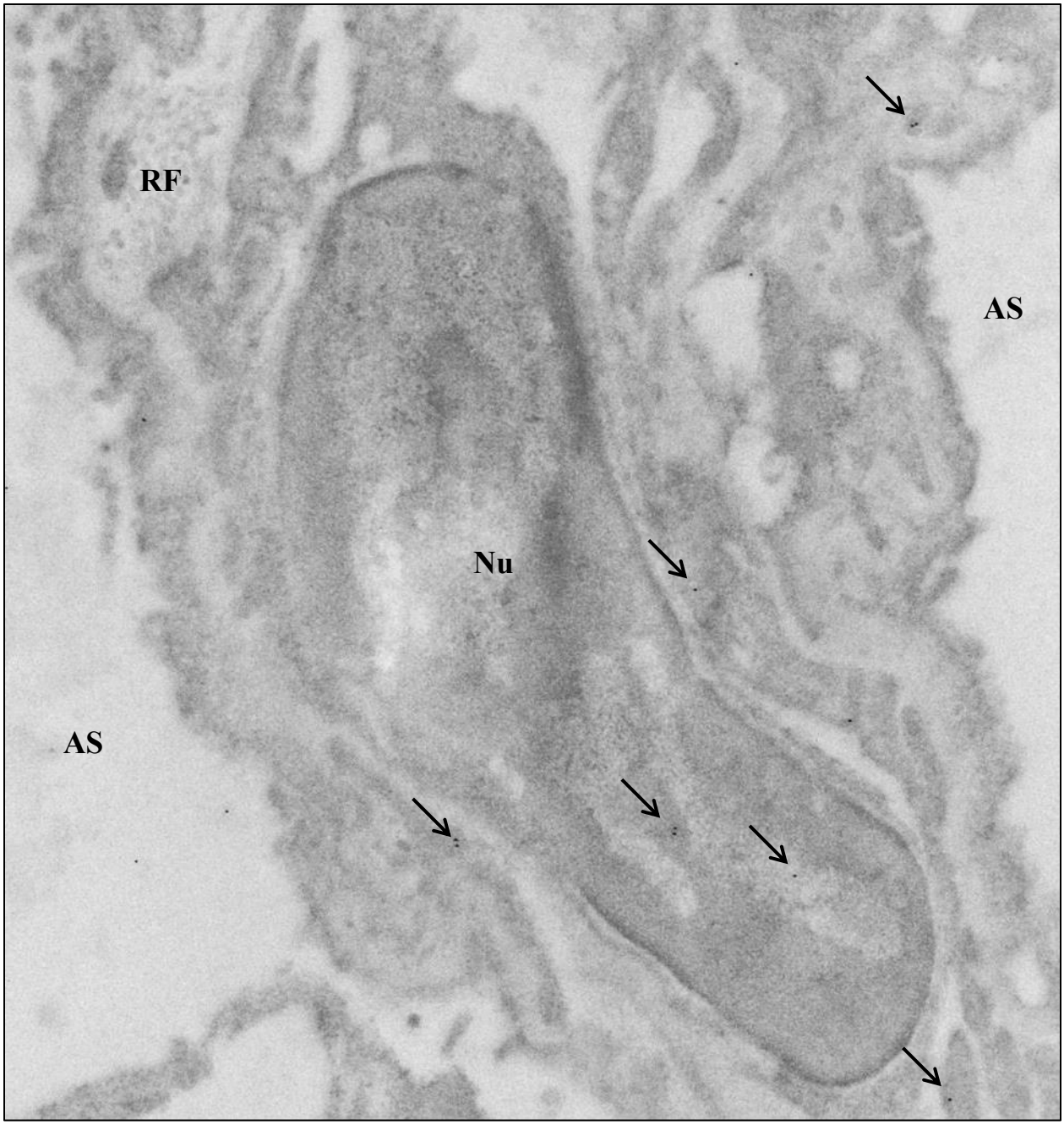

Figure 2.2H: Immuno-gold electron microscopy for NUCB2/nesfatin-1 in PBS-treated mouse lung. Type I pneumocyte of a mouse lung treated with PBS for 9 hours shows NUCB2/nesfatin-1 (arrows) (n=6). Nu: Nucleus; AS: alveolar space; RF: reticular fibres. Original magnification: X15,000.

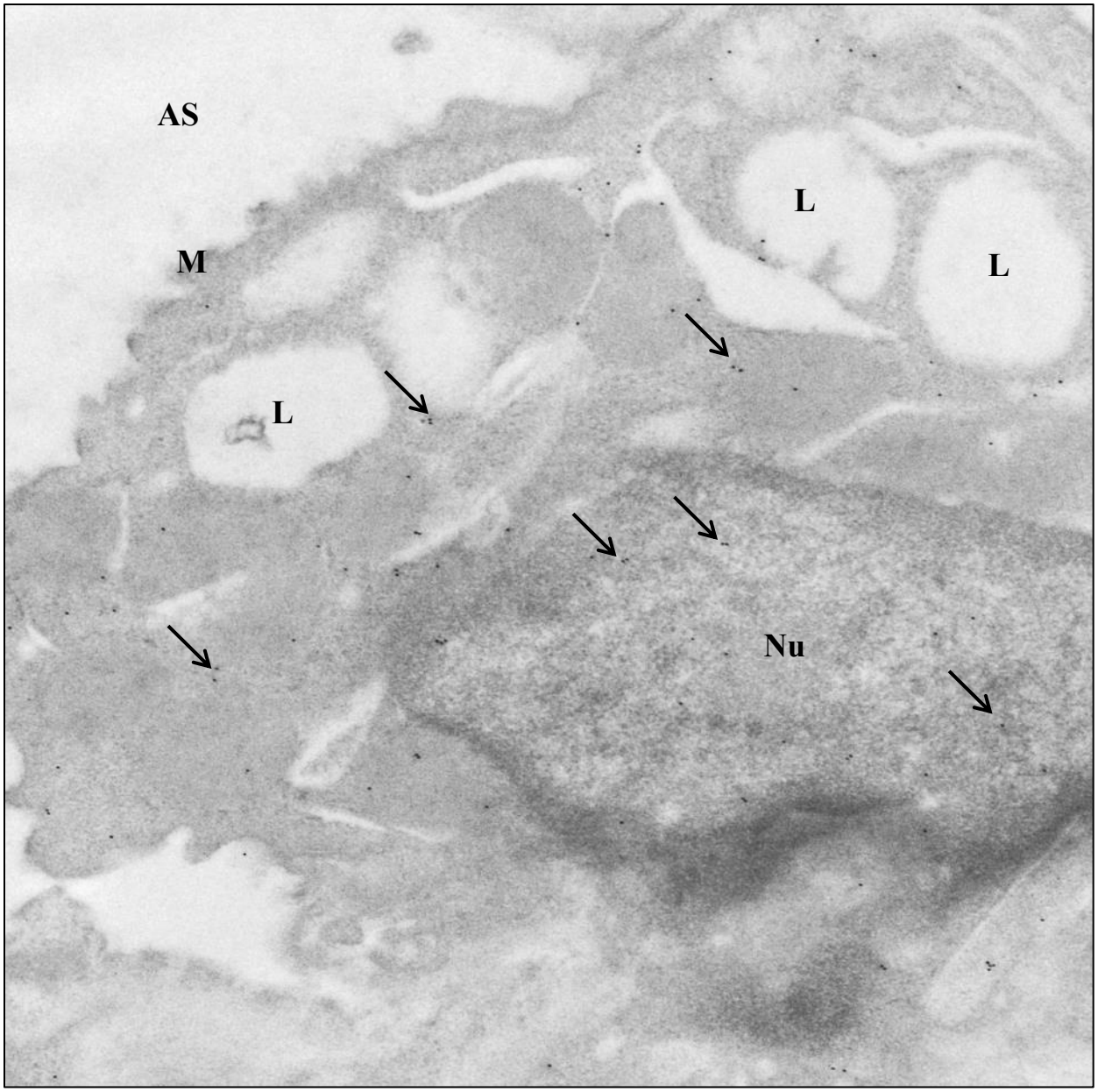

Figure 2.2I: Immuno-gold electron microscopy for NUCB2/nesfatin-1 in PBS-treated mouse lung. Type II pneumocyte of a mouse lung treated with PBS for 9 hours shows NUCB2/nesfatin-1 (arrows) (n=6). Nu: Nucleus; L: lamellar bodies; M: microvilli; AS: alveolar space. Original magnification: X15,000.

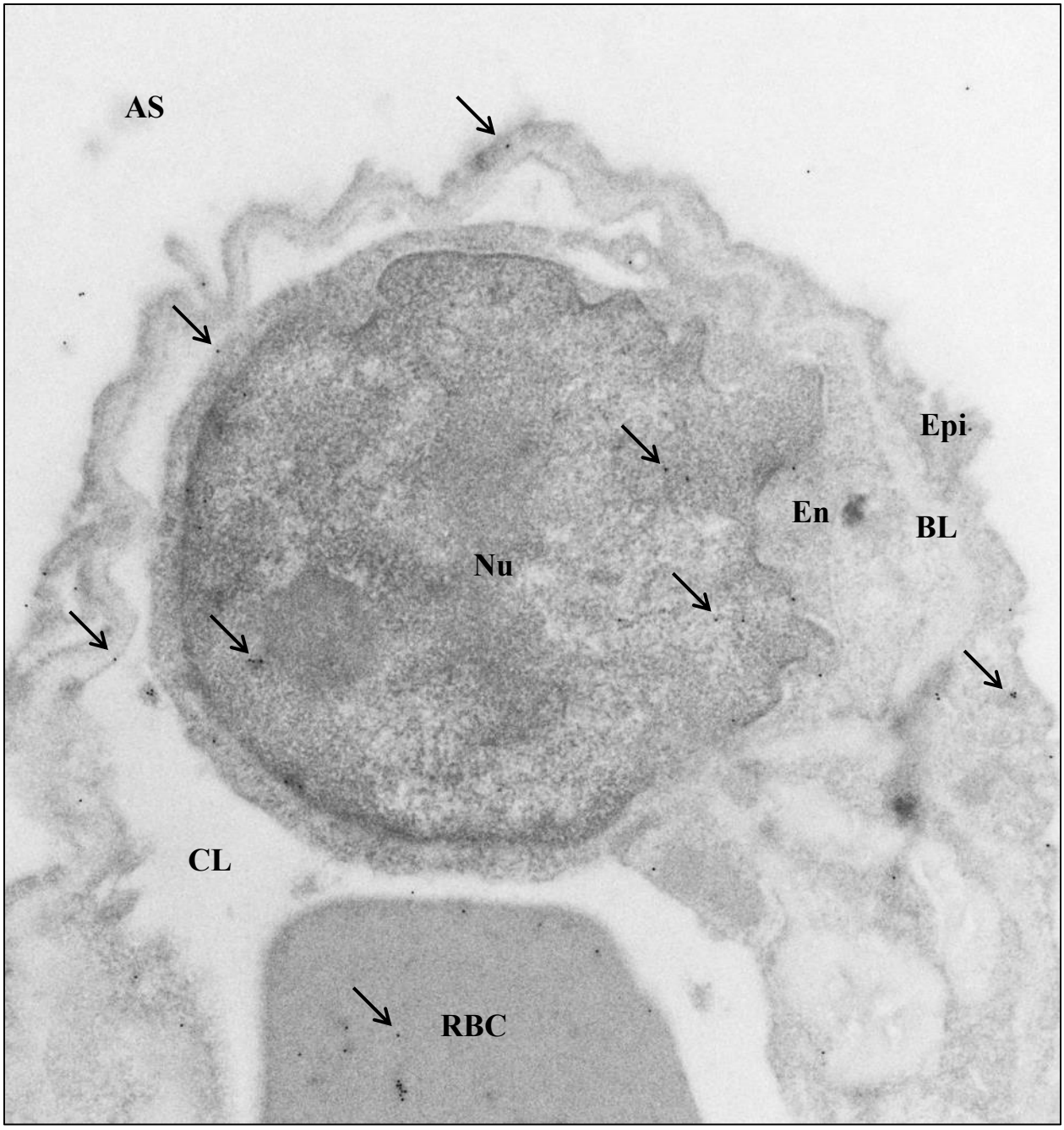

Figure 2.2J: Immuno-gold electron microscopy for NUCB2/nesfatin-1 in PBS-treated mouse lung. Endothelial cell of a mouse lung treated with PBS for 9 hours shows NUCB2/nesfatin-1 (arrows) (n=6). Nu: Nucleus; RBC: red blood cell; CL: capillary lumen; En: endothelium; BL: basal lamina; Epi: epithelium; AS: alveolar space. Original magnification: X15,000.

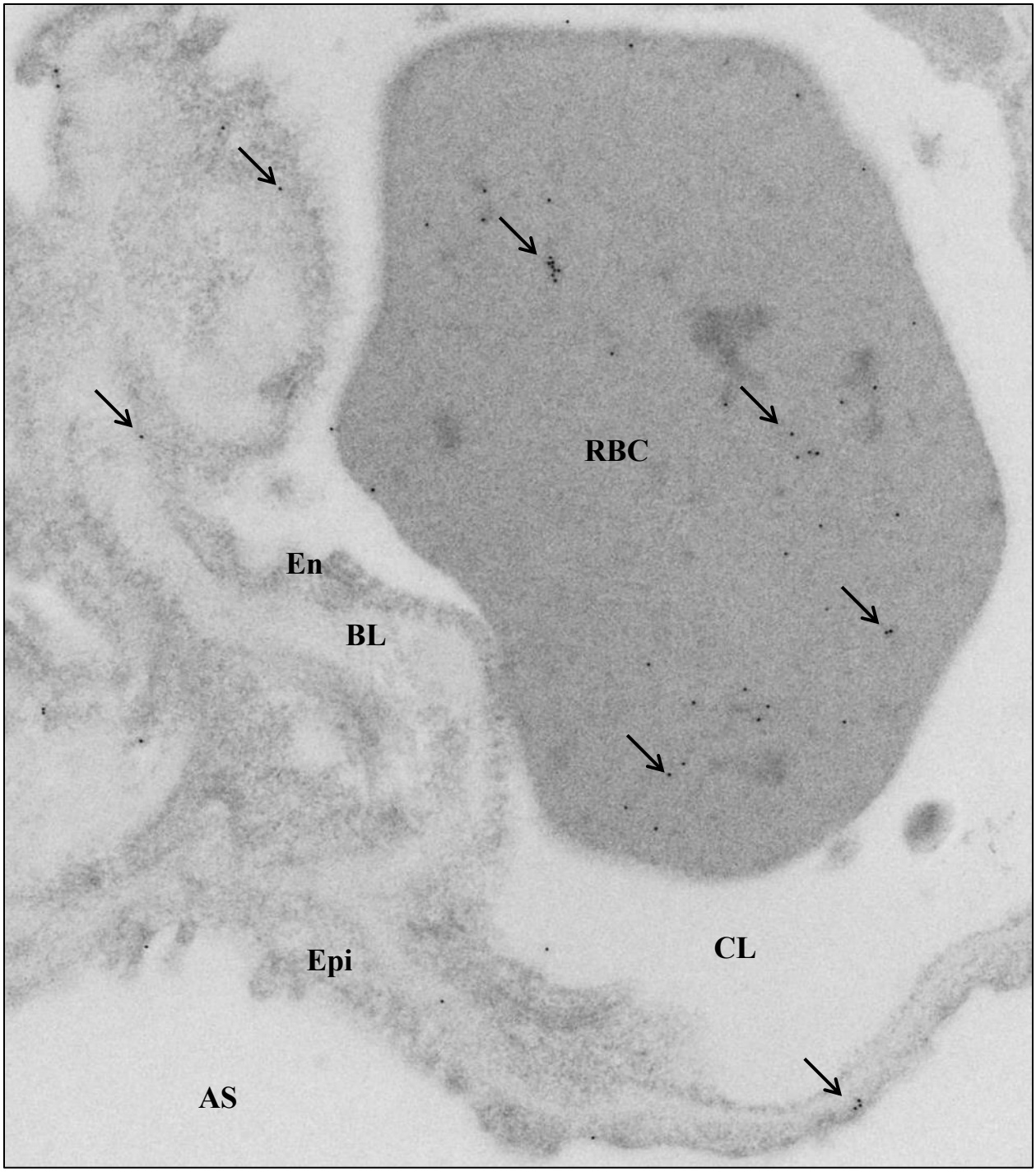

Figure 2.2K: Immuno-gold electron microscopy for NUCB2/nesfatin-1 in PBS-treated mouse lung. Red blood cell and alveolar capillary of a mouse lung treated with PBS for 9 hours shows NUCB2/nesfatin-1 (arrows) (n=6). RBC: Red blood cell; CL: capillary lumen; En: endothelium; BL: basal lamina; Epi: epithelium; AS: alveolar space. Original magnification: X15,000.

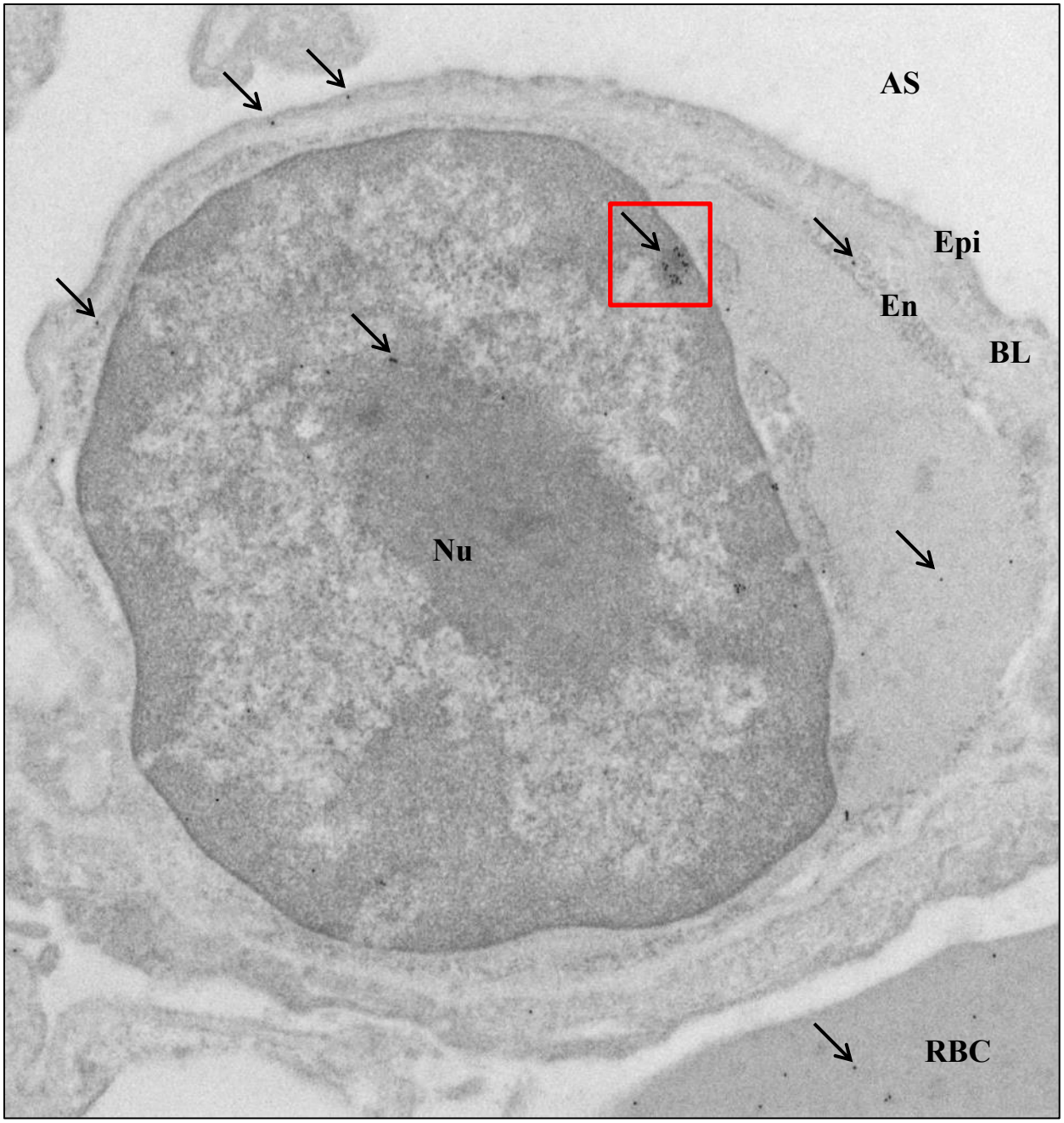

Figure 2.2L: Immuno-gold electron microscopy for NUCB2/nesfatin-1 in PBS-treated mouse lung. Monocyte and alveolar capillary of a mouse lung treated with PBS for 9 hours shows NUCB2/nesfatin-1 (arrows) with staining clustered within monocyte (red box) (n=6). Nu: Nucleus; En: endothelium; BL: basal lamina; Epi: epithelium; RBC: red blood cell; AS: alveolar space. Original magnification: X15,000.

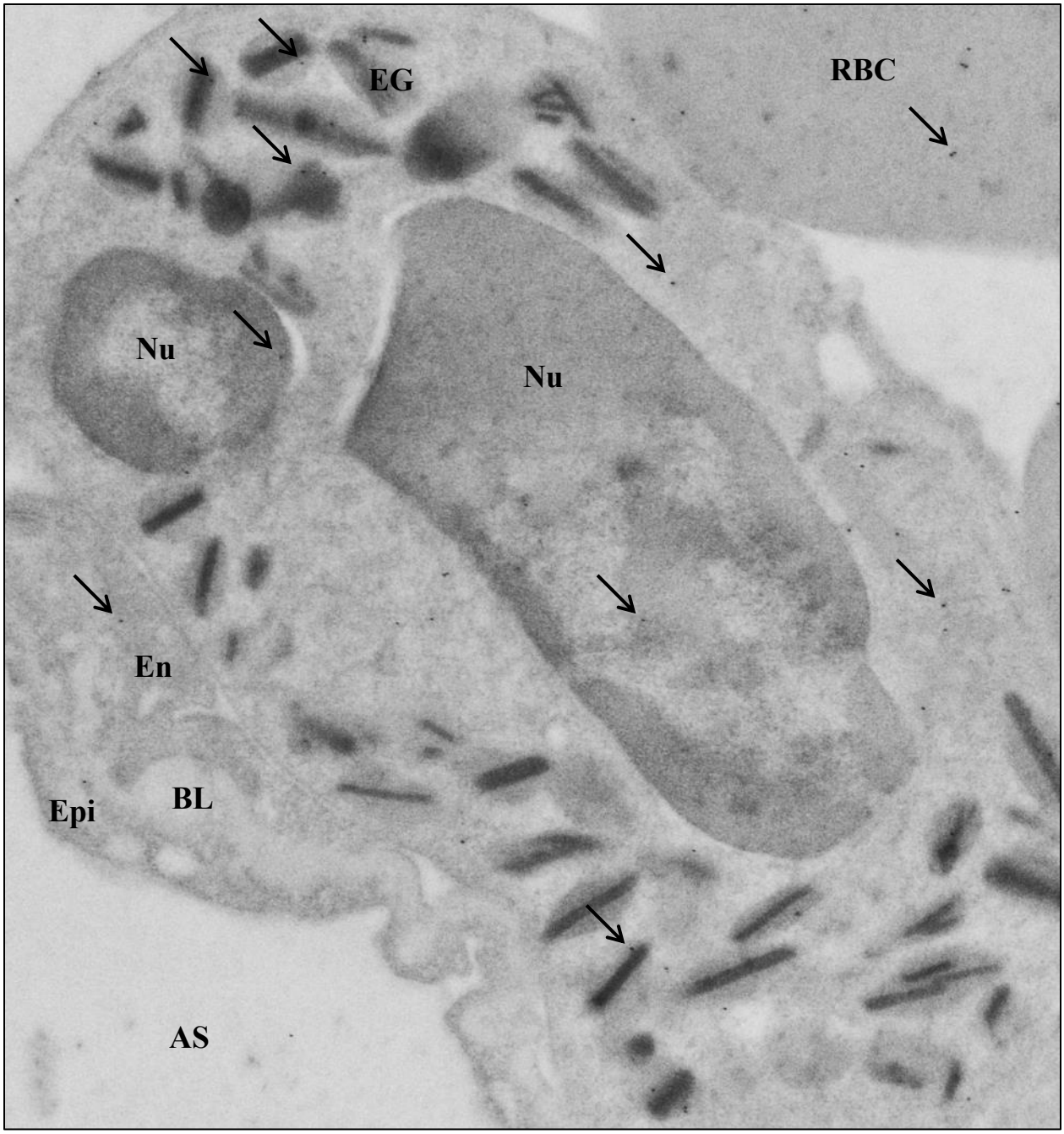

Figure 2.2M: Immuno-gold electron microscopy for NUCB2/nesfatin-1 in PBS-treated mouse lung. Eosinophil in a mouse lung simulated by PBS for 9 hours shows NUCB2/nesfatin-1 (arrows) (n=6). Nu: Nucleus; EG: eosinophil granules; RBC: red blood cell; En: endothelium; BL: basal lamina; Epi: epithelium; AS: alveolar space. Original magnification: X15,000.

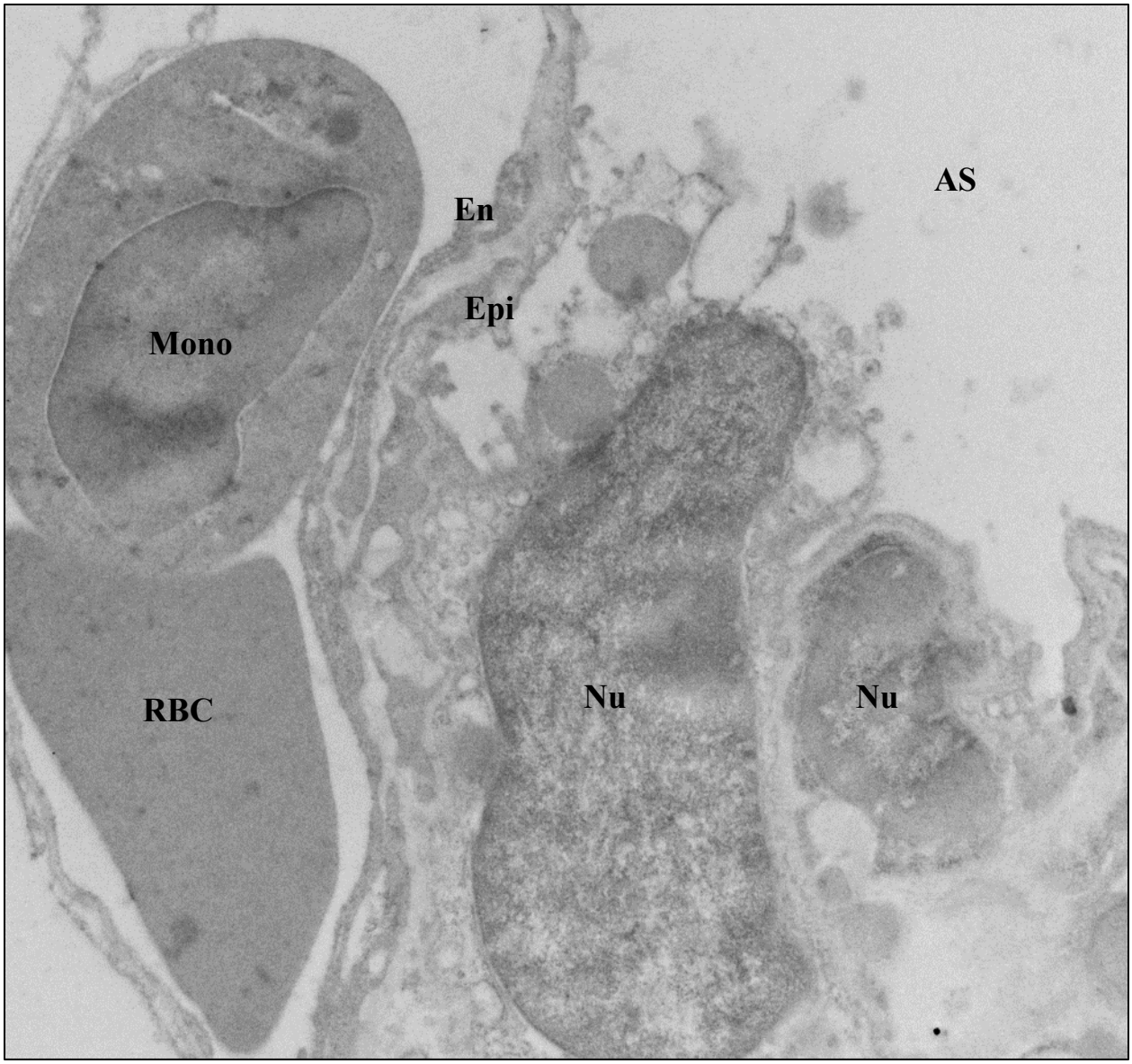

Figure 2.2N: Negative control for immuno-gold electron microscopy of mouse lung.
Sample is devoid of gold particle staining. Nu: Nucleus; RBC: red blood cell; Mono: monocyte; En: endothelium; Epi: epithelium; AS: alveolar space. Original magnification: X10,000.

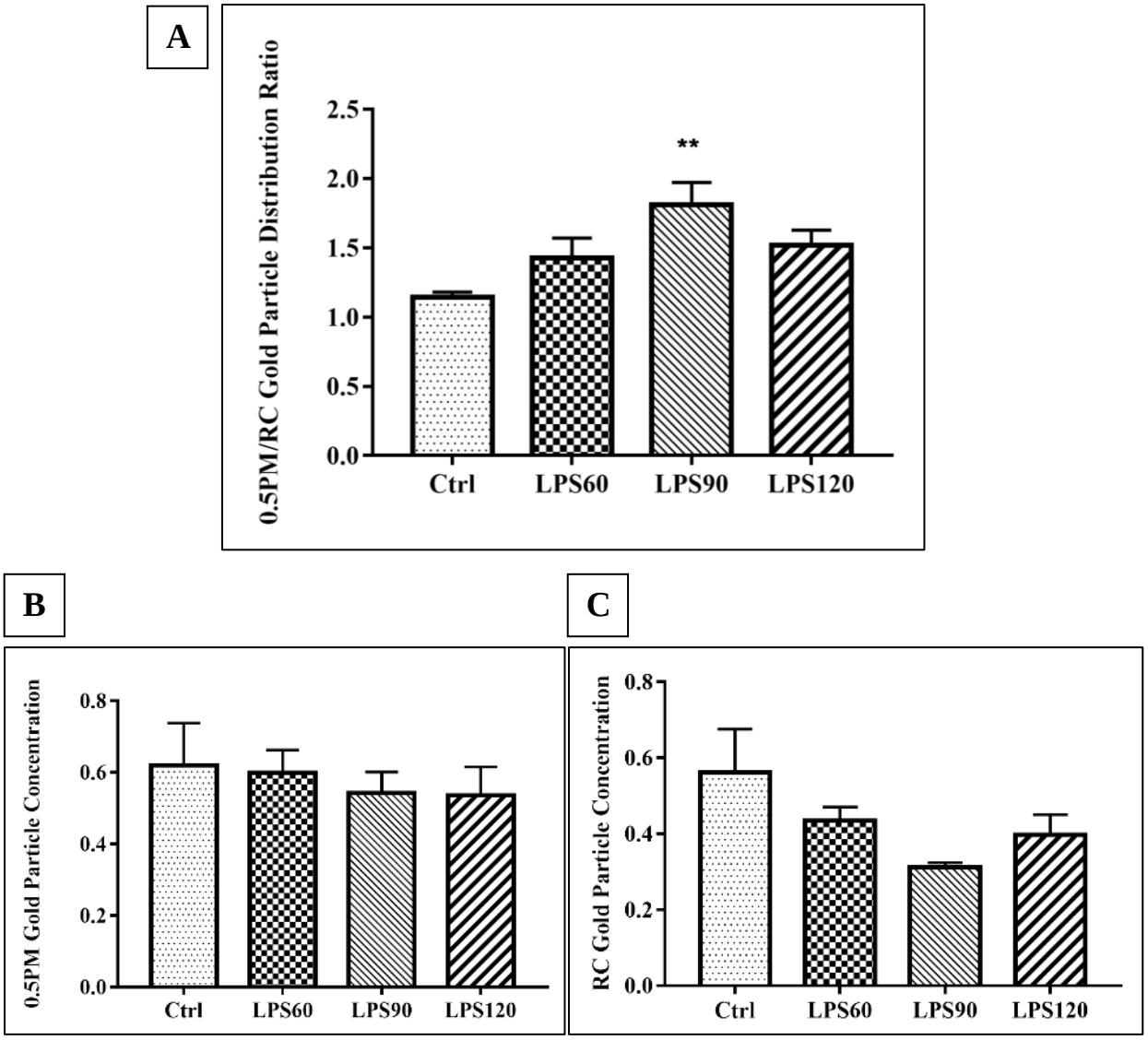

Figure 2.3: 0.5PM/RC NUCB2/nesfatin-3 distribution ratio in human neutrophils on LPS challenge. NUCB2/nesfatin-3 was labelled with immunogold particles and quantified. **(A)** Distribution ratios of NUCB2/nesfatin-3 after human neutrophils were challenged for 0, 60, 90, and 120mins with LPS (1ng/mL) were obtained by dividing the concentration of immunogold particles within 0.5µm of plasma membrane (0.5PM) by the concentration of immunogold particles in the remainder of the cytosol (RC). Repeated measures one-way ANOVA revealed statistical difference between groups ($p=0.010$); Dunnett's multiple comparisons test determined that Ctrl and LPS90 were statistically different ($p=0.017$). **(B, C)** One-way ANOVA on NUCB2/nesfatin-3 concentrations in the 0.5PM or RC compartment alone revealed no statistical difference throughout time ($p=0.626$ and 0.187 respectively). Notably, however, when a t-test comparing Ctrl and LPS90 in the RC compartment was performed, results were close to achieving statistical significance ($p=0.073$). (**$p\leq0.01$ compared to control; data shown as mean ± SEM; n=5).

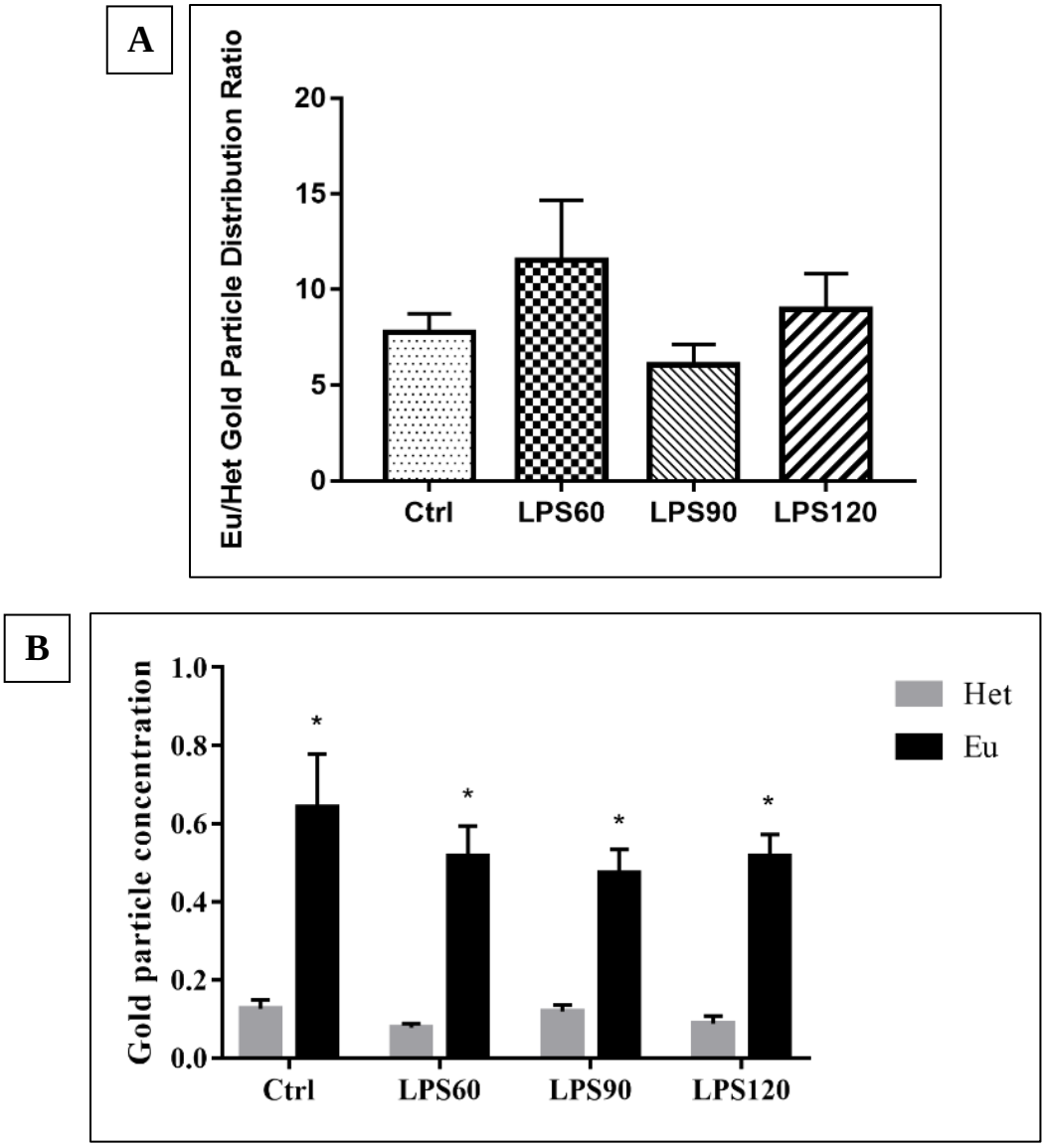

Figure 2.4: Eu/Het NUCB2/nesfatin-3 distribution ratio in human neutrophils on LPS challenge. NUCB2/nesfatin-3 was labelled with immunogold particles and quantified. **(A)** Distribution ratios of NUCB2/nesfatin-3 after human neutrophils were challenged for 0, 60, 90, and 120mins with LPS (1ng/mL) were obtained by dividing the concentration of immunogold particles within the euchromatin portion of nuclei (Eu) by the concentration of immunogold particles in the heterochromatin portion of nuclei (Het). Repeated measures one-way ANOVA revealed no statistical significant difference between groups ($p=0.265$). **(B)** Following, immunogold labelling of Eu and Het compartments throughout time was compared. Repeated measures two-way ANOVA reveals significant difference between compartments ($p=0.001$), but no difference in each compartment across time ($p=0.467$). Sidak's multiple comparisons test reveals that the significant difference between compartments was true across all time points ($p<0.003$). (*$p<0.003$; Data shown as mean ± SEM; n=5).

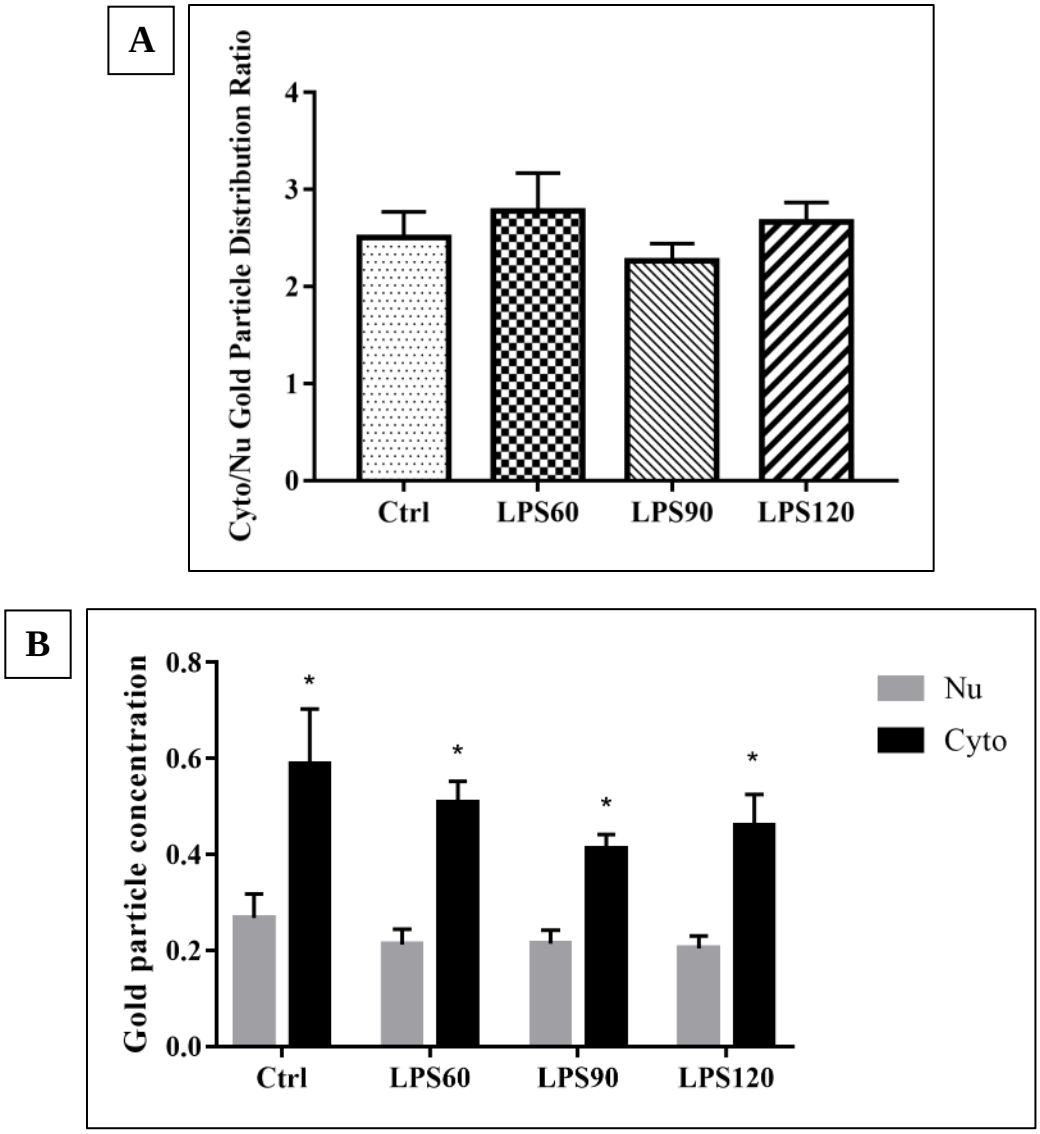

Figure 2.5: Cyto/Nu NUCB2/nesfatin-3 distribution ratio in human neutrophils on LPS challenge. NUCB2/nesfatin-3 was labelled with immunogold particles and quantified. **(A)** Distribution ratios of NUCB2/nesfatin-3 after human neutrophils were challenged for 0, 60, 90, and 120mins with LPS (1ng/mL) were obtained by dividing the concentration of immunogold particles within the cytoplasm (Cyto) by the concentration of immunogold particles in nuclei (Nu). Repeated measure one-way ANOVA revealed no statistical significant difference between groups ($p=0.276$). **(B)** Following, immunogold labelling of Cyto and Nu compartments throughout time was compared. Repeated measures two-way ANOVA reveals significant difference between compartments ($p=0.001$), but no difference in each compartment across time ($p=0.401$). Sidak's multiple comparisons test reveals that the significant difference between compartments was true for all time points (*$p<0.003$; Data shown as mean ± SEM; $n=5$).

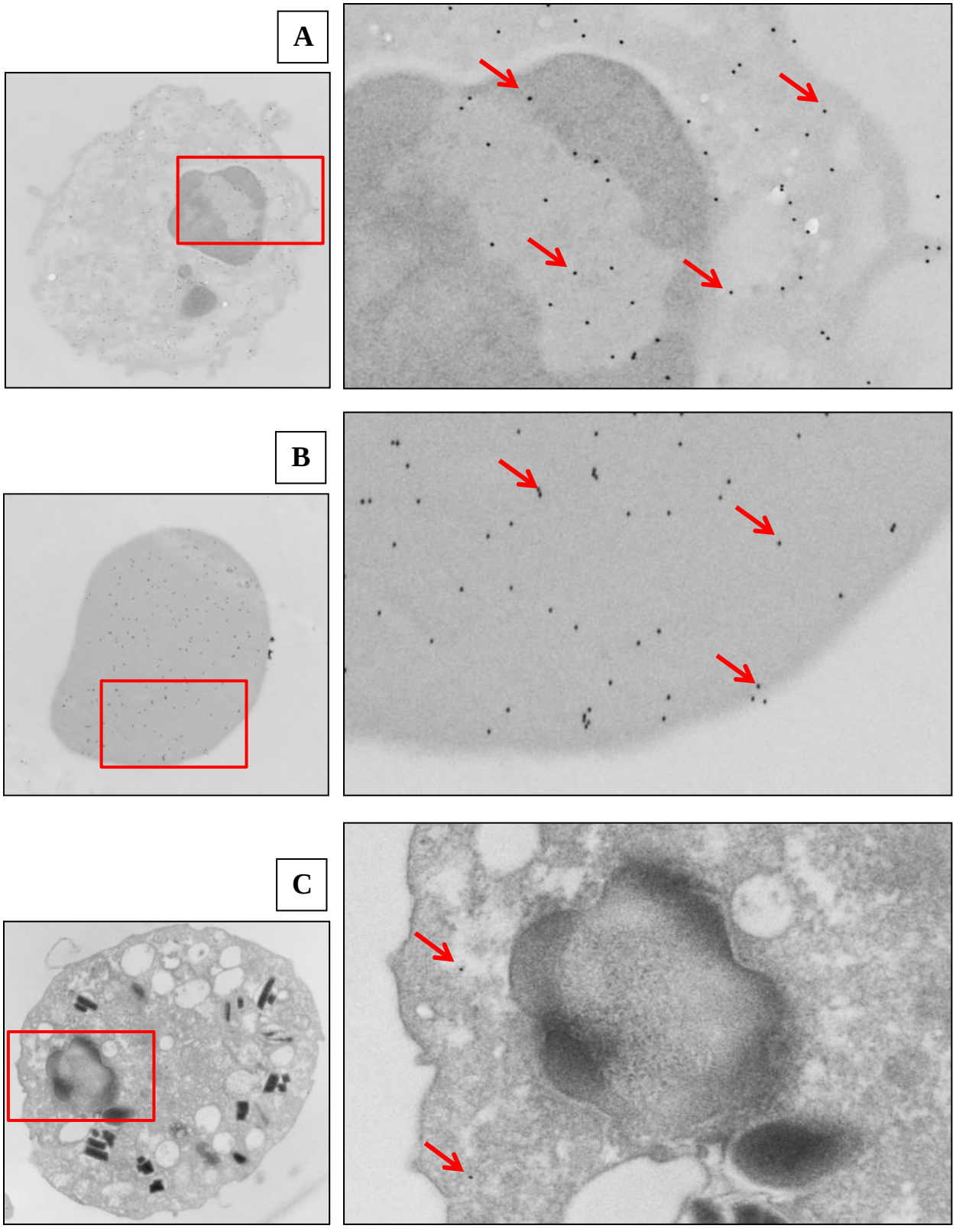
A
B
C

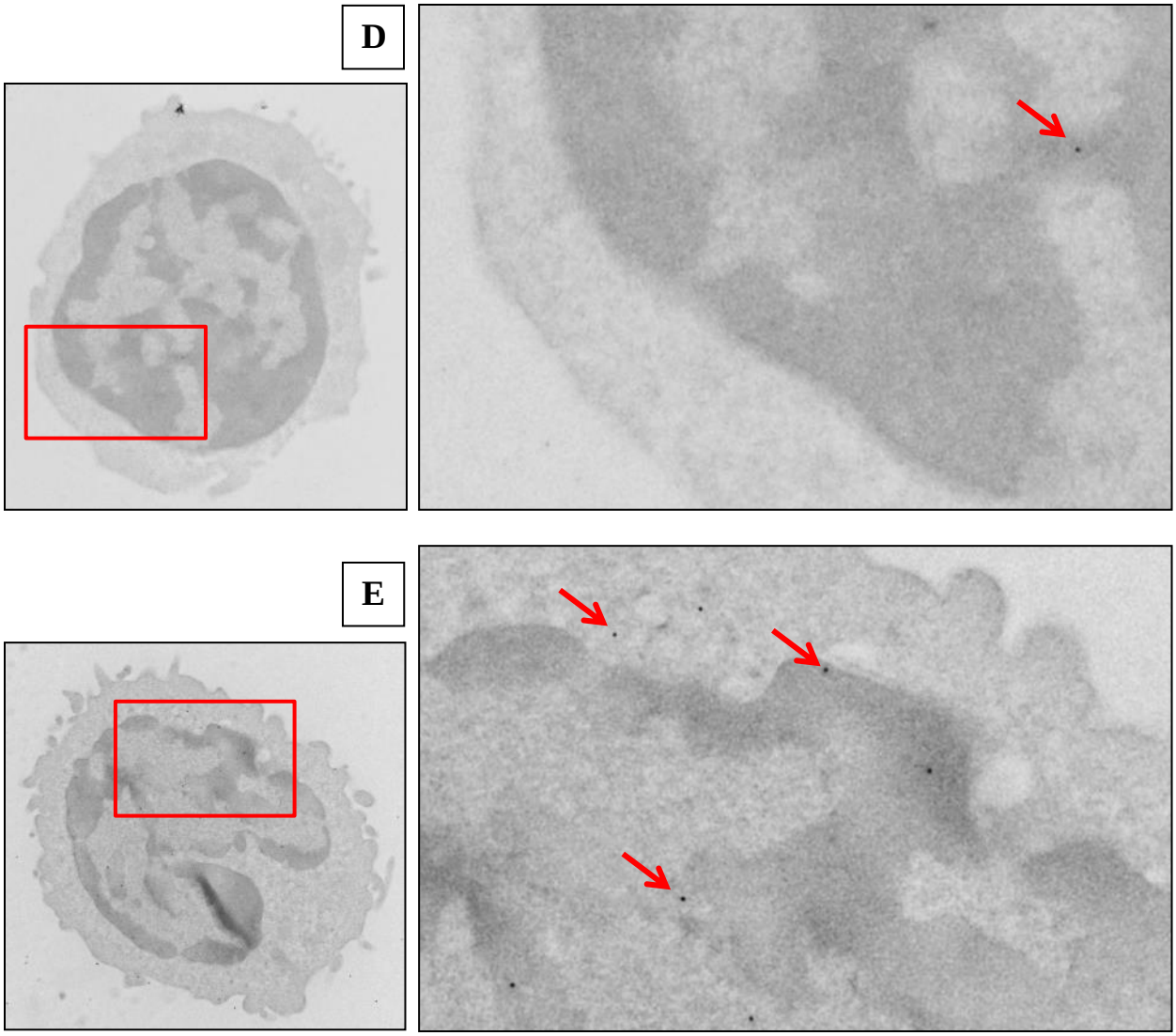

Figure 2.6: Immuno-gold electron microscopy for NUCB2/nesfatin-3 in LPS-treated human immune cells.

Immune cells present as impurities in human neutrophil samples were imaged. Along with **(A)** neutrophils, (**B)** red blood cells, **(C)** eosinophils, **(D)** lymphocytes, and **(E)** monocytes, identified from LPS-stimulated samples, were stained for NUCB2/nesfatin-3 (arrows). Original magnification: X15,000.

2.5 Discussion

NUCB2/nesfatin-1 is expressed in adult mouse lungs, albeit at lower levels compared to the fetal stage (Chung *et al.*, 2013; Kim *et al.*, 2014). In addition, mRNA expression in female mouse lungs has been shown to be significantly lower than male (Kim *et al.*, 2014). Knowing that the protein is also expressed in reproductive organs, and fluctuates in serum of rat mothers during pregnancy, there is also a chance its expression would be affected by the estrous cycle (Kim *et al.*, 2014; Garces *et al.*, 2014). With these considerations in mind, all samples collected, with the exception of human lungs, are from males. Mice used are classified as mature adults, age varying from 3-5months, with a fully developed immune system not yet affected by senescence (The Jackson Laboratory, 2015). The custom rabbit NUCB2/nesfatin-1 antibody (1mg/mL; Pacific Immunology, CA, USA) used on mouse and human lungs detects both NUCB2 and, its post-translational product, nesfatin-1; our results do not distinguish between the two and refer to the proteins collectively as NUCB2/nesfatin-1. Similarly, the polyclonal rabbit NUCB2/nesfatin-3 antibody (NBP1-87383, Novus Biologicals, ON, Canada) used on human neutrophils detects NUCB2 and nesfatin-3. Nesfatin-1 (~10kDa) and nesfatin-3 (~28kDa) were not detected during Western blot analysis of mouse lung homogenates and human neutrophil lysates respectively, therefore signals from immunocytochemistry are expected to predominantly arise from full length NUCB2 (~50kDa) (Appendix II, Figure II.III and II.IVA). Nonetheless, NUCB2/nesfatin-1, NUCB2/nesfatin-3, or NUCB2/nesfatin-1/nesfatin-3 will be used during the discussion of our findings. A detailed discussion on antibodies used can be found in Appendix II.

While studies have shown NUCB2/nesfatin-1 expression to increase following inflammatory stimulus (Ramanjaneya *et al.*, 2010; Leivo-Korpela *et al.*, 2014; Scotece *et al.*, 2014), no significant quantitative or qualitative differences were observed in immunohistological staining of normal and inflamed mouse or human lungs. In both normal and inflamed mouse lungs, heavy NUCB2/nesfatin-1 staining was notably present in immune cells, while red blood cells, alveolar septum, vascular endothelium and bronchiole epithelium were stained to a lesser degree. In both normal and inflamed human lungs, immune cells displayed varying degrees of staining, from heavy to absent. Since we cannot definitively differentiate between immune cell types with these images, it is possible these immune cells belong to different populations. Another possibility for this variability may be the age of sample blocks which have been stored

for at least 5 years, resulting in reduced signal for proteins (Nuovo *et al.*, 2013). Similar to mouse lungs, human lungs also displayed staining in red blood cells, alveolar septum, vascular endothelium and bronchiole epithelium. In addition, we observed that staining was completely absent in adipose tissues and hyaline cartilage. Where the tunica adventitia of arteries (composed mostly of connective tissue and fibroblasts) carried substantial staining, smooth muscle fibers of the tunica media did not stain.

Similar to our immunohistological results, immunoelectron microscopy also revealed little qualitative difference in staining between normal and inflamed mouse lungs. NUCB2/nesfatin-1 was present in the nucleus and cytoplasm of epithelial and endothelial cells as well as immune cells such as eosinophils, neutrophils and monocytes. The protein was not confined to secretory granules; however, a notable amount was observed within eosinophil granules. Immunoelectron microscopy images of various human blood cell types build upon observations from human lung immunohistochemistry: NUCB2/nesfatin-1/nesfatin-3 is present in different quantities amongst immune cells. Neutrophils and red bleed cells carried the most staining, monocytes showed substantially less, and staining was scarce in eosinophils and lymphocytes. We observed that staining was present in the nucleus and cytoplasm of neutrophils, lymphocytes and monocytes whereas staining was only observed in the cytoplasm but not the nucleus of eosinophils. In contrast to mouse eosinophils, NUCB2/nesfatin-1/nesfatin-3 did not appear to accumulate in human eosinophilic granules.

Quantitative analysis of gold particle distribution within human neutrophils stimulated for 0, 60, 90 and 120mins with 1ng/mL LPS revealed that NUCB2/nesfatin-3 accumulated within 0.5μm of the plasma membrane after 90mins of LPS treatment. The protein was notably depleted from the central portions of cytosol while concentrations remained unchanged close to the plasma membrane. This change may indicate an interaction of NUCB2/nesfatin-3 with proteins located at the cytoplasmic periphery, or proteins that migrate towards the plasma membrane upon neutrophil activation. Future studies may use co-immunoprecipitation after LPS stimulation to explore such potential interactions. Further, we found that NUCB2/nesfatin-3 was consistently 5 times as concentrated in the euchromatin relative to the heterochromatin portion of the nucleus. Considering the lack of an identifiable nuclear translocation signal (Barnikol-Watanabe *et al.*, 1994), the protein may have been trafficked into the nucleus through associating with another

protein. Its locational preference for the euchromatin, which contains highly decondensed chromatin often under active transcription, may also indicate a role in transcriptional regulation. Comparing NUCB2/nesfatin-3 concentrations between the cytoplasm and nucleus revealed a consistent 2 times higher mean concentration in the cytoplasm, indicating that the majority of the protein was cytoplasmic despite its ability to enter the nucleus. To further investigate the potential role of NUCB2/nesfatin-1 in transcription, a pilot experiment was conducted in attempt to identify DNA sequences that NUCB2/nesfatin-1 interacted with through chromatin immunoprecipitation sequencing; although ultimately unsuccessful, details of progress made can be found in Appendix III.

It is worth noting that during the course of immunohistochemistry studies, we attempted to create additional controls such as knockout and antigen preabsorption controls without success (Appendix II). Although Western blot results using lung and neutrophil homogenates indicated that all antibodies used have sufficient immunoreactivity towards NUCB2, it is likely that cross-reactivity is present (Appendix II). Considering the limited options currently commercially available, that our custom antibody has an advantage over others in detecting NUCB2/nesfatin-1 without cross-reaction with its homolog, NUCB1, and that our NUCB2/nesfatin-3 antibody is the only one tested to achieve an amount of immunogold staining in IEM suitable for quantitative comparisons, our current results demonstrate the extent of localization information that could be obtained through immunological methods. Pilot experiments using immunofluorescence microscopy were conducted on mouse neutrophils for further NUCB2/nesfatin-1 localization results. Although findings were concurrent with our aforementioned results, negative controls showed non-specific staining and hence failed to validate the protocol used (Appendix III).

TRANSITION

In this study, we expand from the knowledge of NUCB2/nesfatin-1/nesfatin-3 localization to what role the protein might play in normal and inflamed lungs and neutrophils. Although studies have shown NUCB2/nesfatin-1 to be expressed in lungs and involved in inflammatory responses, this following study is the first to describe its role in acute lung injury.

Through the use of WT and NUCB2 KO mice, we examine our hypotheses that absence of NUCB2/nesfatin-1 increases lung inflammation, and NUCB2/nesfatin-1 mRNA and protein expression increase with LPS stimulation. Our findings reveal increased adherent neutrophil accumulation and inflammatory cytokine expression with the loss of NUCB2/nesfatin-1. In mouse neutrophils, the loss of NUCB2/nesfatin-1 resulted in decreased inflammatory cytokine expression. Lastly, NUCB2/nesfatin-1 mRNA and protein expression in lungs and neutrophils did not appear to change with inflammatory status. The following chapter details my research on the role of NUCB2/nesfatin-1 in response to inflammatory stimulus in mouse lungs and neutrophils.

Contributions of co-authors: Dr. Aulakh provided technical support, helped with conducting experiments, data analysis and interpretation, and provided feedback on thesis writing. Dr. Unniappan provided mice used in experiments, feedback on thesis writing, and shared his expertise on NUCB2/nesfatin-1. I designed and conducted experiments, analyzed results and compiled the thesis. Dr. Singh provided research directions, infrastructure, funding and feedback on thesis writing.

CHAPTER 3. ROLE OF NUCLEOBINDIN2/NESFATIN-1 IN INFLAMMATORY RESPONSE OF MOUSE LUNGS AND NEUTROPHILS

3.1 Abstract

Cell culture studies of chondrocytes and adipocytes have shown increased NUCB2/nesfatin-1 expression following inflammatory stimulus. Moreover nesfatin-1 treatment was found to increase expression of pro-inflammatory cytokines chondrocytes. In contrast, animal studies with rat models of subarachnoid hemorrhage-induced oxidative brain damage and traumatic brain injury suggest that nesfatin-1 plays in anti-inflammatory and anti-apoptotic role. Since no studies thus far have looked into the role of NUCB2/nesfatin-1 in lung inflammation, our project would be the first to use WT and NUCB2 KO mice to examine its role in LPS-induced acute lung injury. In addition, we also explore the response of WT and NUCB2 KO bone marrow isolated mouse neutrophils to LPS treatment. Our findings suggest that the absence of NUCB2/nesfatin-1 significantly increases accumulation of adherent neutrophils by approximately 3 times compared to WT within LPS-treated lungs. Integrating this with observations from both BALF and neutrophil cytokine expression, we propose that although neutrophils lacking NUCB2/nesfatin-1 individually secrete less pro-inflammatory cytokines compared to stimulated WT cells, the result of knocking out NUCB2/nesfatin-1 is net pro-inflammatory. No change was found in NUCB2/nesfatin-1 mRNA or protein expression comparing WT LPS and PBS-treated samples. Taken together, our results show that NUCB2/nesfatin-1 is constitutively expressed in mouse lungs and neutrophils, and demonstrates anti-inflammatory properties in mouse lungs during acute lung injury by inhibiting adherent neutrophil accumulation and inflammatory cytokine expression.

3.2 Introduction

Acute lung injury/ acute respiratory distress syndrome (ALI/ARDS) are conditions of acute respiratory failure associated with high morbidity and mortality rates (World Health Organization, 2017). Etiology of ALI/ARDS include sepsis, lung infections, trauma, blood transfusions and more (Flierl *et al*., 2006). Sepsis, in particular, is a predisposing clinical factor with one of the highest incidence of developing ARDS (Rubenfeld *et al.*, 2005). Cellular characteristics of ALI/ARDS generally include loss of alveolar-capillary barrier integrity, increased neutrophil accumulation, and pro-inflammatory mediators (Matthay and Zimmerman, 2005). In one study, researchers identified elevated BAL and plasma levels of IL-6, IL-8 and TNF-α as strong predictors of mortality (Park *et al.*, 2001; Parsons *et al.*, 2005). Neutrophils play an especially important role in ALI/ARDS as they tend to damage the alveolar-capillary barrier through mechanical means as well as release of pro-inflammatory and pro-apoptotic mediators (Zemans *et al.*, 2009). Should the inflammation fail to resolve, progression of injury may lead to additional complications including a transition into chronic obstructive pulmonary disease and multiple organ failure (Matthay and Zimmerman, 2005). Due to various conditions that may accompany ALI/ARDS, treatment tends to be challenging.

Following the previous chapter where results showed that NUCB2/nesfatin-1 localizes in pneumocytes and various immune cells throughout mouse and human lungs without exhibiting spatial changes between PBS or LPS treatment, we aim to determine the importance of its presence during lung inflammation. Previous *in vitro* experiments involving animal models have demonstrated an anti-inflammatory and anti-apoptotic effect of nesfatin-1 in subarachnoid hemorrhage-induced brain damage and the traumatic rat brain (Ozsavci *et al*., 2011; Tang *et al.*, 2012). In these studies, administration of nesfatin-1 not only decreased levels of pro-inflammatory cytokines such as TNF-α, IL-1β and IL-6, oxidative enzymatic activity associated with neutrophil activation and apoptosis also decreased (Ozsavci *et al*., 2011; Tang *et al.*, 2012). Lastly, results demonstrated a protective effect of nesfatin-1 treatment on tissues such as basilar arteries and neurons that would otherwise have suffered oxidative damage (Ozsavci *et al*., 2011; Tang *et al.*, 2012). A previous study of NUCB2/nesfatin-1 in chronic obstructive pulmonary disease (COPD) has also shown a positive correlation between NUCB2/nesfatin-1 levels and

systemic inflammation (Leivo-Korpela *et al.*, 2014). However, no study thus far has been done to examine the role of NUCB2/nesfatin-1 in acute lung inflammation.

Previously, we have mentioned that studies done in cell culture demonstrated an increase in NUCB2/nesfatin-1 mRNA and protein expression upon stimulation with pro-inflammatory cytokines such as IL-1, IL-6 and TNF-α (Ramanjaneya *et al.*, 2010; Scotece *et al.*, 2014). Furthermore, findings from one study seemed contradictory to animal model studies, showing increased pro-inflammatory cytokine expression following nesfatin-1 treatment in a murine chondrogenic cell line and human primary chondrocytes exposed to inflammatory conditions (Scotece *et al.*, 2014). These pro-inflammatory cytokines included IL-6, IL-8 and MIP-1α (Scotece *et al.*, 2014). While neutrophils play central roles in inflammation including acute inflammation in the lungs, there are currently no data showing the effect of NUCB2/nesfatin-1 on neutrophil cytokine expression.

To examine the role of NUCB2/nesfatin-1 in acute lung inflammation, we used a well-established mouse model of LPS-induced ALI. WT and NUCB2 KO (NKO) mice were treated with LPS and their lungs were assessed for inflammatory response. Considering the central role of neutrophils in ALI, we also evaluated cytokine expression in bone marrow derived neutrophils from WT and NKO mice. Lastly, our studies evaluate whether inflammatory stimulus causes any NUCB2/nesfatin-1 mRNA or protein expression changes.

3.3 Materials and Methods

3.3.1 Animal sample collection

Animals used were described in the previous chapter. Briefly, they are a total of 24 WT and NKO mice treated with 50 μL PBS or *E. coli* O55:B5 LPS (L2880, Sigma-Aldrich, MO, USA) for 9 hours. All treatment groups have n=6 with the exception of NKO LPS where n=4. Samples in the experiments of this chapter include the paraffinized sections of left mouse lungs, BALF, and right mouse lungs collected as previously described, as well as peripheral blood. Peripheral blood was collected during the exsanguination of animals through cardiac puncture with a needle coated in heparin. Samples were kept at room temperature and sent to Prairie Diagnostic Services on the same day for complete blood cell count and differential blood count. From our lab's previous experience of inducing ALI through LPS inhalation, 9 hours treatment time was chosen as the experimental end point where inflammatory response peaks. While experimental mice were bred on a C57BL/6 background, a previous study has found this strain to be hyporesponsive towards inhaled LPS which resulted in low immune cell counts in BALF (Lorenz *et al.*, 2001). This is worth noting during result interpretation, but variation may also be present due to other factors such as mouse sub-strain, type of LPS used, and time of stimulation.

WT and NKO mouse neutrophils were extracted from the bone marrow of subjects treated with PBS for 9 hours. To make up one biological replicate, bones from 2 WT or KO mice were pooled; 3 biological replicates were used in downstream experiments. During sample collection, mice pelvis, femur, and tibia were collected and stored in extraction buffer (PBS with 2% FBS and 1 mM EDTA) on ice for same-day processing. Bones were crushed with a mortar and pestle in 3 washes of 1mL extraction buffer to release bone marrow cells. Neutrophils were then extracted using the EasySep™ Mouse Neutrophil Enrichment Kit (19762, STEMCELL Technologies, BC, Canada) following the exact protocols for purifying from the starting material of $2x10^8$cells. Two cytospins of ~$5x10^5$ isolated cells are used to assess purity of processed samples; 100-150cells were counted for each and determined to have ≥90% neutrophil content before proceeding. Isolated cells were resuspended in IMDM media (ATCC) with 10% FBS (Life Technologies, CA, USA) at a concentration of $5x10^6$cells/mL.

3.3.2 Mouse neutrophil stimulation

Mouse neutrophils suspended at $5x10^6$ cells in 1mL were plated into 12-well plates. Cells were then stimulated with 1 ng/mL *E. coli* O55:B5 LPS (L2880, Sigma-Aldrich, MO, USA) for 0, 60, 90 and 120 mins respectively, and incubated at 37°C with 5% CO_2. After stimulation, cells were resuspended through gentle pipetting, collected and separated from the culture media through centrifugation (100 RCF). Protease inhibitor cocktail was added to culture media samples, which were then stored at -80°C. Cells were lysed in 100 µL T-PER Tissue Protein Extraction Reagent (78510; Thermo Fisher Scientific, MA, USA) with protease inhibitor cocktail and stored in -80°C.

3.3.3 Haematoxylin and eosin staining

To evaluate histological evidence of tissue injury, paraffinized sections of left mouse lungs as described in the previous chapter were stained with haematoxylin and eosin. Samples were first deparaffinized with xylene followed by decreasing concentrations of ethanol and dH_2O. Samples were then placed in haematoxylin for 5 mins. The stain is washed off with tap water, dipped into 0.3% HCl in 70% ethanol 2 times, dipped into warm tap water 3 times and left in dH_2O until all samples were processed. Samples were then placed into eosin for 6 mins. Excess solution was rinsed off with dH_2O, and samples were quickly dehydrated with increasing concentrations of ethanol and xylene. Finally, samples were mounted and visualized under a light microscope.

Two researchers independently evaluated the slides, non-blinded, and qualitatively scored inflammation in perivascular, peribronchial and septal spaces. Scores are expressed as (+) no inflammation, (+ +) mild inflammation, (+ + +) moderate inflammation, and (+ + + +) heavy inflammation.

3.3.4 Immunohistochemistry

Next, we specifically examined neutrophil accumulation in LPS and PBS-treated mouse lungs by staining a neutrophil marker, Gr-1. Similar to previously described procedures, paraffinized sections were deparaffinized with xylene, and rehydrated with decreasing concentrations of ethanol, and dH_2O. Samples were then placed in 0.5% H_2O_2 for 20 mins. After washing in PBS, pepsin (2 mg/mL in 0.01N HCl) was added to samples and incubated for 45

mins. Samples were then washed in PBS, blocked with 5% BSA for 30 mins, and incubated overnight in rat anti-mouse Gr-1 antibody (1:100; 550291; BD Biosciences, ON, Canada). The next day, samples were washed, and incubated in HRP-conjugated anti-rat secondary antibody (1:200; P0450; Dako, CA, USA) for 30 mins. Samples were washed in PBS, and color was developed using VECTOR VIP Peroxidase Substrate Kit (VECTOR Laboratories, ON, Canada) for 5 mins. Slides were washed in dH_2O and counter-stained in methyl green for 1 min, washed in dH_2O and dehydrated using increasing concentrations of ethanol followed by xylene. Lastly, samples were mounted and visualized under a light microscope. Isotype and negative controls were included with this set of samples.

In order to separately evaluate neutrophil accumulation in alveolar spaces and interstitial spaces, 5 pictures of each region were taken at high power magnification to establish neutrophil counts. Since Intratracheal administration of LPS is known to result in patchy injury where areas of the lung may be spared, randomly selected areas were only chosen if they were also representative of injury (Matute-Bello *et al*., 2010).

3.3.5 BALF processing

To examine the alteration of alveolar capillary barrier as a result of inflammation, changes in protein concentration in BALF is measured. In addition, inflammatory response can also be measured through an absolute count of immune cells, an absolute count of neutrophils, and the differences of cytokine concentrations in BALF.

After collecting BALF through the trachea with 3 aspirations of 0.5 mL PBS, samples were immediately stored on ice. Cell counts were performed on the same day where cells from the BALF were spun down at 100RCF for 5 mins, resuspended in 1 mL, and counted using a haemocytometer. Following absolute counts of immune cells, samples were once again spun down and resuspended in 200 µL PBS to produce 2 cytospin slides (100 RCF, 3 mins). The slides were then stained using the Hemacolor® Stain Set (65044-93; Millipore Sigma, ON, Canada) and visualized under a light microscope where pictures were taken for differential cell counting; around 100 cells were counted per sample and absolute neutrophil counts were estimated using absolute immune cell counts. BALF supernatant were stored in -80°C for ELISA that would be performed later.

3.3.6 Protein assay

In order to determine the differences in protein concentration of BALF samples, a DC™ protein assay (5000112; Bio-Rad, CA, USA) was performed exactly as instructed by Bio-Rad protocols. Samples were incubated for 15 mins and analyzed with a plate reader. Sample values were averaged between replicates, and a standard curve of BSA was included to quantify sample signals. Total protein concentration was calculated by multiplying protein concentration by BALF volume and dividing by total volume of PBS used (1.5 mL).

3.3.7 ELISA

To determine the difference in cytokine concentration of BALF from WT and NKO LPS and PBS-treated lungs, 50 μL of undiluted sample from each mouse was analyzed with a Bio-Plex Pro™ Mouse Cytokine 23-plex assay (#M60009RDPD; Bio-Rad, CA, USA) following the supplier's protocol. Samples were loaded in duplicates, and signal detection was done using the Luminex Bio-Plex 200 system. The exact same procedure was then repeated on cell culture media samples of mouse neutrophils to elucidate cytokine concentration differences between WT and NKO samples treated 0, 60, 90 and 120 mins with 1 ng/mL LPS. ELISA results from BALF were normalized through multiplying the cytokine concentration by the volume of BALF, then dividing the total cytokine concentration by total PBS used for BALF extraction (1.5 mL).

3.3.8 Myeloperoxidase Assay

As an indirect method of quantifying neutrophils remaining in the lungs after BALF extraction, a myeloperoxidase (MPO) assay is performed. A section of the right mouse lung (stored at -80°C) was first homogenized in 500 μL 50 mM HEPES (pH 8.0) using the Retsch MM400 oscillating mill (frequency: 30/s; 30 secs). Samples were then centrifuged at 10,000 g for 20 mins. Supernatant was discarded, the pellet was resuspended in 500 μL 0.5% CTAC and homogenized again. After centrifuging the sample once more, supernatant was aliquot into new tubes. A standard curve was made up using myeloperoxidase from human leukocytes (M6908-5UN; Sigma-Aldrich). In each well, 10 μL of homogenized sample was combined with 65 μL phosphate citrate; samples were analyzed in duplicates. Afterwards, 100 μL of TMB substrate was added and color was allowed to develop for 5 mins. 150 μL stop solution was added upon completion, and signals were measured at O.D. 450 nm with a plate reader.

In order to standardize readings to the amount of protein present, an accompanying protein assay was also performed as described in section 3.3.6.

3.3.9 Reverse transcription quantitative PCR (RT-qPCR)

To assess NUCB2/nesfatin-1 mRNA expression in mouse lungs, a section of the right mouse lung (previously stored in -80°C) was homogenized in 1 mL TRIzol™ (15596026; Thermo Fisher Scientific, MA, USA) using the VC300 VibraCell sonicator (30 secs ON, 1 min OFF; 2 cycles). RNA was then extracted using the exact protocol provided by Invitrogen. RNA pellets were dissolved in 30 µL RNase-free water and quantified with a Nanodrop. Reverse transcription was then performed with the QuantiTect Reverse Transcription Kit (205311; QIAGEN) following the exact protocol provided for 1 µg starting material. Quantitative real-time PCR was performed using Bio-Rad CFX96 Touch™ instrument and SsoAdvanced Universal SYBR Green Supermix (1725272; Bio-Rad, CA, USA). NUCB2 (FP: 3' CCAGTGGAAAATGCAAGGAT 5' and RP: 3' GCTCATCCAGTCTCGTCCTC 5') and GAPDH (FP: 3' CTCAACGACCACTTTGTCAAGCTCA 5' and RP: 3' GGTCTTACTCCTTGGAGGCCATGTG 5') primers were obtained from Invitrogen (CA, USA). Melting curves, no template and no reverse transcription controls were analyzed after each run to ensure specificity. GAPDH was used as a reference gene for sample normalization.

3.3.10 Western blot

NUCB2/nesfatin-1 protein expression in WT mouse lungs, and neutrophils stimulated with LPS for 0, 60, 90 and 120 mins, were examined through Western blots. Mouse lungs were homogenized in T-PER Tissue Protein Extraction Reagent (Thermo Fisher Scientific, MA, USA) with protease inhibitor cocktail at frequency of 30/s for 30 secs using the Retsch MM400 oscillating mill, and mouse neutrophils ($5x10^6$ cells per sample) were lysed in 100 µL RIPA buffer with protease inhibitor cocktail.

Samples were heated in Laemmli buffer at 95°C for 5 mins, run on 12% SDS-PAGE gels and transferred onto nitrocellulose membranes. Membranes were blocked for 1 hour using 5% skim milk in TBS-T. All antibodies were diluted in 5% skim milk in TBS-T. A custom rabbit anti-NUCB2 antibody (1:1000; 1mg/mL; Pacific Immunology, CA, USA) raised against a synthetic peptide, VDKTKVHNTEPVENARIEP-Cys (20 AA), was used as the primary

antibody and incubated overnight. Following, anti-rabbit Alexa Fluor® 488 (1:5000; A-11008; Thermo Fisher Scientific, MA, USA) was used as the secondary antibody and incubated for 30 mins at RT. Signal detection was done on the GE Healthcare Typhoon 9400 imager. The blot was then stripped and reprobed using rabbit anti-β-actin antibody (1:2000; ab8227; Abcam, ON, Canada), incubated overnight, incubated in anti-rabbit Alexa Fluor® 488 (1:5000; A-11008; Thermo Fisher Scientific, MA, USA) for 30mins at RT and imaged. All densitometry was performed using Image J.

3.3.11 Data Analysis

2-sample t-tests and repeated measures one-way ANOVA were used for sample comparisons; p-values ≤ 0.05 were considered statistically significant. Results are presented as Mean ± SEM with 6 biological replicates per group, except in the NKO LPS group where n=4. GraphPad Prism 7 (Avenida de la Playa, CA, USA) was used for all analysis.

3.4 Results

3.4.1 NKO mouse lungs show slightly more immune cell accumulation compared to WT in LPS treated samples

To assess histological evidence of tissue injury, mouse lungs were stained with haematoxylin and eosin where 3 regions- perivascular, peribronchiolar and septal spaces- were then scored for signs of inflammation such as immune cell accumulation, presence of hyaline membrane, proteinaceous debris in alveolar spaces and alveolar septal thickening (Matute-Bello *et al*., 2010). As structural damage is not expected in ALI models, the following assessment mostly account for immune cell accumulation (Matute-Bello *et al*., 2010). Table 3.1 summarizes our findings in the 4 groups of animals. We observed that none of the WT and NKO PBS-treated samples showed any signs of inflammation. In contrast, WT LPS-treated samples showed moderate inflammation, and NKO LPS-treated samples showed moderate to heavy levels of inflammation in all regions assessed. To illustrate these differences, Figure 3.1 shows representative images for each group. Figure 3.1C and D, in particular, demonstrate the higher immune cell accumulation observed in perivascular and septal spaces of NKO LPS-treated lungs compared to WT.

No other signs of tissue injury including presence of hyaline membranes, fibrin strands or thickened alveolar walls were observed. Similar to WT mice, we confirm that LPS-treatment in NKO mice did not result in pulmonary structural damage. As can be seen in Figure 3.1, the alveolar septa of all samples remain intact. There are no signs of cells sloughing in bronchioles, or presence of hyaline membranes.

3.4.2 Loss of NUCB2/nesfatin-1 increases neutrophil accumulation in LPS-treated mouse lungs

Next, we looked more specifically into neutrophil accumulation in PBS or LPS-treated lungs through immunohistochemistry using a neutrophil marker, Gr-1. Regions representative of injury were randomly selected in each sample, and neutrophils were counted at high power magnification (40X) for 2 regions of interest: alveolar spaces (n=5) and interstitial spaces (n=5).

In alveolar spaces of LPS-treated samples, mean neutrophil counts were 3 times higher in NKO than WT lungs ($p=0.038$; Figure 3.2A). Counts were not significantly different in interstitial spaces ($p=0.072$; Figure 3.2B). Figure 3.2C shows representative images of LPS-

treated samples, illustrating the difference in neutrophil accumulation between NKO and WT lungs. Since non-adherent neutrophils were collected during the BALF extraction process, this population is representative of adherent neutrophils.

In PBS-treated samples, neutrophils were scarce throughout WT and NKO lungs and counts were not significantly different (Figure 3.2D). During this assessment, we were able to confirm the presence of marginated neutrophils in both groups, indicating that the process is not affected by the absence of NUCB2.

Negative and isotype controls performed support the validity of the IHC protocol (Figure 3.2E).

3.4.3 Vascular permeability is not significantly different between WT and NKO PBS or LPS-treated samples

To determine whether knocking out NUCB2 results in alteration of alveolar capillary barrier, a protein assay was performed on BALF extracted from PBS or LPS-treated WT and NKO mouse lungs.

Total protein concentration between WT and NKO LPS or PBS-treated samples were not significantly different (Figure 3.3). However, LPS treatment does increase vascular permeability in both genotypes compared to PBS treatment. WT LPS samples had 1.7 times the mean total protein concentration of PBS-treated samples ($p=0.044$), while NKO LPS samples had 2.4 times the mean total protein concentration of NKO PBS samples ($p<0.001$).

3.4.4 Absolute immune cell and neutrophil counts in BALF of NKO and WT mice do not significantly differ

To measure inflammatory response of NKO and WT mouse lungs, we first examined absolute immune cell counts in BALF, and then looked more specifically at absolute neutrophil counts. Since these neutrophils were flushed out during the process of BALF collection, they represent the population of non-adherent neutrophils within each sample. Around 100 cells examined during differential cell counts and absolute neutrophil counts were estimated based on absolute immune cell counts.

Although the number of total immune cells and neutrophils in BALF increased with LPS treatment compared to PBS treatment, WT and NKO samples were not significantly different following PBS or LPS-treatment ($p=0.778$ and $p=0.334$ respectively; Figure 3.4). In LPS-treated groups, we note that the mean absolute immune cell count and mean absolute neutrophil count were both 1.7 times and higher in NKO samples compared to WT ($p=0.334$ and $p=0.326$ respectively).

3.4.5 Myeloperoxidase activity is not significantly different between NKO and WT LPS-treated lungs

Next, we used an indirect method to quantify adherent neutrophils where myeloperoxidase (MPO), an anti-microbial protein abundant in activated neutrophils, is assayed using lung homogenates. A corresponding protein assay was performed to normalize readings, and MPO activity is expressed in terms of U/mg protein.

MPO activity between NKO and WT PBS or LPS-treated lungs were not statistically different (Figure 3.5). In LPS-treated samples, we observed that the mean MPO activity in NKO mouse lungs was 1.4 times higher than WT ($p=0.074$). MPO activity in LPS-treated NKO mouse lungs was also 2.6 times higher than those treated with PBS ($p<0.0001$). In comparison, LPS-treated WT lungs had 1.9 times higher MPO activity compared to those given PBS ($p=0.010$).

3.4.6 Loss of NUCB2/nesfatin-1 increases concentration of cytokines associated with inflammatory response in BALF

To determine whether knocking out NUCB2 changes the concentration of cytokines involved in inflammatory responses, an ELISA was performed on BALF samples for a panel of 23 different cytokines.

Amongst the 23 cytokines, 5 were found to be statistically different between LPS-treated WT and NKO samples (Figure 3.6A; Table 3.2). Starting from the largest effect size, IL-5 in NKO samples was 2.3 times higher in mean total concentration than WT ($p=0.014$); TNFα, 2.2 times ($p=0.028$); MIP-1β, 2.1 times ($p=0.001$); MIP-1α, 2.0 times ($p=0.029$); G-CSF, 1.6 times ($p=0.029$).

Close to the significance value of $p \leq 0.05$, IL-6 was expressed in NKO samples at 1.8 times higher mean total concentration than WT ($p=0.052$; Figure 3.6B).

IL-17 ($p=0.079$), KC ($p=0.100$), GM-CSF ($p=0.109$), IFN-γ ($p=0.134$), IL-13 ($p=0.143$), IL-12(p70) ($p=0.161$), RANTES ($p=0.307$), IL-1α ($p=0.328$), IL-12(p40) ($p=0.344$), IL-1β ($p=0.461$), MCP-1 ($p=0.482$), IL-10 ($p=0.517$) and eotaxin ($p=0.649$) were not statistically different (Figure 3.6B). Signals were not detected for the following assayed cytokines: IL-2, IL-3, IL-4 and IL-9 (data not shown).

3.4.7 Loss of NUCB2/nesfatin-1 does not affect peripheral blood cell counts in PBS or LPS treated mice

Next, we assessed whether NUCB2/nesfatin-1 had any systemic influence on peripheral blood counts following PBS or LPS treatment. Specific parameters tested include absolute immune cell, lymphocyte and neutrophil counts, neutrophil-total white blood cell (WBC) ratio and neutrophil-lymphocyte ratio (NLR).

Results of peripheral blood analysis are shown in Figure 3.7. When LPS-treated WT and NKO mice were compared, there were no significant differences in absolute immune cell ($p=0.133$), lymphocyte ($p=0.470$) and neutrophil ($p=0.073$) counts, or NLR ($p=0.331$). Similarly, PBS-treated WT and NKO mice showed no significant differences in absolute immune cell ($p=0.421$), lymphocyte ($p=0.582$) and neutrophil ($p=0.193$) counts, or NLR ($p=0.475$).

Close to the significance value, the ratio of neutrophils to total WBC show that the mean ratio in NKO samples is 0.9 times that of WT in LPS-treated samples ($p=0.057$).

3.4.8 NUCB2/nesfatin-1 mRNA and protein expression in mouse lungs do not change with LPS stimulation

To determine whether mRNA or protein expression of NUCB2/nesfatin-1 changes with inflammation of mouse lungs, we performed RT-qPCR and Western blots respectively on mRNA and protein isolated from portions of frozen lung tissue.

Using GAPDH as the reference gene in RT-qPCR, samples were normalized and the ΔΔCq calculation method was used to compare between PBS and LPS-treated WT samples. Results revealed no significant difference in mRNA expression between the two groups (Figure

3.8A). Similarly, Western blot analysis using β-actin to normalize between samples revealed no significant difference in protein expression between the two groups (Figure 3.8B, C).

3.4.9 Inflammatory cytokine concentrations following LPS stimulation were not significantly different between WT and NKO mouse neutrophils

Following the comparison of inflammatory cytokine concentrations in BAL fluid of WT and NKO mouse lungs with LPS treatment, we wanted to more specifically examine the role of neutrophils in our observations. To this end, bone marrow neutrophils were extracted from PBS-treated mice and stimulated with LPS for 0, 60, 90 and 120 mins. Each biological replicate was composed of pooled neutrophils from 2 mice (n=3). Cell culture media, containing all secreted cytokines, were then analyzed with a 23-plex ELISA. Results indicated that only 7 cytokines were present at detectable levels: IL-1α, IL-6, TNF-α, RANTES, MIP-1α, MIP-1β, and IL-12(p70).

Repeated measures two-way ANOVA revealed an interaction between LPS stimulation time and genotype on the concentration of IL-6 in culture supernatant ($p=0.036$). Subsequent Sidak's multiple comparisons test revealed that knocking out NUCB2 led to a significant decrease of IL-6 at LPS120 ($p=0.017$; Figure 3.9).

With all other cytokines, time ($p<0.005$) but not genotype ($p>0.164$) was the significant source of variation. In both WT and NKO samples, expression of these cytokines increased with LPS stimulation time, but no significant differences were identified comparing WT and NKO samples at each time point.

3.4.10 NUCB2/nesfatin-1 protein expression in mouse neutrophils does not change with LPS stimulation

Lastly, Western blots were used to determine whether NUCB2/nesfatin-1 expression in mouse neutrophils change with 0, 60, 90 and 120mins of LPS stimulation (n=3). β-actin was used as the reference gene for normalization. Densitometry was performed and data was analyzed using repeated measaures one-way ANOVA.

Results revealed no significant difference in NUCB2/nesfatin-1 expression between time points ($p=0.436$; Figure 3.10).

	Perivascular	Peribronchiolar	Septal
WT PBS	+	+	+
NKO PBS	+	+	+
WT LPS	+ + +	+ + +	+ + +
NKO LPS	+ + +/+ + + +	+ + +	+ + +/+ + + +

Table 3.1: Scoring of perivascular, peribronchiolar and septal spaces for inflammation.
(+: no inflammation, + + mild inflammation, + + + moderate inflammation, + + + + heavy inflammation)

	NKO/WT Total Protein Concentration (LPS-treated)	p-value
IL-5	2.3	0.014
TNFα	2.2	0.028
MIP-1β	2.1	0.001
MIP-1α	2.0	0.029
G-CSF	1.6	0.029
IL-6	1.8	0.052
IL-17	1.2	0.079
KC	1.6	0.100
GM-CSF	1.8	0.109
IFN-γ	1.1	0.134
IL-13	1.3	0.143
IL-12(p70)	1.4	0.161
RANTES	1.3	0.307
IL-1α	1.3	0.328
IL-12(p40)	1.3	0.344
IL-1β	1.1	0.461
MCP-1	1.3	0.482
IL-10	1.1	0.517
Eotaxin	0.8	0.649

Table 3.2: ELISA of BALF from LPS-treated mouse lungs.
To emphasize effect size, this table compares cytokine concentrations by dividing concentrations in NKO samples by that in WT (n=4-6). P-values represent the degree of statistical significance when the 2 groups are compared through a student's t-test. Statistically significant results are arranged in order of effect size; statistically insignificant results ($p \geq 0.05$; below red line) are arranged by p-values.

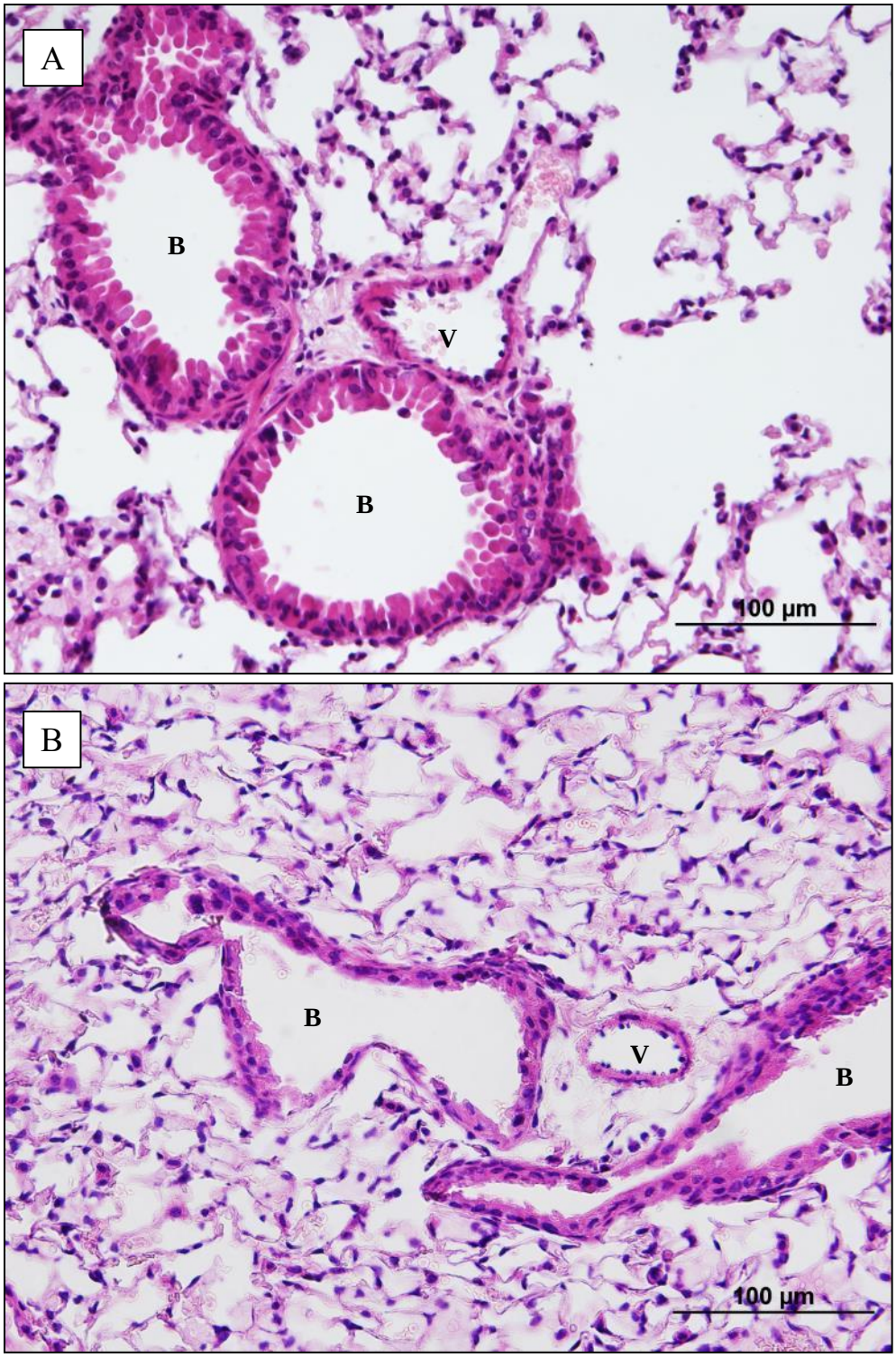
A
B
V
B
100 µm
B
B
V
B
100 µm

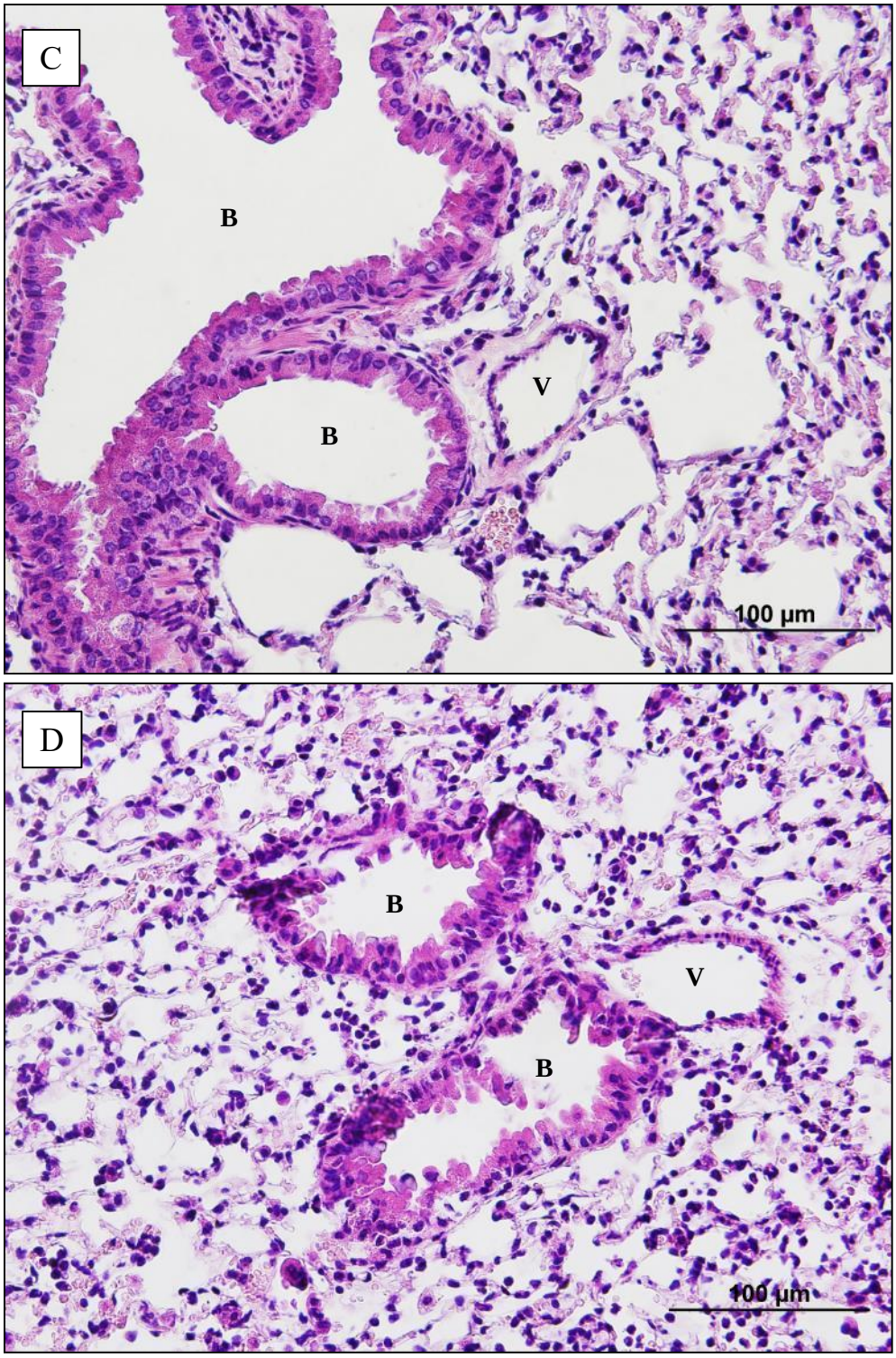

Figure 3.1: Haematoxylin and eosin staining.
Representative images of **(A)** WT PBS, **(B)** NKO PBS, **(C)** WT LPS, and **(D)** NKO LPS mouse lung sections stained with haematoxylin and eosin (n=4-6). B: Bronchiole; V: vein. Scale bar = 100 µm

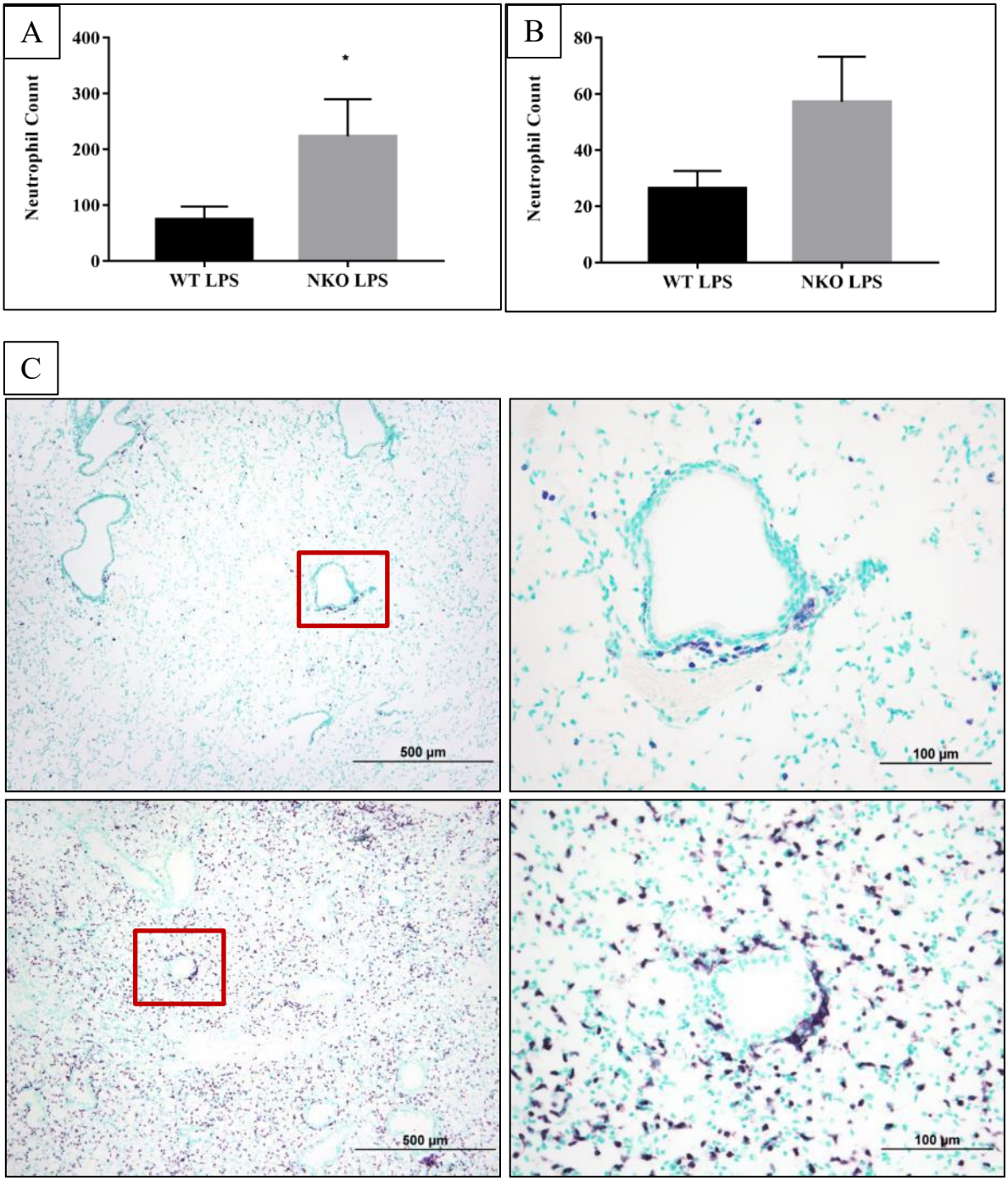
A
Neutrophil Count
400
300
200
100
0
*
WT LPS
NKO LPS
B
Neutrophil Count
80
60
40
20
0
WT LPS
NKO LPS
C
WT LPS
NKO LPS
500 µm
100 µm
500 µm
100 µm

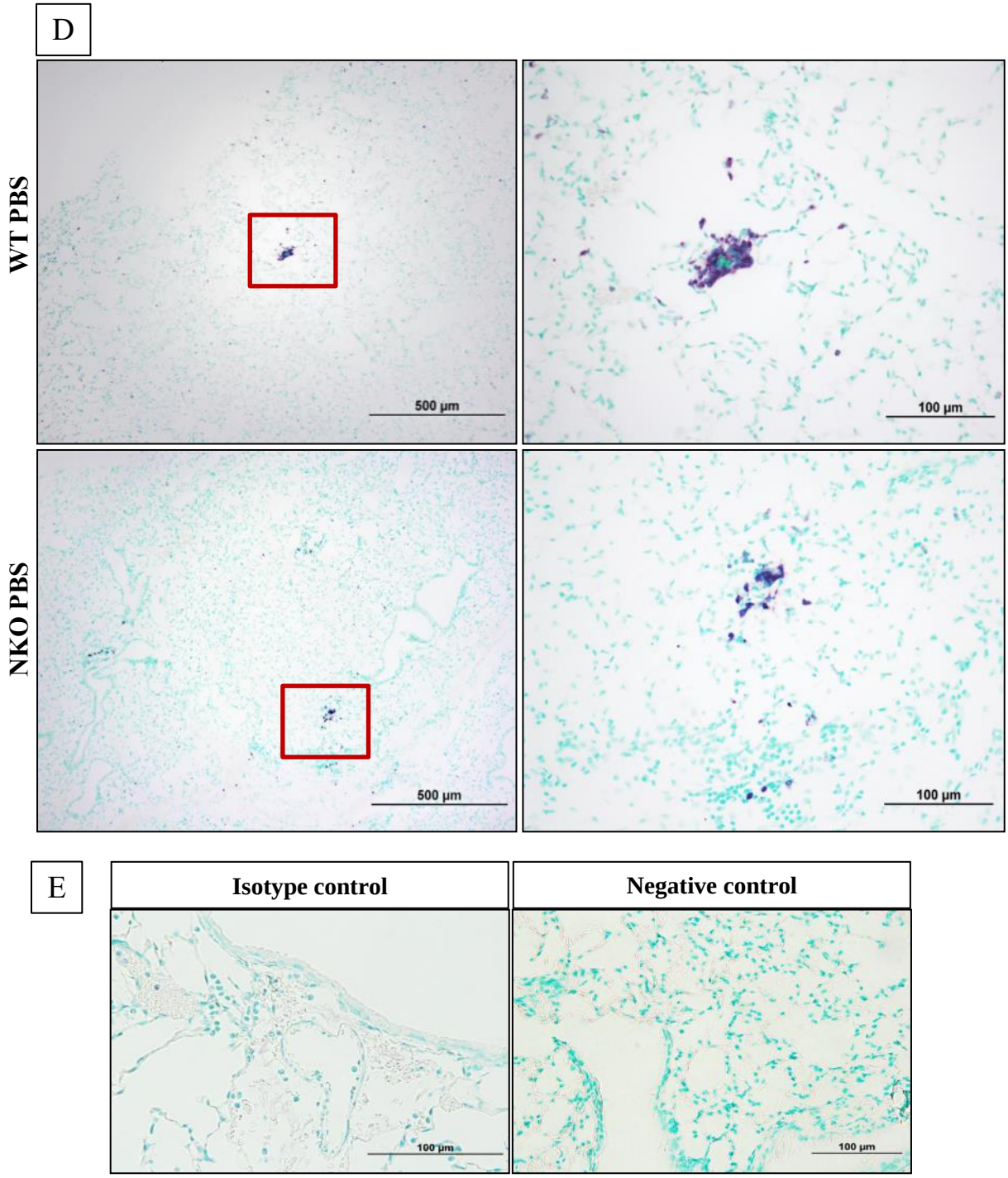

Figure 3.2: Neutrophil counts at high power magnification (40X) through immunohistochemistry of Gr-1.

Neutrophils identified through immunohistochemical staining of Gr-1 were counted at high power magnification (40X) for **(A)** alveolar spaces, and **(B)** interstitial spaces; counts were averaged between 5 fields per sample. Representative images for **(C)** LPS-treated samples show neutrophil accumulation in interstitial and alveolar spaces, and **(D)** PBS-treated samples show neutrophil margination around small capillaries and resident neutrophils in alveolar spaces. **(E)** Controls included secondary antibody only

(negative control) and staining with Rat IgG2b (isotype control). Raw data were analyzed through 2-sample t-tests (*$p \leq 0.05$; n=4-6; results presented as Mean ± SEM).

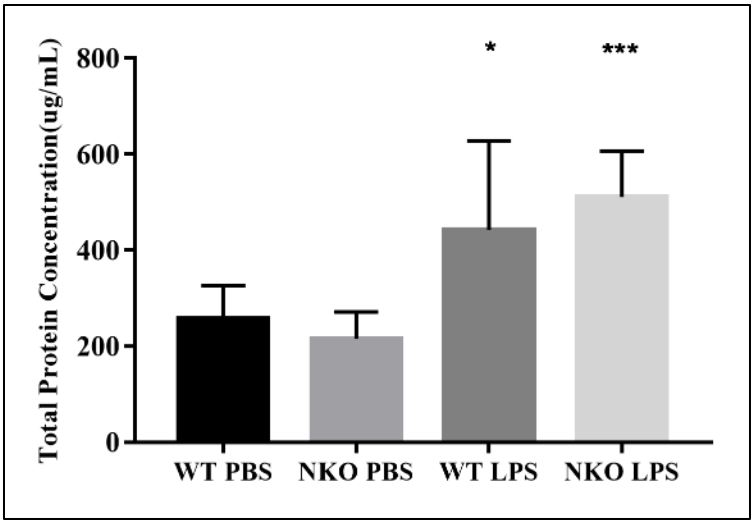

Figure 3.3: Total protein concentration in BALF.

Total protein concentration of BALF was determined through a DC protein assay. There were no significant differences between WT and NKO LPS or PBS-treated samples. (*$p \leq 0.05$ compared to WT PBS; ***$p \leq 0.001$ compared to NKO PBS; n=4-6; results presented as Mean ± SEM).

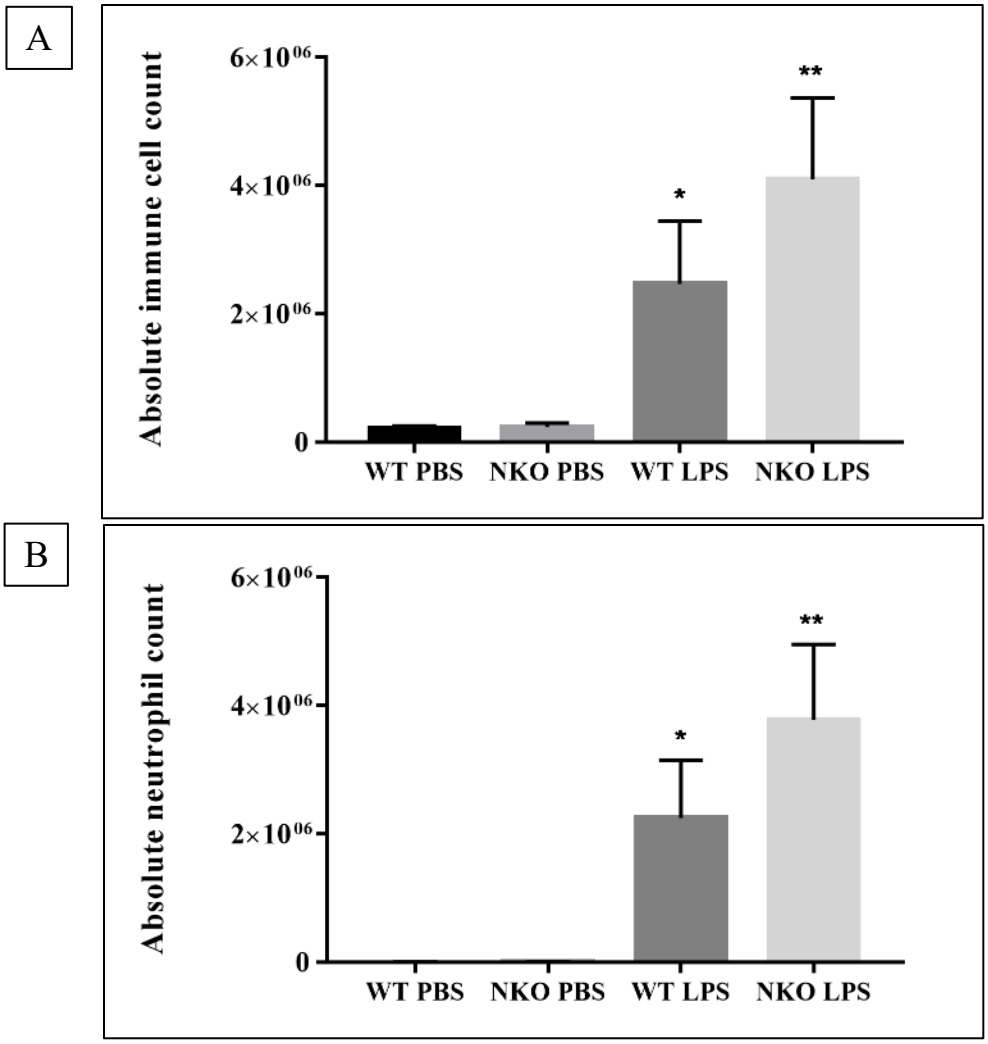

Figure 3.4: Absolute cell counts in BALF.
(A) Absolute immune cell counts were performed on BALF extracted. **(B)** Following, differential cell counts were performed on around 100 cells per sample and absolute neutrophil counts were estimated based on absolute immune cell counts. Results revealed no significant difference between WT and NKO samples; statistical significance only found when comparing PBS and LPS treatments of the same genotype (*$p \leq 0.05$, **$p \leq 0.01$ compared to PBS treatment of the same genotype; n=4-6; results presented as Mean ± SEM).

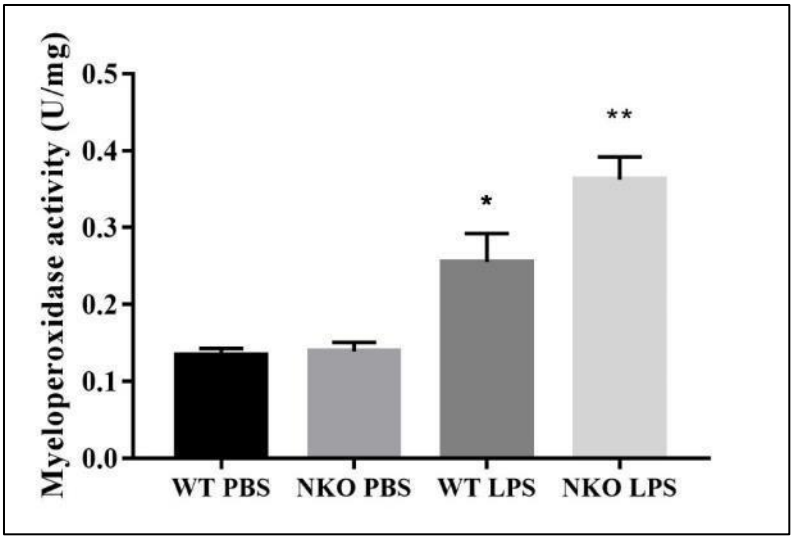

Figure 3.5: Assay of myeloperoxidase activity in mouse lung homogenates.
A uniform volume of mouse lung homogenate was assayed for each sample to determine its myeloperoxidase activity, and then normalized against sample protein concentration to produce final data. Differences between LPS-treated WT and NKO samples were close to achieving statistical significance ($p=0.074$). PBS and LPS treatments were statistically different within the same genotype. (*$p \leq 0.05$, **$p \leq 0.0001$ compared to PBS treatment of the same genotype; n=4-6; results presented as Mean ± SEM).

A

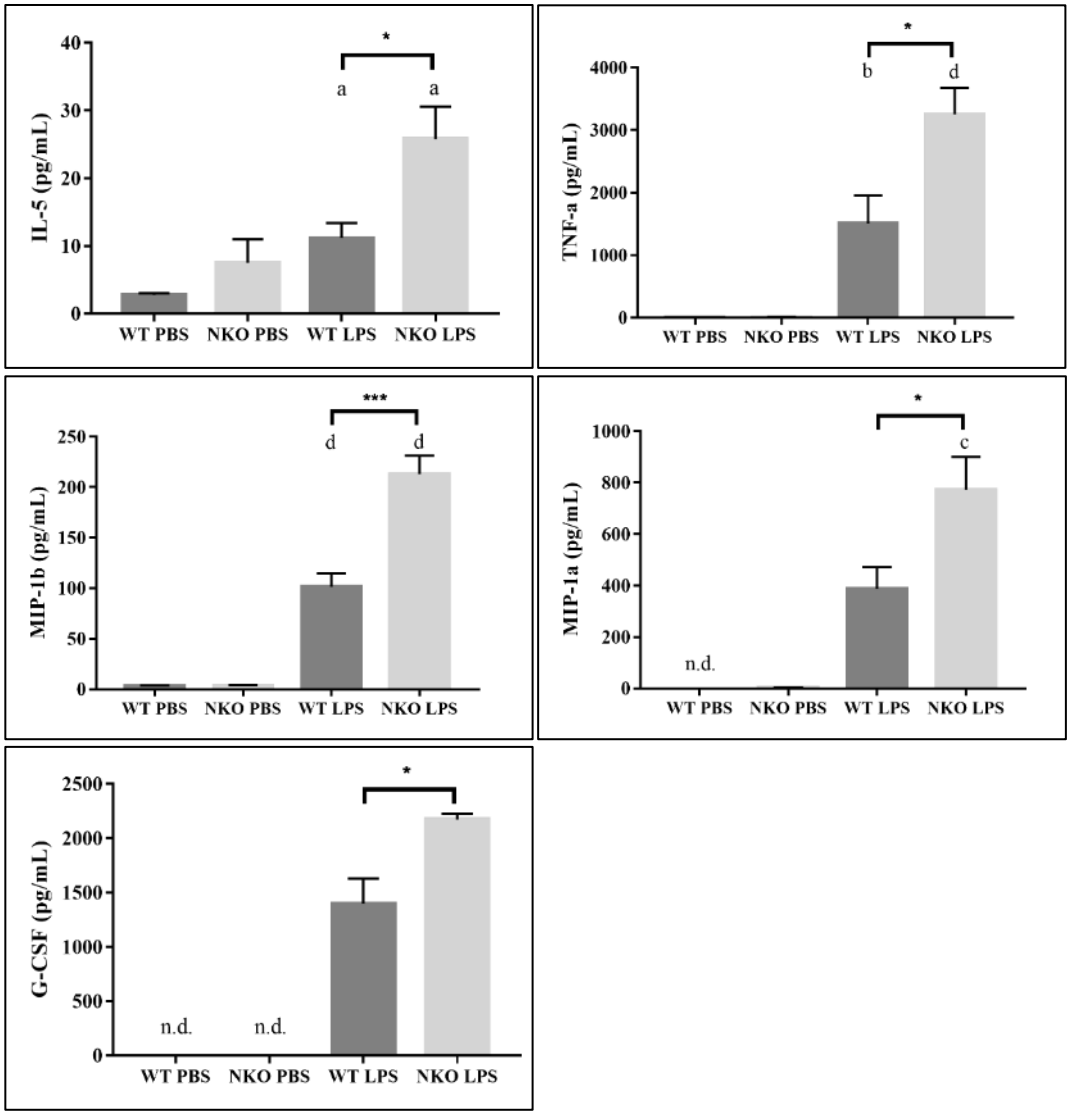
IL-5 (pg/mL)
40
30
20
10
0
*
a
a
WT PBS
NKO PBS
WT LPS
NKO LPS
TNF-a (pg/mL)
4000
3000
2000
1000
0
*
b
d
WT PBS
NKO PBS
WT LPS
NKO LPS
MIP-1b (pg/mL)
250
200
150
100
50
0
***
d
d
WT PBS
NKO PBS
WT LPS
NKO LPS
MIP-1a (pg/mL)
1000
800
600
400
200
0
*
c
n.d.
WT PBS
NKO PBS
WT LPS
NKO LPS
G-CSF (pg/mL)
2500
2000
1500
1000
500
0
*
n.d.
n.d.
WT PBS
NKO PBS
WT LPS
NKO LPS

B

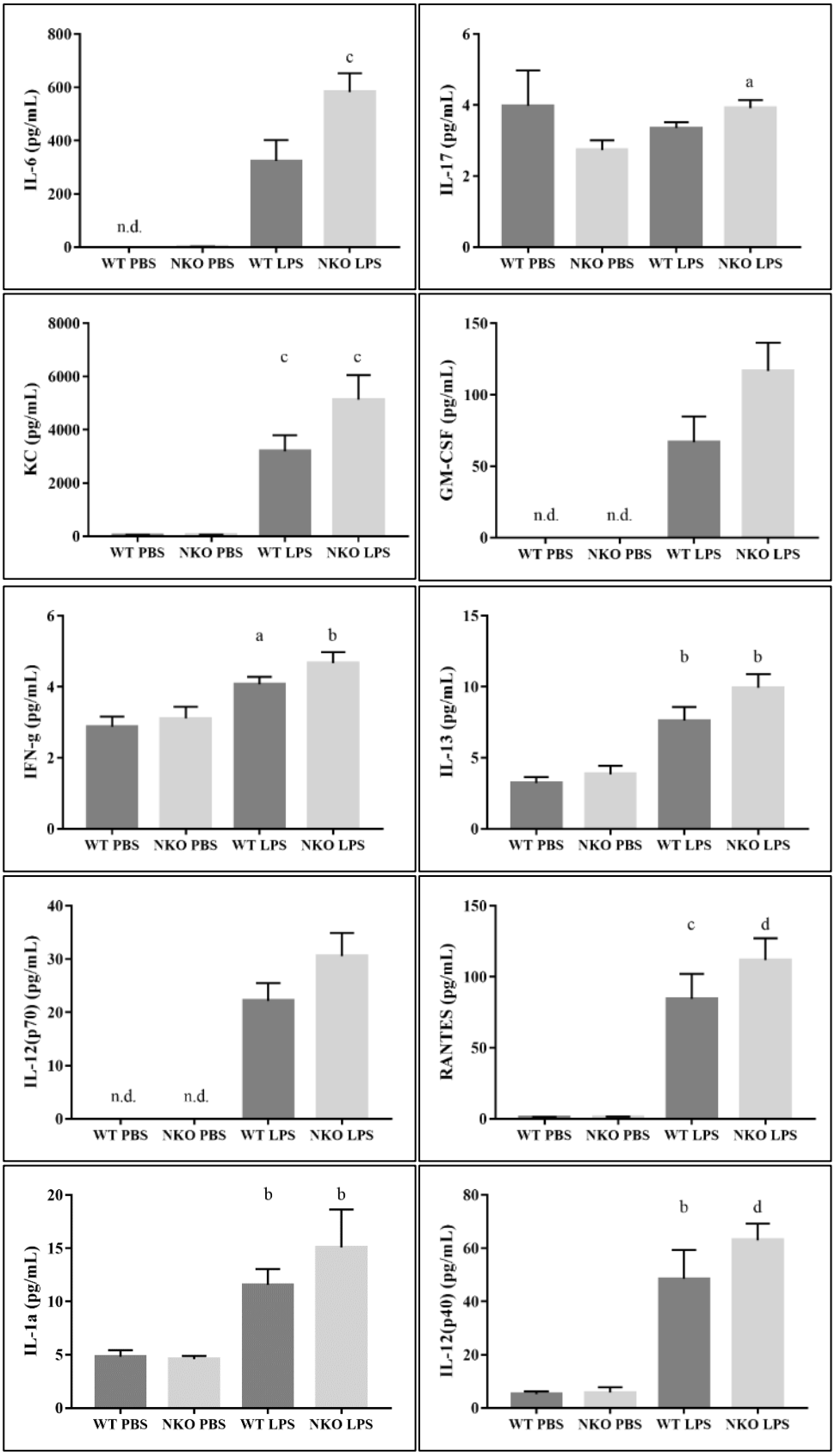
IL-6 (pg/mL)
800
600
400
200
0
n.d.
c
WT PBS NKO PBS WT LPS NKO LPS
IL-17 (pg/mL)
6
4
2
0
a
WT PBS NKO PBS WT LPS NKO LPS
KC (pg/mL)
8000
6000
4000
2000
0
c
c
WT PBS NKO PBS WT LPS NKO LPS
GM-CSF (pg/mL)
150
100
50
0
n.d.
n.d.
WT PBS NKO PBS WT LPS NKO LPS
IFN-g (pg/mL)
6
4
2
0
a
b
WT PBS NKO PBS WT LPS NKO LPS
IL-13 (pg/mL)
15
10
5
0
b
b
WT PBS NKO PBS WT LPS NKO LPS
IL-12(p70) (pg/mL)
40
30
20
10
0
n.d.
n.d.
WT PBS NKO PBS WT LPS NKO LPS
RANTES (pg/mL)
150
100
50
0
c
d
WT PBS NKO PBS WT LPS NKO LPS
IL-1a (pg/mL)
20
15
10
5
0
b
b
WT PBS NKO PBS WT LPS NKO LPS
IL-12(p40) (pg/mL)
80
60
40
20
0
b
d
WT PBS NKO PBS WT LPS NKO LPS

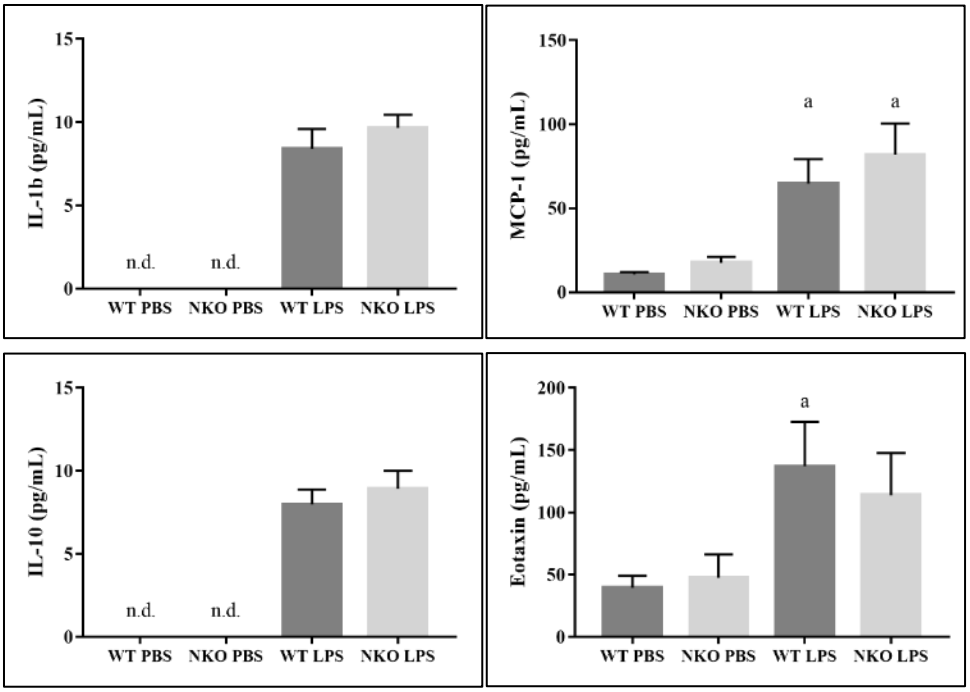

Figure 3.6: 23-plex ELISA of BALF.

An ELISA performed on the BALF of LPS or PBS-treated mouse lungs reveal **(A)** statistically significant differences between NKO and WT groups treated with LPS in concentrations of IL-5, TNF-α, MIP-1β, MIP-1α and G-CSF ordered according to effect size. **(B)** Results for IL-6, IL-17, KC, GM-CSF, IFN-γ, IL-13, IL-12(p70), RANTES, IL-1α, IL-12(p40), IL-1β, MCP-1, IL-10 and eotaxin were not statistically significant. Signals for IL-2, IL-3, IL-4 and IL-9 were not within detectable range (data not shown). (*$p \leq 0.05$, ***$p \leq 0.001$. Letters represent statistically significant differences compared with its PBS counterpart, a: $p \leq 0.05$, b: $p \leq 0.01$, c: $p \leq 0.001$, d: $p \leq 0.0001$. Groups with ≥4 samples below detection limit are categorized as not detected (n.d.); n=4-6. Results are presented as mean ± SEM.)

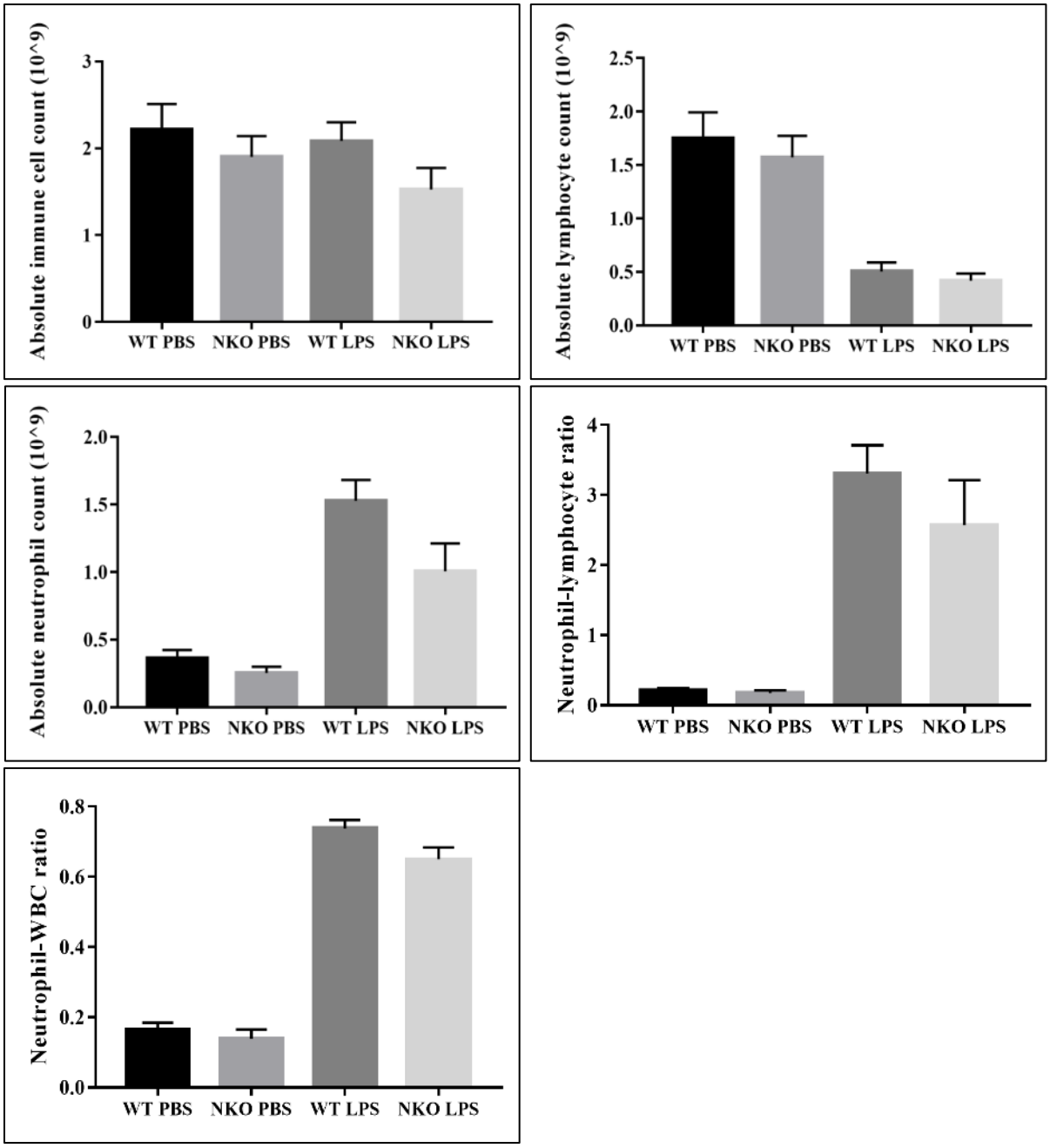

Figure 3.7: Peripheral blood analysis.

Peripheral blood from WT and NKO mice treated with LPS or PBS were analyzed in terms of absolute immune cell, lymphocyte and neutrophil count, neutrophil-lymphocyte ratio, and neutrophil-WBC ratio. Results were not statistically significant ($p \leq 0.05$). (Results are presented as mean ± SEM)

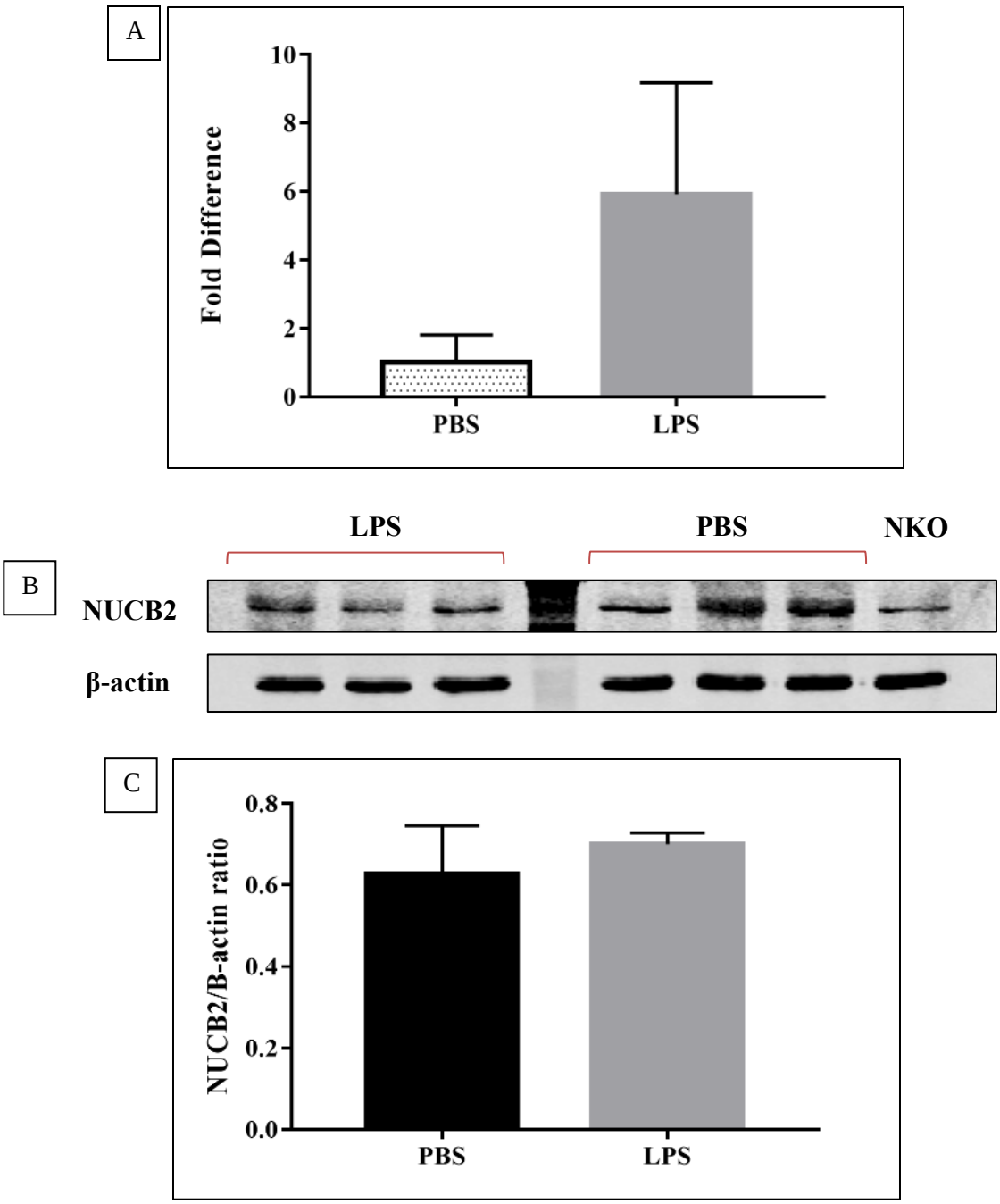

Figure 3.8: RT-qPCR quantification and Western blot of NUCB2/nesfatin-1 in WT PBS and LPS-treated mouse lungs.

Quantification of NUCB2/nesfatin-1 **(A)**mRNA expression through RT-qPCR and **(B)**protein expression through Western blots in WT PBS and LPS-treated mouse lungs revealed no significant difference between the two groups (n=6). NKO sample shows the presence of antibody non-specificity. **(C)** Graphical representation of Western blot densitometry analysis (n=6). (Results presented as Mean ± SEM.)

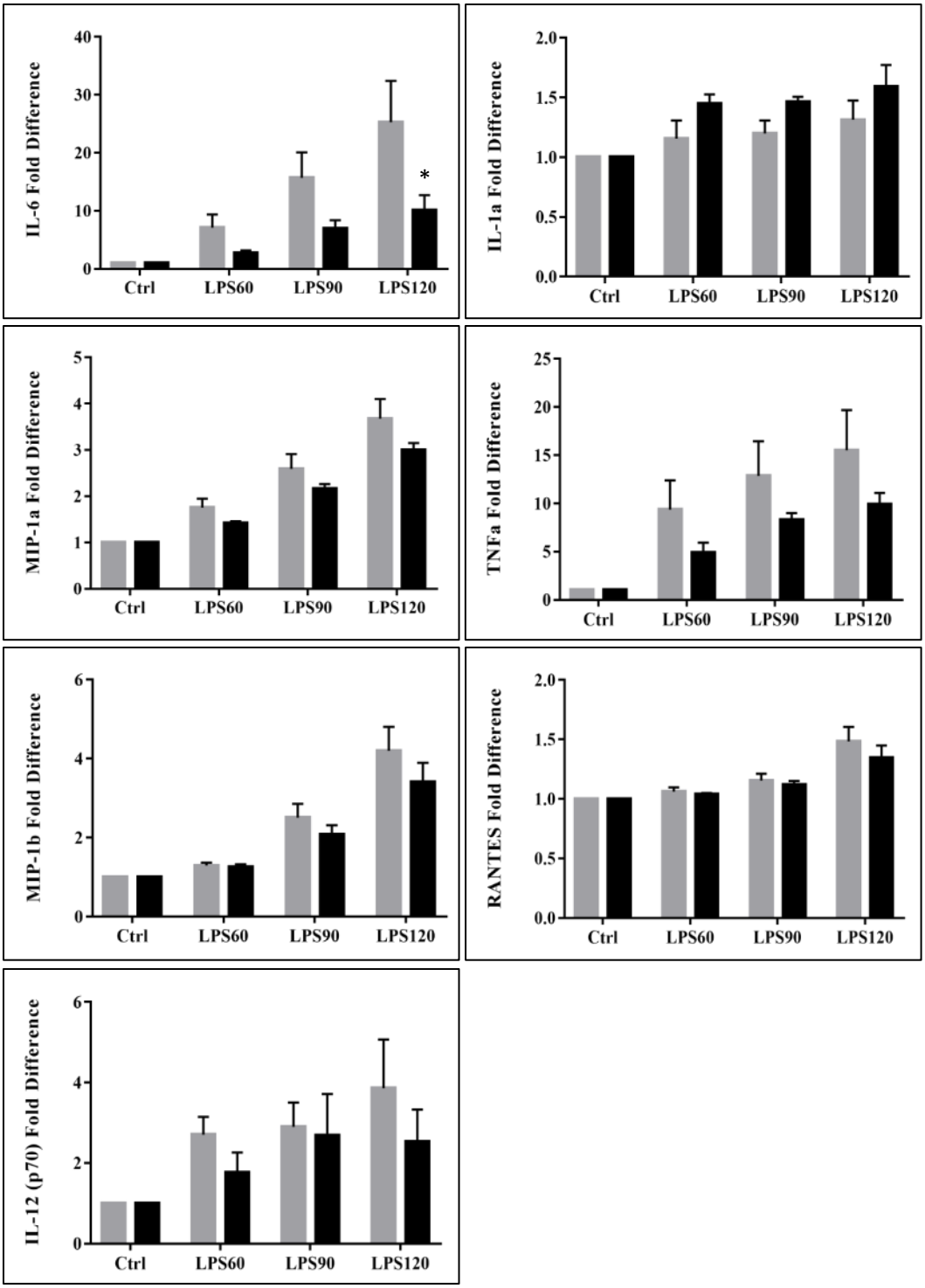

Figure 3.9: 23-plex ELISA of mouse neutrophil culture supernatant.

An ELISA performed on the culture supernatant of mouse neutrophils stimulated with 1ng/mL LPS for 0, 60, 90 and 12mins reveal no significant differences between WT (grey) and NKO (black) for IL-1α, TNF-α, RANTES, MIP-1α, MIP-1β, and IL-12(p70) cytokine expression ($p>0.121$). Sidak's multiple comparisons following a repeated measures two-way ANOVA indicated that IL-6 was significantly lower at LPS120 in NKO samples ($p=0.017$). All LPS stimulated samples were standardized against their

respective control samples. Signals for other assayed cytokines were not within detectable range (data not shown). (Results are presented as Mean ± SEM.)

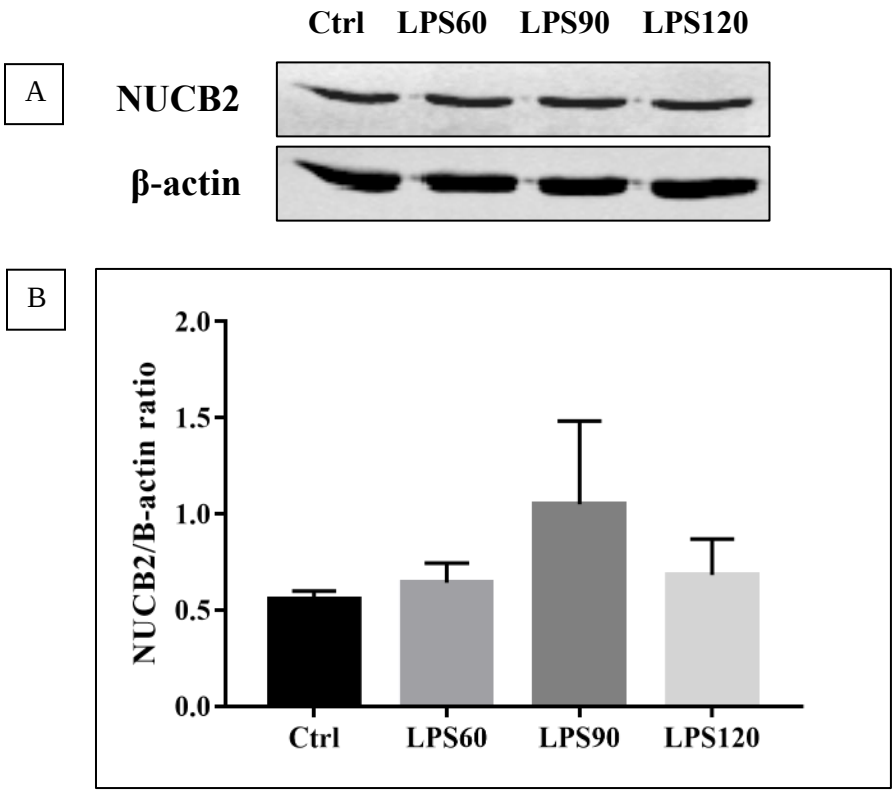

Figure 3.10: Western blot of NUCB2/nesfatin-1 in WT neutrophils.
Quantification of NUCB2/nesfatin-1 in WT mouse neutrophils treated with 1ng/mL LPS for 0(Ctrl), 60, 90 and 120mins. **(A)** Representative image of Western blot results for one set of samples. **(B)** Graphical representation of Western blot densitometry analysis (n=3). Results analyzed using repeated measures one-way ANOVA revealed no significant difference in NUCB2/nesfatin-1 protein expression (p=0.436). (Results presented as Mean ± SEM.)

3.5 Discussion

Acute lung injury(ALI) is a pulmonary inflammatory condition with multiple causes that can broadly be divided into local injuries such as pneumonia, ventilatory damage and blunt chest trauma, and systemic risk factors such as sepsis, large volume blood transfusions and burn injuries (Flierl *et al*., 2006). While no animal model is capable of replicating all symptoms of human ALI, parameters determined upon consensus of researchers surveyed by the American Thoracic Society have been established to assess ALI in mouse models (Matute-Bello *et al*., 2010). These characteristics of ALI include histological evidence of tissue injury, change in alveolar-capillary membrane integrity, inflammatory response, and physiological evidence of dysfunction (Matute-Bello *et al*., 2010). In our ALI mouse model, we addressed the first 3 of these characteristics using adult (3-5 months old) male C57BL/6-$^{Tyrc\text{-}Brd}$ WT and NUCB2 KO(NKO) mice intranasally stimulated with E. coli O55:B5 LPS for 9 hours to induce ALI caused by neutrophil infiltration and sepsis. The above parameters are important since any variation would alter the degree or nature of responses. Our experiments mainly focus on differences between WT and NKO mouse lungs and neutrophils to elucidate the potential role of NUCB2/nesfatin-1 in lung inflammation. Nonetheless, the role of the above parameters on our results will be briefly discussed to highlight possible refinements to our experiments. While previous studies of NUCB2/nesfatin-1 in inflammation all involve the addition of nesfatin-1 into their experimental model, our studies are unique in the use of NKO mice, and insight through inducing inflammation in the absence of our protein of interest.

In assessing the characteristics of ALI, our results showed a significant increase in neutrophil and inflammatory cytokine accumulation in NKO mouse lungs compared to WT. While previous studies have shown significantly reduced levels myeloperoxidase (MPO) activity- an indirect measure of neutrophil infiltration- in brain tissues of nesfatin-1 treated rats compared to untreated samples (Ozsavci *et al*., 2011), our immunohistological results of Gr-1 stained neutrophils are the first to present illustrative evidence of enhanced neutrophil accumulation in the absence of NUCB2/nesfatin-1. Our results showed mean neutrophil counts at high power magnification to be 3 times higher in NKO samples compared to WT. Since we know that ALI induced through intranasal injection of LPS would result in patchy injury, our method of assessing neutrophil infiltration through counts enables us to randomly select areas

representative of injury. This advantage to experimental relevance comes at the cost of possible experimenter bias. Hence to support our findings, an assay to compare MPO activity between WT and NKO mouse lung homogenates was also performed. A small section of each mouse lung was randomly sampled without knowledge of its state of injury. Although the results were not statistically significant, the 1.4 times higher MPO activity in NKO samples compared to WT ($p=0.074$) was supportive of our findings. Further, taking into consideration our small sample size of 6 animals per group, we propose that statistical significance for this particular experiment would only be a matter of increasing animal numbers. Another interpretation of present results is that myeloperoxidase may be less active in the absence of NUCB2/nesfatin-1, which in turn affected the ability of an MPO assay to indirectly quantify neutrophils. Increased neutrophil infiltration in the absence of NUCB2/nesfatin-1 not only implicates the potential for increased oxidative damage and pro-inflammatory cytokine release, but also additional stress on macrophages during clearance to resolve inflammation. This will be further discussed later as we specifically examine WT and NKO mouse neutrophils.

In terms of changes in alveolar-capillary permeability, there results showed no statistically significant differences in total protein concentration of BALF between WT and NKO LPS or PBS-treated samples. Both WT and NKO total protein concentrations were higher in LPS-treated samples compared to PBS samples, signaling that vascular permeability was increased as a result of inflammatory stimulation.

In our final measure of ALI, absolute immune cell and neutrophil counts, and cytokine expression in BALF of NKO and WT mice were used to assess inflammatory response. The expression of 5 cytokines were significantly elevated in NKO samples compared to WT, but no significant difference was found between WT and NKO absolute immune cell and neutrophil counts. While the loss of NUCB2/nesfatin-1 increases the adherent population of neutrophils in mouse lungs, these results suggest the non-adherent neutrophil population remains unaffected. Previous studies have found C57BL/6 mice to be LPS-hyporesponsive, displaying consistently low concentrations of polymorphonuclear leukocytes, TNF-α, and MIP-2 in BALF compared to other mouse strains such as 129/Svlm and C3H/BfeJ (Lorenz *et al.*, 2001). As such, our experimental model may simply not be sensitive enough to detect any significant difference between treatment groups.

Amongst the many inflammatory cytokines, previous research on human lung inflammation induced by intratracheal instillation of LPS showed increased levels of TNF-α, IL-1β, IL-6, G-CSF, IL-8, MCP-1, MIP-1α and MIP-1β (O'Grady *et al.*, 2001). From our results, TNF-α, G-CSF, MIP-1α and MIP-1β were expressed at significantly higher levels in LPS-treated NKO BALF samples compared to WT. These observations provide important hints as to which cytokines relevant to LPS-induced human lung inflammation are affected by NUCB2/nesfatin-1. At length, our results showed that IL-5, TNF-α, MIP-1α, MIP-1β and G-CSF expression were significantly higher in NKO than WT; IL-6 also had higher expression in NKO samples than WT, but was slightly short of statistical significance ($p=0.052$); results for IL-17, KC, GM-CSF, IFN-γ, IL-13, IL-12(p70), RANTES, IL-1α, IL-12(p40), IL-1β, MCP-1, IL-10 and eotaxin were not statistically significant; IL-2, IL-3, IL-4 and IL-9 expression was below detectable levels. Cytokines expressed at significantly higher levels in NKO samples could be divided into pro-inflammatory cytokines (TNF-α and G-CSF) and chemokines (MIP-1α and MIP-1β) that participate in the acute phase reaction, and a mediator of allergic inflammation (IL-5) (Xu *et al.*, 1996; Tumpey *et al.*, 2002; Lee *et al.*, 2014). These results agree with previous findings in animal studies where NUCB2/nesfatin-1 was shown to play an anti-inflammatory role (Ozsavci *et al*., 2011; Tang *et al.*, 2012). While LPS treatment itself is not expected to produce allergic inflammation in mice, the elevated levels of IL-5 with LPS treatment could be an indication of previous exposure to allergens (Lee *et al.*, 2014). Differential cell counts performed on BALF showing elevated lymphocyte counts in 4 out of 12 PBS-treated samples, but none of the LPS-treated samples, implicate this as a possibility. These results suggest that the increased neutrophil accumulation observed in NKO mice contributes to increased pro-inflammatory cytokine expression. While not explored in this experiment, we propose that NUCB2/nesfatin-1 may also increase macrophage pro-inflammatory cytokine expression since TNF-α, MIP-1α, MIP-1β and G-CSF are all cytokines secreted by macrophages to initiate acute inflammation (O'Grady *et al.*, 1999; Xu *et al.*, 2000; Duque and Descoteaux, 2014).

In addition to the parameters above that help us assess the extent of ALI in WT and NKO mouse lungs, we observed that the absence of NUCB2/nesfatin-1 in mouse lungs did not compromise its macroscopic structural integrity during PBS or LPS treatment. Neutrophil margination appeared, likewise, unaffected in PBS-treated lungs. A brief analysis of peripheral blood counts revealed no significant difference between WT and NKO animals treated with LPS

or PBS. However, we do note the 0.9 times neutrophil to total white blood cell ratio in LPS-treated NKO samples compared to WT that was close to statistical significance ($p=0.057$). This provides additional support to the observed increased neutrophil recruitment to the lungs as they are depleted from peripheral circulation.

To take a more specific look into the role of NUCB2/nesfatin-1 in mouse neutrophils during ALI, we performed an identical 23-plex ELISA on the neutrophil culture supernatant after $5x10^6$ cells were stimulated for 0, 60, 90 and 120 mins with 1 ng/mL LPS. The 1 ng/mL LPS concentration was selected based on previous studies in human neutrophils demonstrating different dosages that enhanced phagocytosis and oxidative burst compared to LPS-free controls (Bohmer *et al.*, 1992). It was also determined to be a physiologically relevant dosage based on endotoxin levels present in serum of septic patients (Levin *et al.*, 1970). Our results showed that the only cytokines present at detectable levels were IL-6, IL-1α, MIP-1α, MIP-1β, TNF-α, RANTES and IL-12(p70). After normalizing results against their respective controls, we found that only NKO neutrophils after 120 mins of LPS stimulation had significantly lower expression of IL-6 than WT. Previous studies have shown IL-6 to enhance neutrophil migration towards IL-8, reduce neutrophil deformability, and stimulate neutrophil release from bone marrow in response to LPS treatment (Walker et al., 2008; Wright *et al.*, 2014). However, it is worth noting that macrophages are also a major source of IL-6 (Duque and Descoteaux, 2014), hence decreased expression from neutrophils alone should be interpreted with caution. Although statistically insignificant, we observed that all detected cytokines except IL-1α were secreted at higher concentrations by WT neutrophils than NKO after LPS stimulation; cytokine concentrations in the supernatant generally increased with stimulation time. Since only 3 biological replicates were performed; an increase in sample size is expected to increase sensitivity to the observed change in effect size. Our observations agree with previous findings where expression of inflammatory cytokines was upregulated with the presence of NUCB2/nesfatin-1 (Scotece *et al.*, 2014). With our observation that NKO mouse lungs had approximately 3 times the adherent neutrophil population of WT, our findings integrate the seemingly contradictory results of NUCB2/nesfatin-1 being anti-inflammatory and pro-inflammatory in animal and cell culture studies respectively (Ozsavci *et al.*, 2011; Tang *et al.*, 2012; Scotece *et al.*, 2014). We propose that while neutrophils individually secrete less

inflammatory cytokines the absence of NUCB2/nesfatin-1, increased accumulation results in an effect that is net pro-inflammatory.

Last, while studies have shown that NUCB2/nesfatin-1 mRNA and protein expression in adipocytes and chondrocytes increased with pro-inflammatory stimulus, our results revealed no change of mRNA and protein expression in mouse lung homogenates, and no change of protein expression in mouse neutrophil lysates following LPS treatment (Ramanjaneya *et al.*, 2010; Scotece *et al.*, 2014).

Taken together, our findings suggest NUCB2/nesfatin-1 to be an anti-inflammatory cytokine. The absence of NUC2/nesfatin-1 not only significantly increased adherent neutrophil accumulation, but also pro-inflammatory cytokines and chemokines. Vascular permeability was not significantly affected by the loss of NUCB2/nesfatin-1. Inflammatory stimulus with LPS in WT mice also did not change NUCB2/nesfatin-1 mRNA and protein expression in mouse lungs, or protein expression in mouse neutrophils.

CHAPTER 4. GENERAL DISCUSSION AND FUTURE DIRECTIONS

The primary objectives of this project were to determine the localization, expression and function of NUCB2/nesfatin-1 in normal and inflamed human and mouse lungs. Experiments were carried out with a focus on the role of neutrophils during inflammatory conditions as they are important mediators in many pulmonary inflammatory conditions such as chronic obstructive pulmonary disease (COPD) and acute lung injury/acute respiratory distress syndrome (ALI/ARDS) which are typically associated with high mortality rates (Liu *et al.*, 2017). While NUCB2/nesfatin-1 is known to be expressed in mouse lungs (Chung *et al.*, 2013), implicated to have a role in inflammation (Ozsavci *et al*., 2011; Tang *et al.*, 2012), and expressed in plasma at levels that positively correlate with pro-inflammatory cytokines (IL-6, IL-8, TNF-α and MMP-9) during human COPD (Leivo-Korpela *et al.*, 2014), our study is the first to investigate its role in ALI. In contrast to previous studies, our experiments make use of WT and NUCB2 KO (NKO) mice as supposed to administering additional nesfatin-1 to our models. By performing studies on both animal models and cell culture, we also bridge the gap of knowledge as to whether NUCB2/nesfatin-1 has a pro- or anti- inflammatory effect.

In the first part of our studies, we determined the localization of NUCB/nesfatin-1 in normal and inflamed human and mouse lungs and neutrophils. Prior to our experiments, there were only published results of its mRNA and protein expression in mouse lungs; no studies had looked into human lungs or given any localization information (Chung *et al.*, 2013; Kim *et al.*, 2014). In addition, a study by Stengel *et al.* (2011) suggested that NUCB2/nesfatin-1 mRNA was not detectable in rat white blood cells; this was later disputed as Ravussin (2016) demonstrated that NUCB2/nesfatin-1 mRNA was present in macrophages and T cells. Through immunohistochemistry, a custom NUCB2/nesfatin-1 antibody (Pacific Immunology, CA, USA) confirmed to not cross-react with NUCB1, a homolog to NUCB2, was used to determine the localization of the protein in normal and inflamed mouse and human lung samples. Results showed that our protein of interest was expressed in the alveolar septa, bronchiolar epithelium, vascular endothelium, immune cells and red blood cells in both mouse and human samples. Human lung samples revealed that NUCB2/nesfatin-1 was absent in adipose tissues, hyaline cartilage and smooth muscle fibers of the tunica media. Further, localization did not change with inflammatory status. Afterwards, subcellular localization of NUCB2/nesfatin-1 in mouse lungs

was determined through immunoelectron microscopy using the same antibody. Results revealed that the protein localized in the cytoplasm and nucleus of pulmonary and immune cells; similarly, this did not change with inflammatory status. Lastly, analysis of immunoelectron microscopy images of human neutrophils stimulated for 0, 60, 90 and 120 mins with 1 ng/mL LPS using a polyclonal NUCB2/nesfatin-3 antibody (NBP1-87383, Novus Biologicals, ON, Canada) revealed that the protein accumulated within 0.5 μm of the plasma membrane after 90 mins of LPS treatment. The protein was consistently present at 5 times the mean concentration in the euchromatin compared to heterochromatin portion of the nucleus, and 2 times the mean concentration in the cytoplasm compared to nucleus. These observations suggest that NUCB2/nesfatin-3 may have a role in transcription regulation, as well as provide important clues for potential function and interaction with other molecules.

In the second part of our studies, we examine the role of NUCB2/nesfatin-1 in the development of ALI using WT and NKO mice stimulated for 9 hours with 50 μL of 1 mg/mL *E. coli* O55:B5 LPS or PBS. Previous animal studies administered nesfatin-1 to rats with subarachnoid hemorrhage-induced oxidative brain damage, and traumatic brain injury, and found nesfatin-1 to have an anti-inflammatory and anti-apoptotic effect (Ozsavci *et al*., 2011, Tang *et al.*, 2012). Expression of pro-inflammatory cytokines, neutrophil-mediated oxidative damage and enzymatic activities, and tissue damage decreased with nesfatin-1 treatment (Ozsavci *et al*., 2011, Tang *et al.*, 2012). In our studies, we examined ALI through 3 parameters deemed most relevant by the American Thoracic Society: histological evidence of tissue injury, changes in alveolar-capillary barrier, inflammatory response and physiological evidence of dysfunction (Matute-Bello *et al*., 2010). Histological analysis through haematoxylin and eosin staining revealed no structural damage and no compromise to neutrophil margination in any treatment group, but slightly more immune cell accumulation in perivascular and septal spaces of LPS-treated NKO samples compared to WT. Immunohistochemistry using Gr-1 antibody to identify neutrophils for high power magnification counts revealed neutrophil numbers 3 times higher in LPS-treated NKO lungs compared to WT. When changes to vascular permeability were examined through a protein assay of bronchoalveolar lavage fluid (BALF), results showed no significant difference between WT and NKO samples with PBS or LPS treatment. Measures of inflammatory response using absolute immune cell and neutrophil counts in BALF revealed no significant difference between WT and NKO mice, notably showing that the loss of

NUCB2/nesfatin-1 does not affect the non-adherent population of neutrophils following LPS-treatment. Next, myeloperoxidase activity was used as an indirect measure to quantify adherent neutrophil. While there is no significant difference between NKO and WT LPS-treated samples, MPO activity in LPS-treated NKO samples was 2.6 times higher than PBS-treated samples, whereas the increase was only 1.9 times in WT samples. Lastly, ELISA performed for 23 inflammatory cytokines in WT and NKO BALF revealed that pro-inflammatory cytokines (TNF-α and G-CSF), chemokines (MIP-1α and MIP-1β) and a mediator of allergic inflammation (IL-5) were significantly upregulated in NKO compared to WT samples. IL-6 expression was also upregulated in NKO samples compared to WT, but was slightly short of statistical significance ($p=0.052$); results for IL-1α, IL-1β, IL-10, IL-12(p40), IL-12(p70), IL-13, IL-17, KC, GM-CSF, IFN-γ, RANTES, MCP-1, and eotaxin were not statistically significant; IL-2, IL-3, IL-4 and IL-9 expression were below detectable levels. While significantly increased cytokine expression of TNF-α, MIP-1α and MIP-1β in LPS-treated mouse lungs may, in part, be a result of neutrophil accumulation, we must note that these pro-inflammatory cytokines are also expressed by macrophages (TNF-α, MIP-1α, MIP-1β) and endothelial cells (TNF-α). Significant differences in IL-5 and G-CSF expression between WT and NKO mouse lungs further suggests NUCB2/nesfatin-1 to regulate other cell types. While our experiments do not specifically investigate other cell types, future studies doing so would provide a more comprehensive picture on the role of NUCB2/nesfatin-1 during acute lung inflammation. Peripheral blood analysis was performed to determine whether NUCB2/nesfatin-1 had any systemic effect on blood counts; results were not statistically significant. Together, these results suggest NUCB2/nesfatin-1 to have an anti-inflammatory role, considering that its absence significantly increases adherent neutrophil accumulation, and pro-inflammatory cytokine expression in mouse lungs.

To more specifically determine the role of mouse neutrophils during acute inflammation, we extracted bone marrow neutrophils from WT and NKO mice and stimulated them with 1ng/mL LPS for 0, 60, 90 and 120mins ($5x10^6$ cells per sample; n=3). Culture supernatant was analyzed using the same ELISA for 23 cytokines. Results only revealed statistical significance in IL-6, where NKO samples expressed 0.4 times the IL-6 of WT samples. Otherwise, only IL-1α, TNF-α, RANTES, MIP-1α, MIP-1β, and IL-12(p70) were present at detectable levels, and results comparing between WT and NKO samples at different time points were not significant. However, the observation that WT samples expresses more cytokines compared to NKO does

agree with previous cell culture findings where the addition of nesfatin-1 to chondrocytes after inflammatory stimulus increases pro-inflammatory cytokine expression (Scotece *et al.*, 2014). Taking into account that neutrophil counts are approximately 3 times in NKO than WT samples, the net effect of knocking out NUCB2/nesfatin-1 is still expected to be pro-inflammatory.

Lastly, since previous studies have shown inflammatory stimulus to increase NUCB2/nesfatin-1 mRNA and protein expression in adipocytes and chondrocytes, we attempted to determine if the same occurs in mouse lung tissues and neutrophils (Ramanjaneya *et al.*, 2010; Scotece *et al.*, 2014). Protein and mRNA were extracted from WT lung homogenates for LPS and PBS-treated samples, and assessed using Western blots and RT-qPCR respectively. Results revealed no significant difference in NUCB2/nesfatin-1 protein or mRNA expression for samples treated with LPS or PBS. Similarly, protein was extracted from mouse neutrophils that were stimulated for 0, 60, 90 and 120 mins, and assessed through Western blots. Again, results showed no statistically significant differences. Our results indicate that NUCB2/nesfatin-1 is constitutively expressed, and not influenced by LPS stimulation.

Taken together, results of our experiments suggest that NUCB2/nesfatin-1 localizes in the nucleus and cytoplasm of pulmonary cells as well as immune cells of human and mice; neither localization nor expression changes with inflammatory status. In addition, NUCB2/nesfatin-1 presence in euchromatin and its apparent ability to regulate cytokine expression suggest that it may be involved with transcription regulation. The protein appears to exert an anti-inflammatory effect by inhibiting adherent neutrophil accumulation and inflammatory cytokine expression. Considering that adherent neutrophil accumulation significantly increases in NKO mice whereas non-adherent neutrophil counts do not change, NUCB2/nesfatin-1 present throughout the epithelium and endothelium of lungs may have a role in inhibiting neutrophil infiltration and adhesion during inflammation. This is further supported by lower levels of inflammatory cytokines, TNF-α and G-CSF, in WT compared to NKO BALF. These results imply that situations which lower levels of circulating NUCB2/nesfatin-1 such as pregnancy or fasting may exacerbate neutrophil-mediated conditions such as ALI or COPD; as the population of adherent neutrophil increases, resolution time may also increase, impeding recovery from neutrophilic inflammation. Future studies should examine whether administration of NUCB2/nesfatin-1 could rescue LPS-treated NKO mice from increased pro-inflammatory conditions, or even decrease

inflammation at a higher dosage. As an extension of the current study, follow-up experiments should also examine more LPS stimulation time points. While our study focused on a 9-hour LPS stimulation where inflammation is expected to be at its peak, future studies could extend time points to 12 and 24hours to examine the progress of inflammatory resolution.

Limitation to our studies include the aforementioned effect of NUCB2/nesfatin-1 on cytokine expression of other cell types including macrophages and endothelial cells during acute lung inflammation. While they may also significantly contribute to the demonstrated anti-inflammatory effect of NUCB2/nesfatin-1, our data is insufficient to make this correlation. In a future study, inflammatory cytokine expression of WT and NKO macrophages and endothelial cells stimulated with LPS should be examined to determine to what extent these cell types contribute to the difference of inflammatory cytokine expression observed in LPS-treated WT and NKO mouse lungs. The specificity of NUCB2/nesfatin-1 antibodies used in our localization study also presents an important limitation. While we can be certain that it detects our protein of interest, we cannot rule of the possibility of cross-reaction. Future studies may consider engineering a mouse model where NUCB2/nesfatin-1 is tagged with a GFP reporter to eliminate this element of uncertainty.

APPENDIX I: Quantification of gold particles in immunoelectron microscopy images

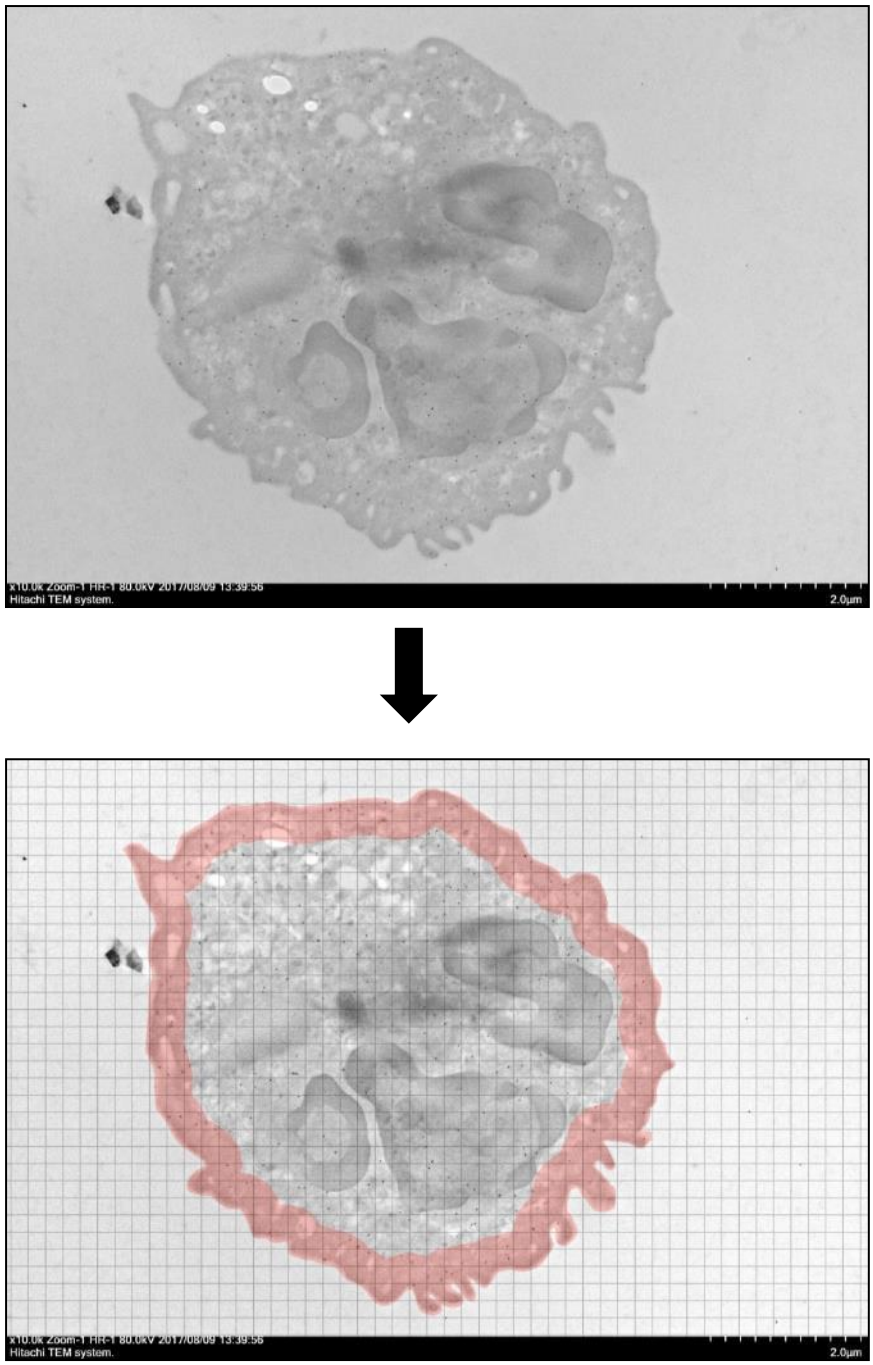

Figure I.I: Processing image for analysis.
An image is taken for each randomly chosen neutrophil at 10,000X (top). The image is then adjusted in Photoshop CS6; a uniformly-spaced grid is placed on top and the region 0.5 μm inside the plasma membrane is highlighted by selecting the cell region with a lasso tool and applying an inner stroke of 209px (bottom).

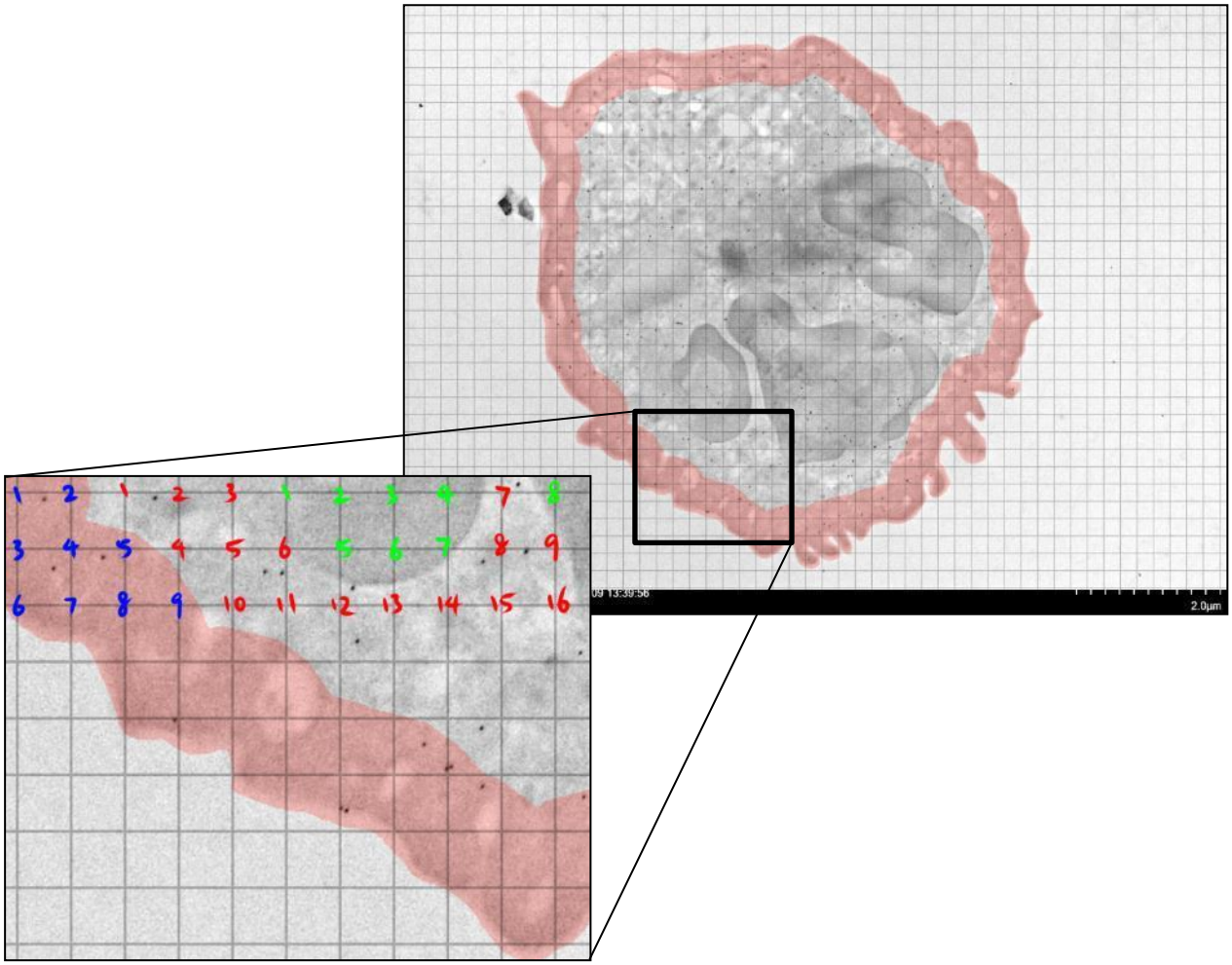

Figure I.II: Estimating area with grid.
The cell is divided into 4 regions of interest: 0.5 µm within plasma membrane, remainder of cytoplasm, euchromatin (lighter portion of nucleus), and heterochromatin (darker portion of nucleus). The profile area of each region is estimated by counting points of intersection. As an example, the above image illustrates area counting of 0.5 µm within plasma membrane (blue), remainder of cytoplasm (red) and heterochromatin (green).

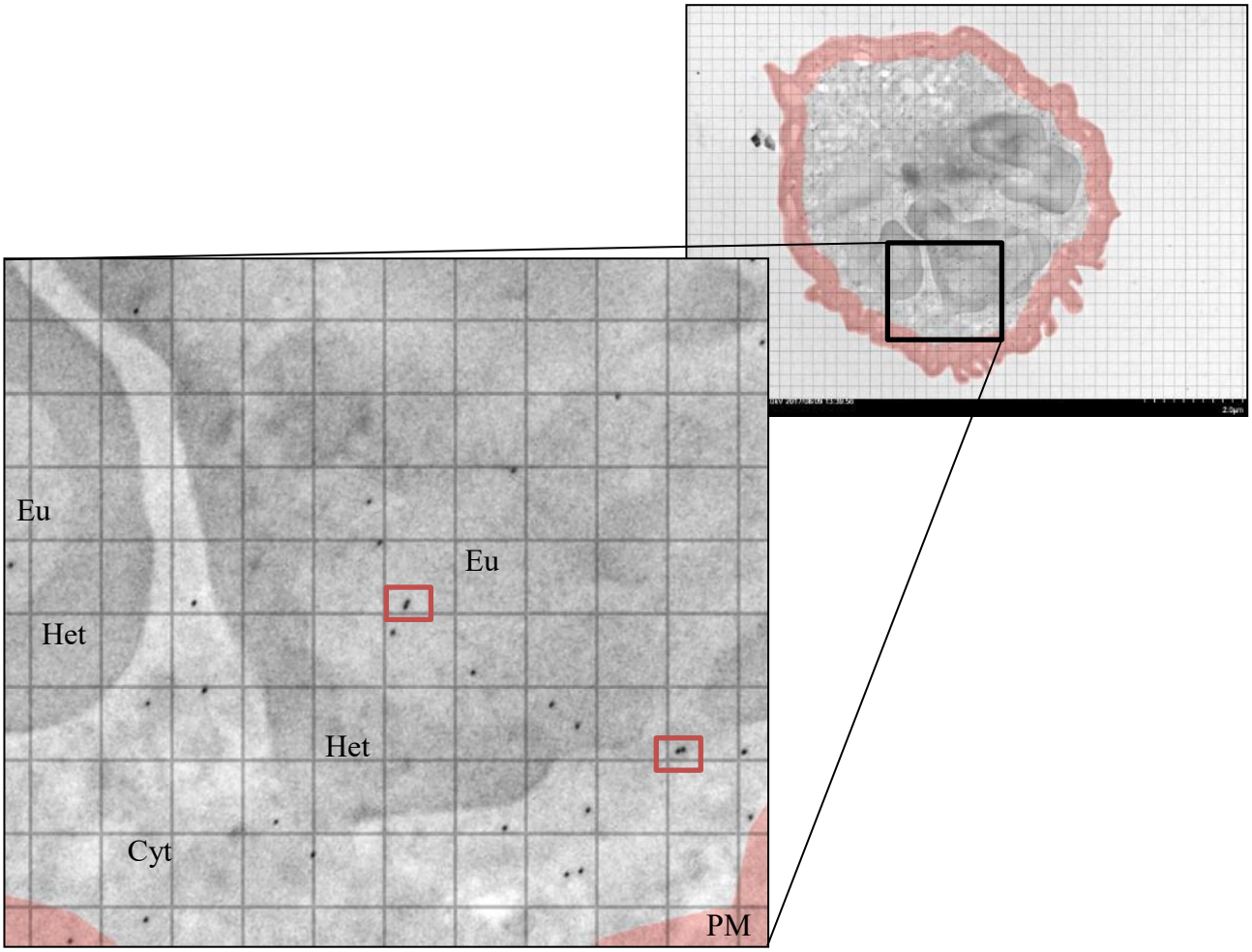

Figure I.III: Counting gold particles.
Gold particles in each region (PM: 0.5 µm within plasma membrane; Cyt: remainder of cytoplasm; Het: heterochromatin; Eu: euchromatin) are quantified accordingly. However, gold particles that are too close together (red box) are counted as 1 due to possibility of polyclonal antibodies reacting to different epitopes on the same protein.

APPENDIX II: Testing for antibody specificity

II.I NUCB2/nesfatin-1 monoclonal antibody (Custom, Pacific Immunology)

NUCB2/nesfatin-1 rabbit monoclonal antibody (Custom; Pacific Immunology, CA, USA) was developed against a synthetic peptide, VDKTKVHNTEPVENARIEP-Cys (20 AA). The sequence is located within nesfatin-1. This antibody was used in localization studies of mouse and human lungs during immunohistochemistry and immunoelectron microscopy, as well as all Western blot studies conducted within this thesis. In order to confirm its specificity, we attempted to create knockout and antigen preabsorption controls. Western blots of mouse lung homogenates were also performed.

Knockout controls were generated using the same immunohistochemistry protocol as described in section 2.3.7. NUCB2 KO (NKO) and WT mouse lung tissues were incubated with 1:50, 1:100, 1:200 and 1:250 dilutions of 1 mg/mL primary antibody. While staining became weaker in WT samples with increasing primary antibody dilution, non-specific staining in NKO samples remained consistent throughout (Figure II.I). Since nesfatin-1 mRNA was verified to be absent in NKO samples through RT-qPCR, it is possible that the antibody is cross-reacting with a highly similar compensatory protein.

Antigen preabsorption controls were generated through incubating synthetic nesfatin-1 peptide (003-22B; Phoenix Pharmaceuticals, CA, USA) with the antibody at a 2:1 concentration overnight. NKO lung tissues were also incubated with the synthetic peptide overnight to block off any unoccupied receptors that might bind with synthetic nesfatin-1 in preabsorbed antibodies. Tissue sections were briefly washed with PBS afterwards, and preabsorbed antibodies were used at a 1:200 dilution. Immunohistochemistry was carried out without further changes. Results showed non-specific staining for epithelial and endothelial layers relatively uniform in strength (Figure II.II).

Western blots were also performed on WT and NKO lung homogenates to determine antibody specificity. ENCODE guidelines (2011) suggest using a combination of characterization methods. In order to meet requirements of specificity using immunoblot analyses, the protein of interest, NUCB2/nesfatin-1, must be detected with a signal larger than 50% the total signal. Figure II.III shows that the majority of signal in all samples are at ~55kDa,

representing the molecular weight of NUCB2. Further, ENCODE guidelines (2011) suggest a sufficiently specific antibody should detect no more than 30% of the WT signal in KO samples. Densitometry was performed for the NUCB2 bands identified at ~55 kDa, revealing that all but 2 WT signals were >30% of the NKO signal. This presents reasonable evidence for antibody specificity; however, we cannot completely rule out the presence of cross-reaction.

During the course of antibody testing, a commercial NUCB2/nesfatin-1 polyclonal antibody from Phoenix Pharmaceuticals, CA, USA (H-003-22) was also examined. Results produced were similar, but the antibody is known to react with NUCB1 and Western blot results have shown a slightly higher degree of non-specificity with more bands than one at ~55 kDa detected (data not shown).

II.II NUCB2/nesfatin-3 polyclonal antibody (NBP1-87383, Novus Biologicals)

NUCB2/nesfatin-3 rabbit polyclonal antibody (NBP1-87383; Novus Biologicals, ON, Canada) was developed against a recombinant protein with the sequence of a segment within nesfatin-3. In order to confirm the specificity of the antibody to be used in immunoelectron microscopy of human neutrophils, Western blots were performed on mouse lung and pancreas homogenates, and human neutrophils. Non-specific binding was blocked with 5% BSA in TBS containing 0.1% Tween 20 (TBS-T) for 1hour at RT. The membrane was then incubated with the aforementioned NUCB2 antibody diluted 1:500 in TBS-T with 3% BSA overnight at 4°C. Afterwards, the membrane was washed with TBS-T and incubated with anti-rabbit Alexa Fluor® 488 (A-11008, Thermo Fisher Scientific, MA, USA) for 1 hour at RT and visualized on the GE Healthcare Typhoon 9400 imager. Adequate specificity of the primary antibody was evaluated according to ENCODE guidelines (ENCODE, 2011). β-actin was used as the reference gene for normalization.

According to ENCODE guidelines (2011) the protein of interest, NUCB2/nesfatin-3, must be detected with a signal larger than 50% the total signal. Figure II.IVA shows the antibody reacting against human neutrophil homogenates with signals at ~50 kDa and ~10 kDa, of which the signal at ~50 kDa represents NUCB2. Densitometry performed shows that all NUCB2 signals ~50 kDa were at least twice of that at ~10 kDa. A secondary mode of characterization was performed to compare signals between WT and NKO tissues with the principle that a

sufficiently specific antibody should detect no more than 30% of the WT signal in KO samples. While Figure II.IVB shows an immunoblot detecting vast amounts of non-specificity associated with lung and pancreas tissue, these were not detected in human neutrophil homogenates. Densitometry was performed for the NUCB2 band identified at ~55 kDa. Results showed a band in pancreas from NKO mice with 5% the WT signal, while the band in lung samples from NKO mice had 10% the weakest (lane 3) and 6% strongest (lane 4) WT band signal.

Altogether, results show that although the possibility of cross-reaction is not completely eliminated, the chosen polyclonal anti-NUCB2/nesfatin-3 antibody (NBP1-87383; Novus Biologicals, ON, Canada) has sufficient specificity for detecting NUCB2/nesfatin-3 in human neutrophils. Aside from this, one of the main reasons for this antibody choice was its ability to achieve a quantifiable amount of immunogold staining during IEM; the chosen anti-NUCB2 polyclonal antibody (NBP1-87383; Novus Biologicals, ON, Canada) out-performs monoclonal anti-NUCB2 antibodies (Custom; Pacific Immunology, CA, USA) (data not shown).

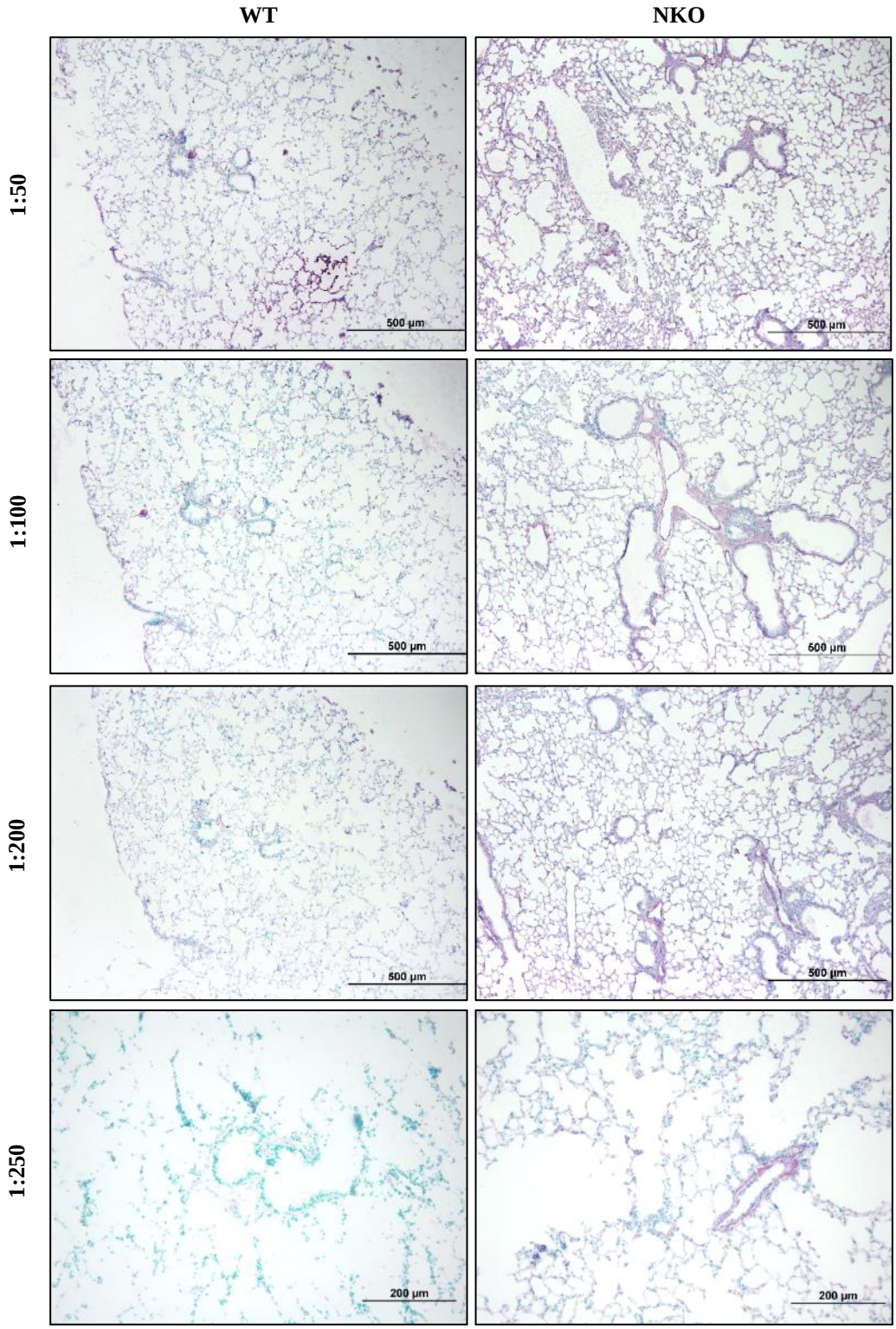

Figure II.I: Immunohistochemistry of WT and NKO mouse lungs.
Immunohistochemistry performed using NUCB2/nesfatin-1 rabbit monoclonal antibody (Custom, Pacific Immunology) on WT and NUCB2 KO mouse lungs at 1:50, 1:100, 1:200 and 1:250 dilution.

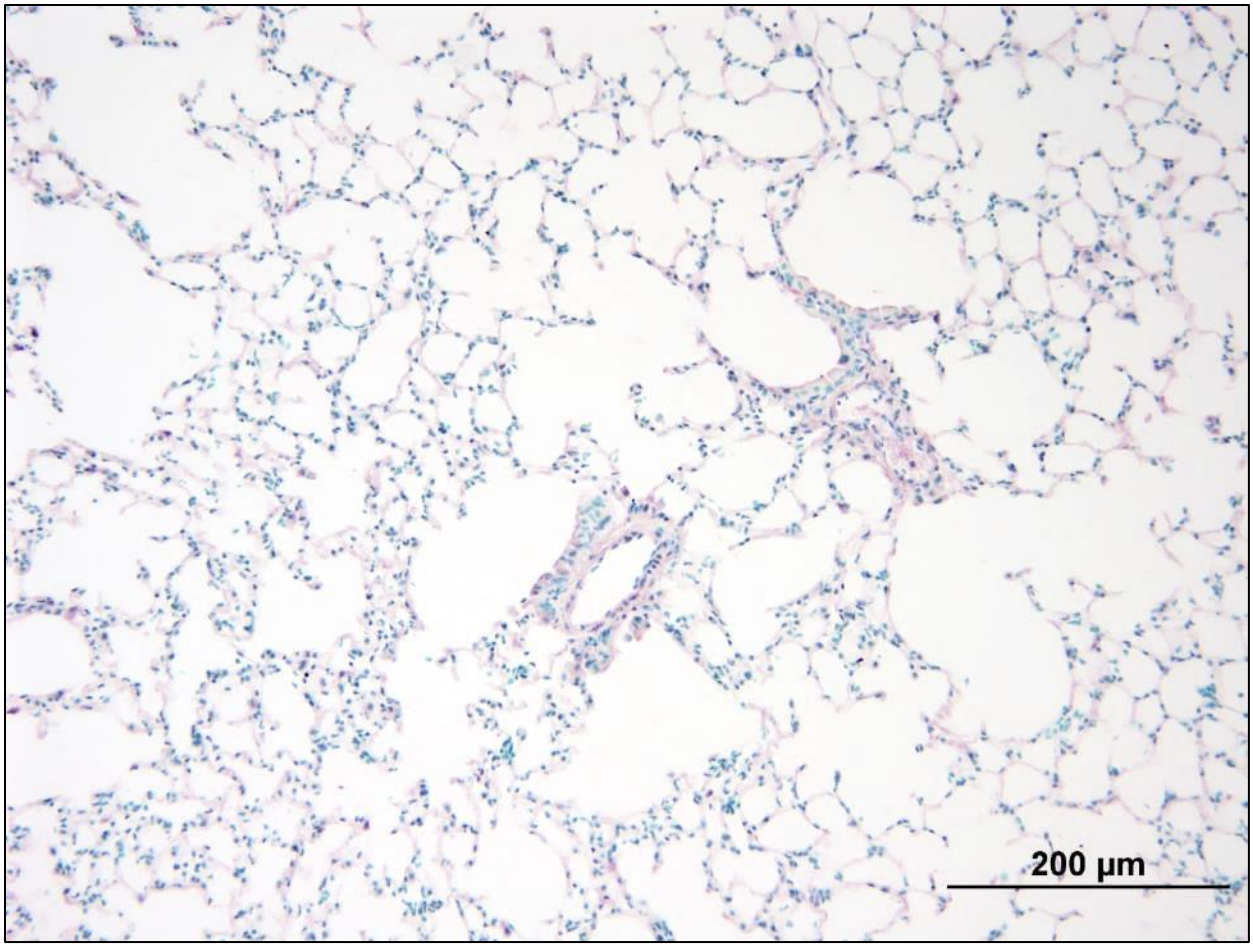

Figure II.II Immunohistochemistry of NKO mouse lungs with preabsorbed antibody.
Immunohistochemistry was performed with rabbit monoclonal NUCB2/nesfatin-1 antibody (Custom, Pacific Immunology) preabsorbed using synthetic nesfatin-1 peptide (003-22B, Phoenix Pharmaceuticals) at 1:200 dilution on NKO mouse lungs previously incubated with the same synthetic nesfatin-1 peptide.

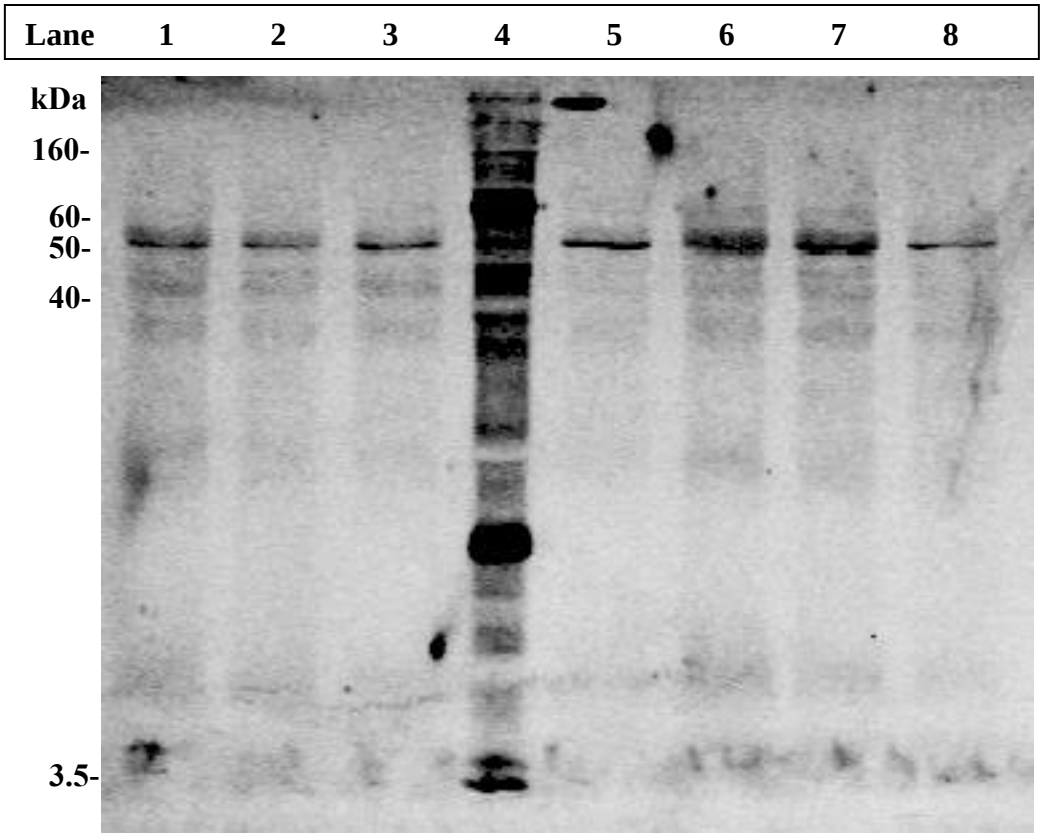

Figure II.III: Western blot analysis of anti-NUCB2/nesfatin-1 antibody specificity.
Western blot specificity testing of anti-NUCB2 antibody/nesfatin-1 (Custom, Pacific Immunology) using protein from lung homogenates of WT LPS (lane 1-3) and PBS-treated (lane 5-7) mice, and NKO (lane 8) mouse. A protein ladder was run on lane 4. Band specific for NUCB2 can be identified ~55kDa.

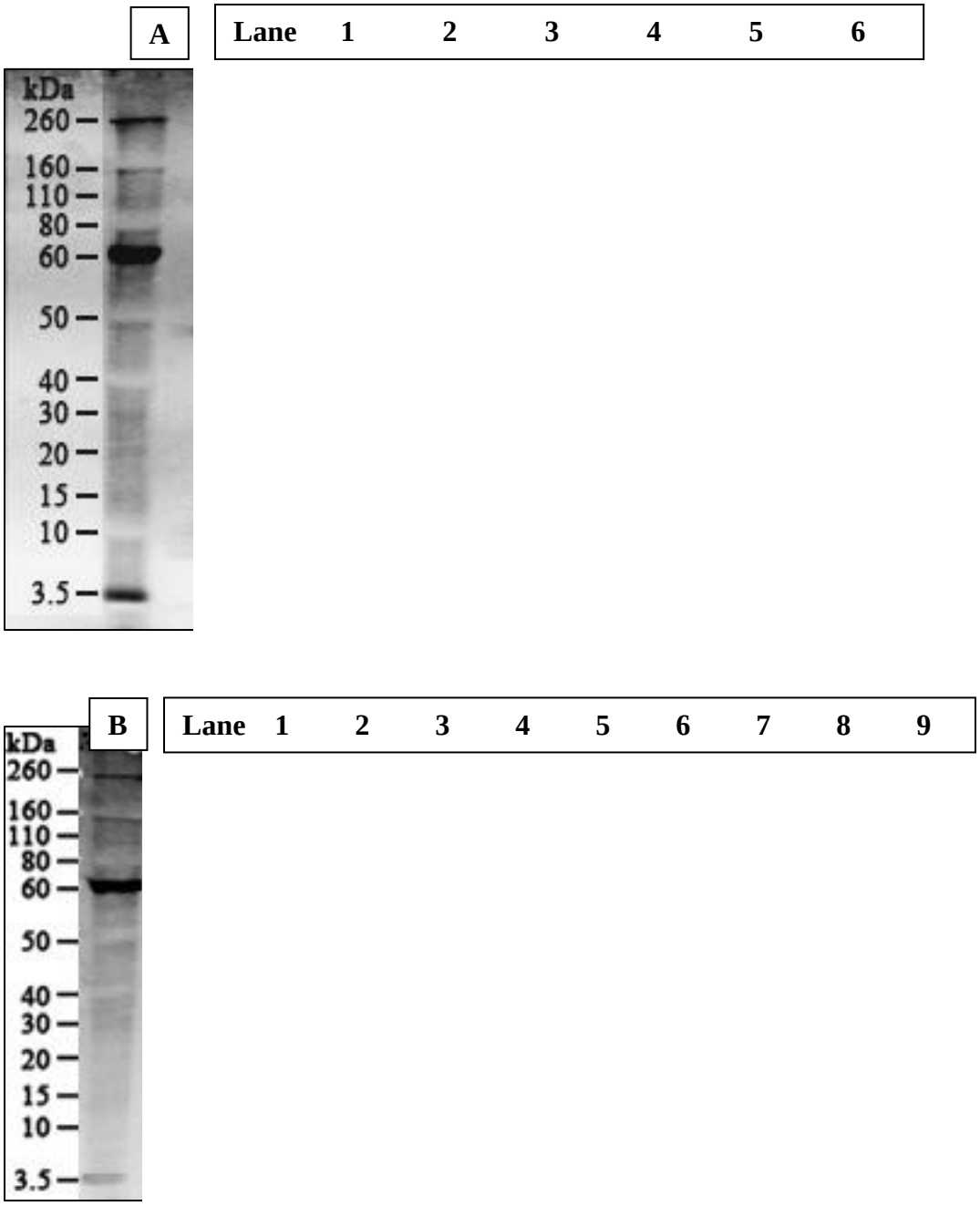

Figure II.IV: Western blot analysis of anti-NUCB2/nesfatin-3 antibody specificity.
Western blot specificity testing of anti-NUCB2/nesfatin-3 antibody (NBP1-87383, Novus Biologicals) using **(A)** protein from human neutrophil (lane 2-5; n=4), and **(B)** WT (lane 2-5; n=4) and NKO (lane 7) mouse lung homogenates, NKO (lane 8) and WT (lane 9) mouse pancreas homogenates. Protein ladders were loaded in lanes 1 and 6 of both blots.

APPENDIX III: Pilot Experiments

Two pilot experiments were carried out during the course of all NUCB/nesfatin-1 characterization studies. The first was initiated upon observation of NUCB2/nesfatin-1 presence in euchromtic portions of human neutrophils through IEM. Its primary objective was to determine potential DNA-binding motifs, establish a genome-wide binding profile and assess binding affinity. An attempt at chromatin immunoprecipitation-sequencing (ChIP-sequencing) was carried out using unstimulated human neutrophils (n=2) to immunoprecipitate chromatin fragments associated with NUCB2/nesfatin-1 within the nuclei. The pilot would allow practice and refinement of a pre-existing protocol developed by Dr. Richard Myers' Lab at the Hudson Alpha Institute for Biotechnology (Myers Lab, 2014). Specifically optimizing it to process human neutrophils using the VC300 VibraCell sonicator, and ultimately isolate sufficient chromatin fragments for sequencing.

Another pilot study was carried out to examine the distribution patterns of NUCB2/nesfatin-1 in WT mouse neutrophils following LPS stimulation through confocal microscopy. The objective was to practice the protocol which would ultimately provide reliable results through a secondary method to support IEM findings in human neutrophils.

III.I Chromatin immunoprecipitation for sequencing

Human blood was collected from healthy volunteers and neutrophils were isolated as described above. All buffers were made according to the Myers lab protocol; $2x10^7$ untreated neutrophils were used as starting material. Chromatin-protein and protein-protein cross-links were formed by adding formaldehyde to the final concentration of 1% and incubating at RT for 10 mins. The reaction was stopped by adding glycine to the final concentration of 0.125 M. Cells were then washed with PBS, resuspended in 1 mL Farnham lysis buffer and incubated on ice for 15 mins. Lysate was then passed through a 20-gauge needle 20 times to facilitate extraction of intact nuclei from the cells. Nuclei were then resuspended in 1mL RIPA buffer (300 µL and 1.2 mL RIPA buffer volumes were tested according to protocol but resulting fragments were too large or too small) and sonicated with the VC300 VibraCell sonicator (630-0418 tapered tip) to produce chromatin fragments. Each cycle of sonication consisted of 30 secs ON (pulser off; output control at 5) and 1 min OFF where samples were left on ice. 5 cycling conditions (2, 4, 6,

8, 10 cycles) were examined to determine optimal conditions where fragments would enrich around 100-500 bp and centre around at 250 bp with the least amount of cycles. As shown in Figure III.I, 6 cycles in 1 mL RIPA buffer produced optimal results. Small aliquots of fragmented chromatin were set aside in -80°C as input control for each successfully sonicated sample while the rest proceeded to downstream immunoprecipitation.

Dynabeads™ M-280 Sheep Anti-rabbit IgG (11203D; Invitrogen, CA, USA) was incubated with 5 µg custom anti-NUCB2 antibody (Pacific Immunology, CA, USA) overnight for conjugation. Afterwards the beads were washed with 5% BSA with protease inhibitor cocktail and incubated with fragmented neutrophil chromatin overnight at 4°C. The final product was washed 5 times in LiCl, once in TE buffer using a magnet and resuspended in IP elution buffer.

Lastly, cross-links with proteins were reversed to extract immune-bound chromatin from magnetic beads by incubating at a 65°C water bath for 1 hour. Beads were separated through centrifugation, the supernatant was collected and incubated at a 65°C water bath overnight to complete cross-link reversal. The QIAquick PCR Purification Kit (28104, Qiagen) was used to elute DNA and the Qubit™ dsDNA HS Assay Kit was used to evaluate DNA yield. Expected DNA recovery in a successful immunoprecipitation is 5-50 ng from $2x10^7$ cells as starting material. This was achieved in both final samples (6 and 7 ng) sent for sequencing library construction. An attempt was made to accommodate for low yield, however library construction was ultimately unsuccessful.

This portion was discontinued due to insufficient DNA recovery for ChIP-seq library construction and time constraints. Low recovery may be the result of nuclear NUCB2/nesfatin-1 being obscured by cytoplasmic NUCB2/nesfatin-1. Future trials to optimize this protocol could consider adding a wash step after Farnham buffer lysis of plasma membranes; however, this poses a risk of diluting the chromatin. Other options would be to first find conditions where NUCB2/nesfatin-1 is up-regulated in nuclei, or to pool 2 or more samples from the same biological source.

III.II Confocal microscopy of LPS-stimulated mouse neutrophils

Bone marrow neutrophils were extracted from 2 WT (C57BL/6J), and 2 PBS-treated WT (C57BL/6NCRL) mice and samples from each pair were pooled. Six well plates were set up to

contain neutrophils at $2x10^6$ cells/mL. Placed at the centre, each well also had an etched glass coverslip that was pre-coated with 20 µL 1mg/mL fibronectin for 45 mins. Cells were stimulated with 1 ng/mL LPS (L2880, Sigma-Aldrich) for 0, 60, 90 and 120 mins respectively, and incubated at 37°C with 5% CO_2. After stimulation, glass coverslips were taken from the wells, washed in PBS and fixed with 4% paraformaldehyde/0.1% TritonX-100 for 2 mins at RT. Cells were then blocked with 5% BSA at RT for 30 mins then incubated with 1:200 rabbit NUCB2 antibody (Custom, Pacific Immunology) at 4°C overnight. The next day, coverslips were incubated with a cocktail of fluorescent antibodies. During the first trial (WT C57BL/6J mice), cells were incubated with goat anti-rabbit IgG-FITC (sc-2012; Santa Cruz Biotechnology, TX, USA) and Alexa Fluor® 555 phalloidin (A34055, Life Technologies); during the second trial (WT C57BL/6NCRL), cells were incubated with goat anti-rabbit Alexa Fluor® 633 (A-21070, Life Technologies, CA, USA) and Alexa Fluor® 488 phalloidin (A12379; Life Technologies, CA, USA). Coverslips were then incubated with 1:10000 DAPI (D3571, Life Technologies) for 5mins in RT and mounted onto microscope slides using ProLong™ Gold Antifade Mountant (P36934, Thermo Fisher Scientific). Slides were left to dry in the dark overnight before storing into a slide box until confocal microscopy.

During the first trial, wash steps may have lasted too long as many neutrophils became washed off; glass coverslips may have also been insufficiently etched. However, an image of NETs was obtained from a sample treated with LPS for 120 mins (Figure III.II), suggesting that NUCB2/nesfatin-1 may be released along with chromatin DNA to form extracellular traps. During the second trial, there were no observations of NETs. Instead, a distinct NUCB/nesfatin-1 distribution pattern was observed where the protein in unstimulated cells was mostly diffuse, and became concentrated towards the plasma membrane as time exposed to LPS increased (Figure III.III). These preliminary results supported observations in human neutrophils seen in IEM where immunostaining shifts towards the plasma membrane after 90 mins LPS stimulation. However, the experiment was not pursued as negative controls did not validate the protocol used.

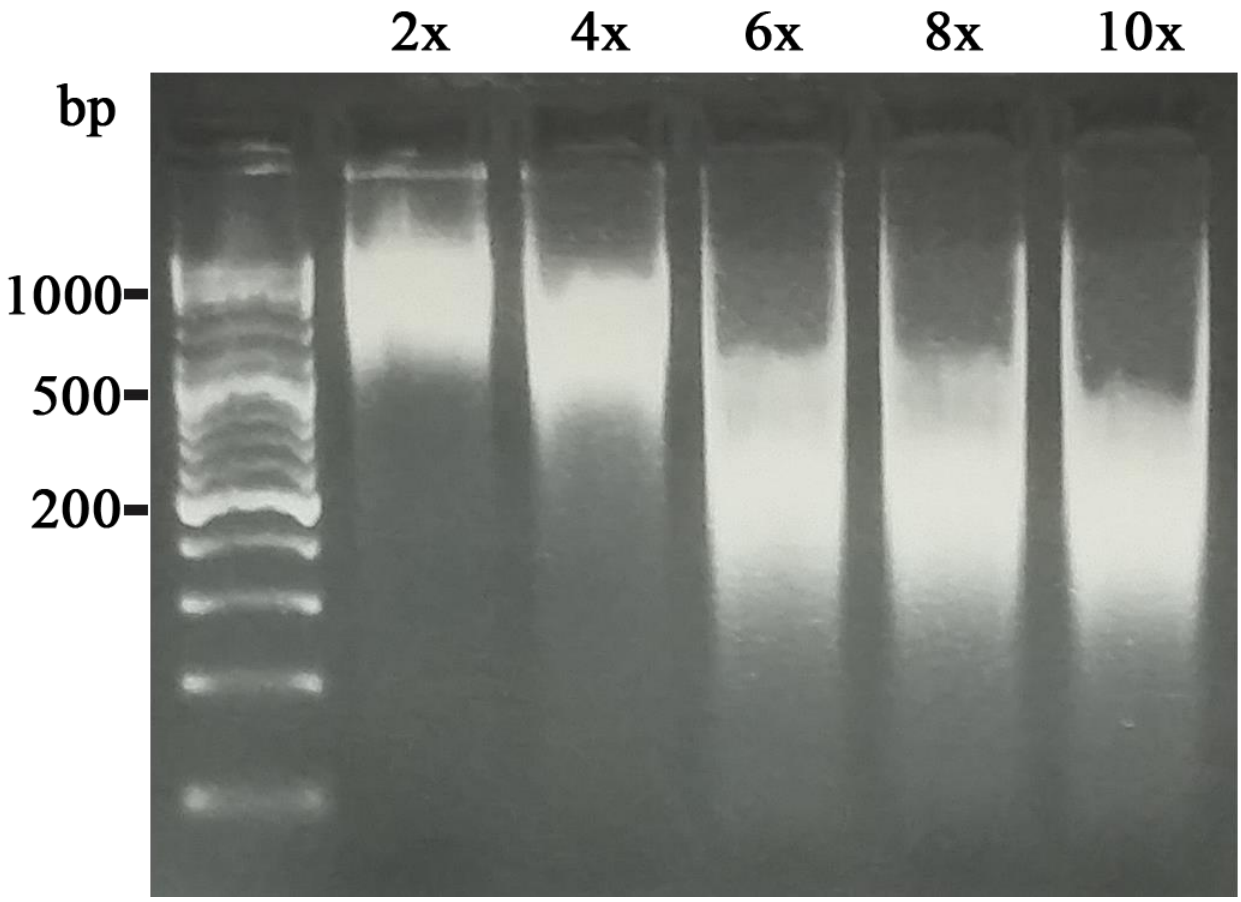

Figure III.I: Gel electrophoresis of human chromatin fragmentation after sonication.
Human neutrophil chromatin was fragmented using the VC300 VibraCell sonicator where each cycle consists of 30 secs ON, 1 min OFF (on ice). The above samples were sonicated for 2, 4, 6, 8, and 10 cycles respectively with 6 being the least amount of cycles needed to result in optimal fragmentation distribution (100-500bp spread).

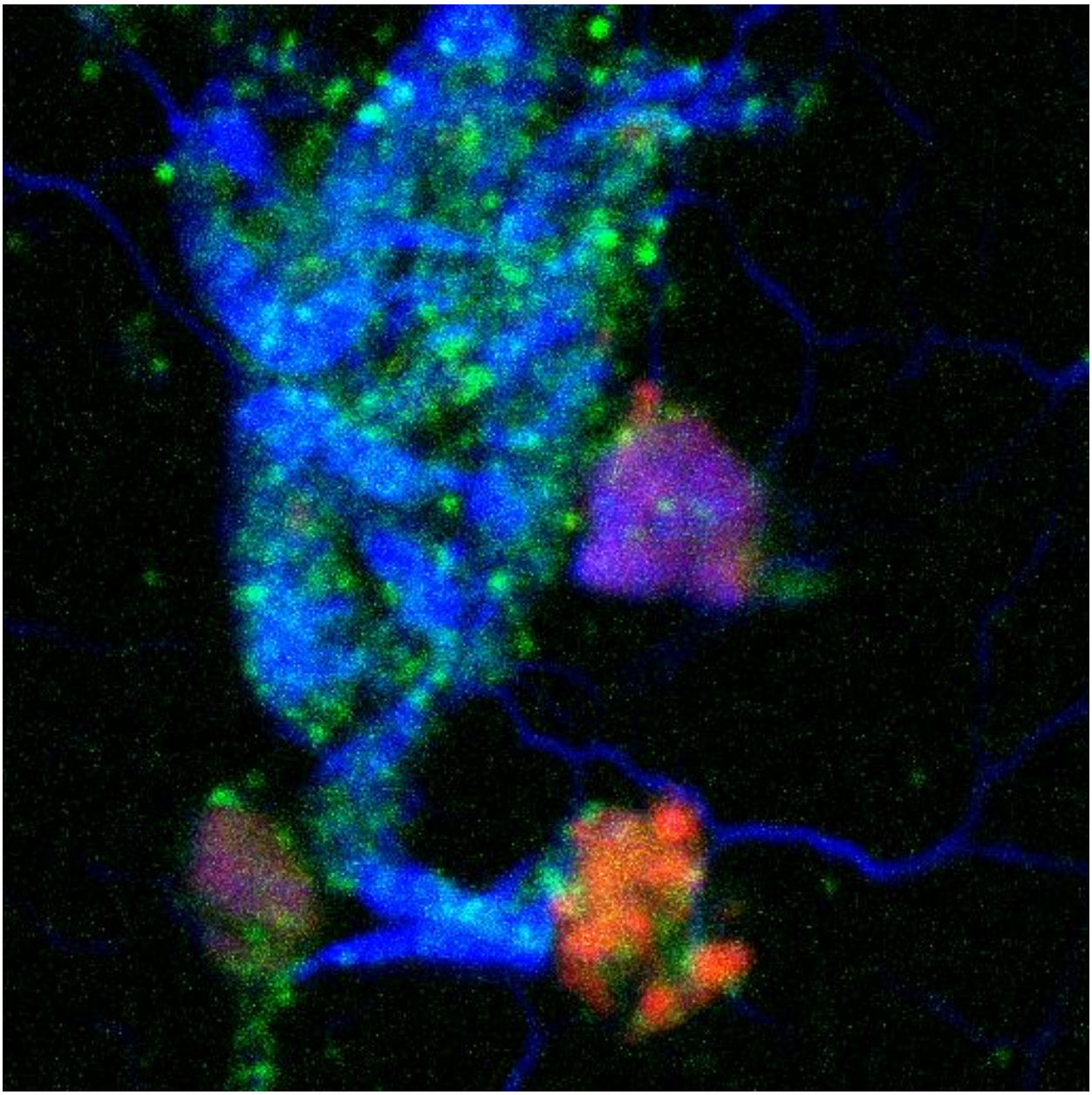

Figure III.II: Confocal image of NUCB2/nesfatin-1 in neutrophil extracellular traps after 120mins 1ng/mL LPS stimulation.

A composite maximum intensity projection (MIP) image was created from a series of z stacks to show NETs and 3 surrounding neutrophils almost devoid of chromatin DNA. (Blue: DAPI, Red: β-actin, Green: NUCB2/nesfatin-1)

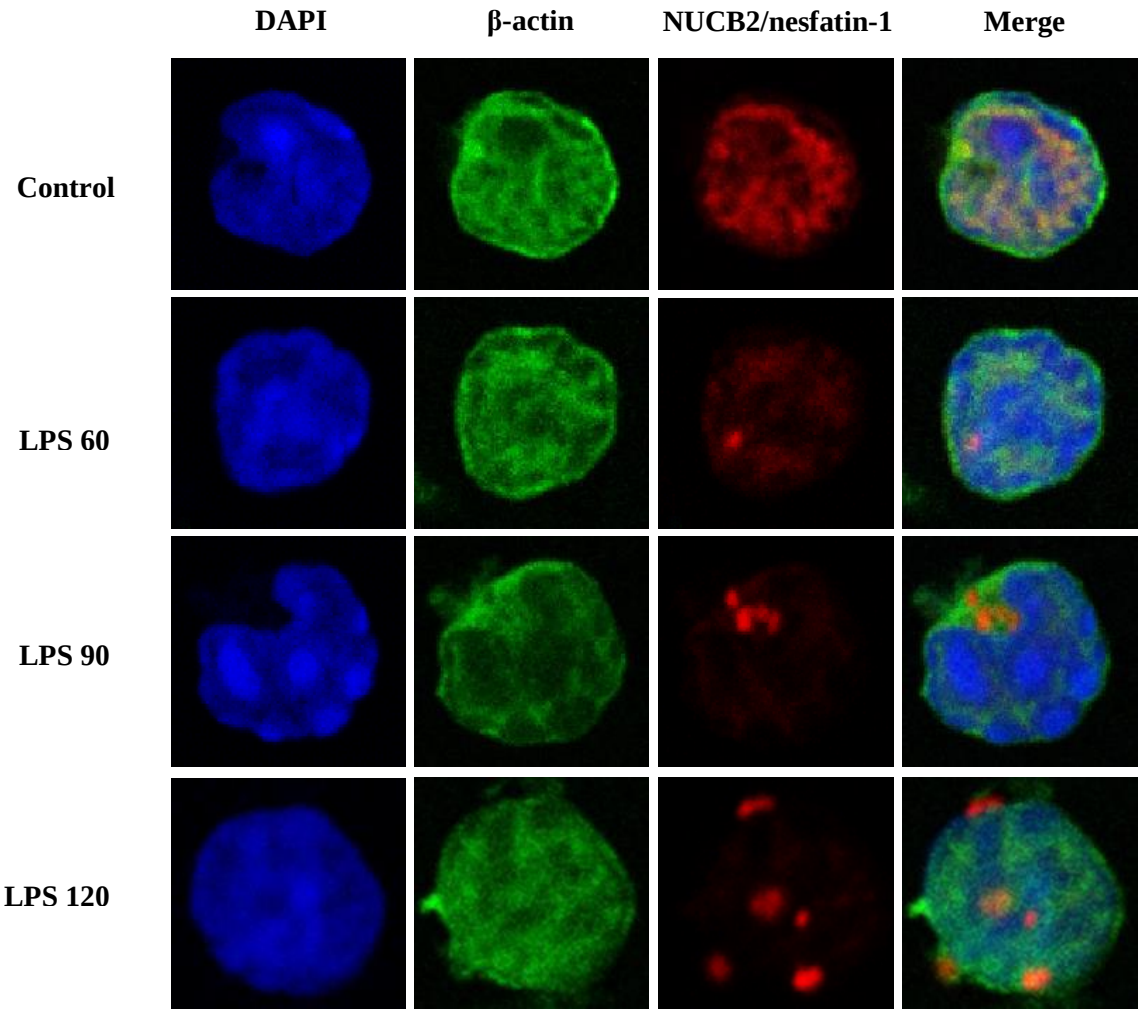

Figure III.III: NUCB2/nesfatin-1 distribution following LPS treatment.
Neutrophils from C57BL/6J WT mice were isolated and challenged with 1 ng/mL LPS for 0, 60, 90, and 120 mins. Neutrophils shown are single plane images representative of 1 biological replicate.

LIST OF REFERENCES

Altemeier, W. A., Hung, C. F., & Matute-Bello, G. (2017). Mouse Models of Acute Lung Injury. In L. M. Schnapp & C. Feghali-Bostwick (Eds.), Acute Lung Injury and Repair: Scientific Fundamentals and Methods (pp. 5-23). Cham: Springer International Publishing.

American Medical Association. (1890). Statistics of breathing. Journal of the American Medical Association, 14, 514.

Barnikol-Watanabe S., Gross N. A., Gotz H., Henkel T., Karabinos A., Kratzin H., . . . Hilschmann N. (1994). Human protein NEFA, a novel DNA binding/EF-hand/leucine zipper protein. Molecular cloning and sequence analysis of the cDNA, isolation and characterization of the protein. Biological Chemistry Hoppe-Seyler, 375(8), 497-512.

Bernard G. R., Artigas A., Brigham K. L., Carlet J., Falke K., Hudson L., . . . Spragg R. (1994). Report of the American-European Consensus conference on acute respiratory distress syndrome: definitions, mechanisms, relevant outcomes, and clinical trial coordination. Journal of Critical Care, 9, 72-81.

Bohmer R. H., Trinkle L. S., & Staneck J. L. (1992). Dose effects of LPS on neutrophils in a whole blood flow cytometric assay of phagocytosis and oxidative burst. Cytometry, 13, 525-531.

Bratton D. L., & Henson P. M. (2011). Neutrophil clearance: when the party's over, cleanup begins. Trends in Immunology, 32(8), 350-357.

Buckley C. D., Ross E. A., McGettrick H. M., Osborne C. E., Haworth O., Schmutz C., . . . Rainger G. E. (2006). Identification of phenotypically and functionally distinct population of long-lived neutrophils in a model of reverse endothelial migration. Journal of Leukocyte Biology, 79(2), 303-311.

Caudrillier A., Kessenbrock K., Gilliss B. M., Nguyen J. X., Marques M. B., Monestier M., . . . Looney M. R. (2012). Platelets induce neutrophil extracellular traps in transfusion-related acute lung injury. The Journal of Clinical Investigation, 122(7), 2661-2671.

Chung Y., Jung E., Kim H., Kim J., & Yang H. (2013). Expression of Nesfatin-1/NUCB2 in fetal, neonatal and adult mice. Development and Reproduction, 17(4), 461-467.

Colotta F., Re F., Polentarutti N., Sozzani S., & Mantovani A. (1992). Modulation of granulocyte survival and programmed cell death by cytokines and bacterial products. Blood, 80, 2012-2020.

Curtis J. L. (2005). Cell-mediated adaptive immune defense of the lungs. Proceedings of the American Thoracic Society, 2(5), 412-416.

Dancey J. T., Deubelbeiss K. A., Harker L. A., & Finch C. A. (1976). Neutrophil kinetics in man. The Journal of Clinical Investigation, 58(3), 705-715.

Demetri G. D., & Griffin J. D. (1991). Granulocyte colony-stimulating factor and its receptor. Blood, 78(11), 2791-2808.

Doeing D. C., Borowicz J. L., & Crockett E. T. (2003). Gender dimorphism in differential peripheral blood leukocyte counts in mice using cardiac, tail, foot, and saphenous vein puncture methods. BMC Clinical Pathology, 3(1), 3.

Doerschuk C. M. (2001). Mechanisms of leukocyte sequestration in inflamed lungs. Microcirculation, 8, 71-88.

Doerschuk C. M., Allard M. F., Martin B. A., MacKenzie A., Autor A. P., & Hogg J. C. (1987). Margination pool of neutrophils in rabbit lungs. Journal of Applied Physiology, 63, 1806-1815.

Doerschuk C. M., Beyers N., Coxson H. O., Wiggs B., & Hogg J. C. (1993). Comparison of neutrophil and capillary diameters and their relation to neutrophil sequestration in the lung. Journal of Applied Physiology, 74, 3040-3045.

Donaldson G. C., Seemungal T. A., Patel I. S., Bhowmik A., Wilkinson T. M., Hurst J. R., . . . Wedzicha J. A. (2005). Airway and systemic inflammation and decline in lung function in patients with COPD. Chest, 128(4), 1995-2004.

Duque G. A., & A., D. (2014). Macrophage cytokines: Involvement in immunity and infectious diseases. Frontiers in Immunology, 5, 491.

Eisner M. D., Thompson T., Hudson L. D., Luce J. M., Hayden D., Schoenfeld D., . . . Acute Respiratory Distress Syndrome Network. (2001). Efficacy of low tidal volume ventilation in patients with different clinical risk factors for acute lung injury and the acute respiratory distress syndrome. American Journal of Respiratory and Critical Care Medicine, 164, 231-236.

Farlex and Partners. (2013). Handbook of Laboratory and Diagnostic Tests Complete blood count, WBC count and differential. Retrieved from http://medical-dictionary.thefreedictionary.com/Complete+Blood+Count%2c+WBC+Count+and+Differential

Flierl M. A., Rittirsch D., Hoesel L. M., Gao H., Zetoune F. S., Huber-Lang M. S., & A., W. P. (2006). Acute lung injury: A challenging transfer from bench to bedside. The Journal for Innovative Ideas in Biomedical Research, 3, 727-738.

Garces M. F., Poveda N. E., Sanchez E., Sanchez A. Y., Bravo S. B., Vazquez M. J., . . . E., C. J. (2014). Regulation of NUCB2/nesfatin-1 throughout rat pregnancy. Physiology & Behavior, 133, 216-222.

Garcia-Marcos M., Kietrsunthorn P. S., Wang H., Ghosh P., & G., F. M. (2011). G Protein Binding Sites on Calnuc (Nucleobindin 1) and NUCB2 (Nucleobindin 2) Define a New Class of Gαi-regulatory Motifs. Journal of Biological Chemistry, 286(32), 28138-28149.

Gompertz S., O'Brien C., Bayley D., Hill S. L., & Stockley R. A. (2001). Changes in bronchial inflammation during acute exacerbations of chronic bronchitis The European Respiratory Journal, 17(6), 1112-1119.

Greene K. E., & E., P. P. (1998). Complement and Endotoxin in Lung Injury. In Marini J. J. & E. T. W. (Eds.), Acute Lung Injury (pp. 54-69). Berlin: Springer-Verlag.

Hasleton P. S. (1972). The internal surface area of the adult human lung. Journal of Anatomy, 112(3), 391-400.

Hoenderdos K., & Condliffe A. (2012). The neutrophil in chronic obstructive pulmonary disease. American Journal of Respiratory Cell and Molecular Biology, 48(5), 531-539.

Kanai Y., Miura K., Uehara T., Amagai M., Takeda O., Tanuma S., & Kurosawa Y. (1993). Natural occurrence of Nuc in the sera of autoimmune-prone MRL/lpr mice. Biochemical and Biophysical Research Communications, 196, 729-736.

Kapoor N., Gupta R., Menon S. T., Folta-Stogniew E., Raleigh D. P., & P., S. T. (2010). Nucleobindin 1 Is a Calcium-regulated Guanine Nucleotide Dissociation Inhibitor of Gαi1. Journal of Biological Chemistry, 285(41), 31647-31660.

Karabinos A., Bhattacharya D., Morys-Wortmann C., Kroll K., Hirschfeld G., Kratzin H.D., . . . N., H. (1996). The divergent domains of the NEFA and nucleobindin proteins are derived from an EF-hand ancestor. Molecular Biology and Evolution, 13(7), 990-998.

Kim J., Chung Y., Kim H., Im E., Lee H., & Yang H. (2014). The tissue distribution of Nesfatin-1/NUCB2 in mouse. Development and Reproduction, 18(4), 301-309.

Kolaczkowska E., & Kubes P. (2013). Neutrophil recruitment and function in health and inflammation. Nature Reviews Immunology, 13(3), 159-175.

Laufe M. D., Simon R. H., Flint A., & Keller J. B. (1986). Adult respiratory distress syndrome in neutropenic patients. The American Journal of Medicine, 80(6), 1022-1026.

Lee N., You S., Shin M. S., Lee W. -W., Kang K. S., Kim S. H., . . . Kang I. (2014). IL-6 receptor a defines effector memory CG8+ T cells producing Th2 cytokines and expanding

in asthma. American Journal of Respiratory and Critical Care Medicine, 190(12), 1383-1394.

Leivo-Korpela S., Lehtimaki L., Hamalainen M., Vuolteenaho K., Koobi L., Jarvenpaa R., . . . Moilanen E. (2014). Adipokines NUCB2/nesfatin-1 and visfatin as novel inflammatory factors in chronic obstructive pulmonary disease. Mediators of Inflammation, 2014, 1-6.

Levin J., Poore T. E., Zauber N. P., & S., O. R. (1970). Detection of endotoxin in the blood of patients with sepsis due to gram-negative bacteria. New England Journal of Medicine, 283, 1313-1316.

Levy B. D., & Serhan C. N. (2014). Resolution of Acute Inflammation in the Lung. Annual Review of Physiology, 76, 467-492.

Lien D. C., Jr Wagner W. W., Capen R. L., Haslett C., Hanson W. L., Hofmeister S. E., . . . Worthen G. S. (1987). Physiological neutrophil sequestration in the lung: visual evidence for localization in capillaries. Journal of Applied Physiology, 62(3), 1236-1243.

Liu J., Pang Z., Wang G., Guan X., Fang K., Wang Z., & Wang F. (2017). Advanced role of neutrophils in common respiratory diseases. Journal of Immunology Research, 2017(6710278), 1-21.

Looney M. R., & Bhattacharya J. (2014). Live imaging of the lung. Annual Review of Physiology, 76, 431-445.

Lorenz E., Jones M., Wohlford-Lenane C., Meyer N., Frees K. L., Arbour N. C., & Schwartz D. A. (2001). Genes other than TLR4 are involved in the response to inhaled LPS. American Journal of Physiology - Lung Cellular and Molecular Physiology, 281(5), L1106-L1114.

Martin T. R., & Frevert C. W. (2005). Innate Immunity in the Lungs. Proceedings of the American Thoracic Society, 2, 403-411.

Mathias J. R., Perrin B. J., Liu T. X., Kanki J., Look A. T., & Huttenlocher A. (2006). Resolution of inflammation by retrograde chemotaxis of neutrophils in transgenic zebrafish. Journal of Leukocyte Biology, 80(6), 1281-1288.

Matthay M. A., & Zimmerman G. A. (2005). Acute lung injury and the acute respiratory distress syndrome: four decades of inquiry into pathogenesis and rational management. American Journal of Respiratory Cell and Molecular Biology, 33, 319-327.

Matute-Bello G., Downey G., Moore B. B., Groshong S. D., Matthay M. A., Slutsky A. S., & Kuebler W. M. (2010). An official American Thoracic Society workshop report: features and measurements of experimental acute lung injury in animals. American Journal of Respiratory and Molecular Biology, 44(5), 725-738.

Megens R. T., Vijayan S., Lievens D., Doring Y., van Zandvoort M. A., Grommes J., . . . Soehnlein O. (2012). Presence of luminal neutrophil extracellular traps in atherosclerosis. Thrombosis and Haemostasis, 107(3), 597-598.

Mescher A. L. (2016). Junqueira's Basic Histology: Text and Atlas Fourteenth Edition: McGraw-Hill Education.

Mestas J., & Hughes C. C. W. (2004). Of mice and not men: Differences between mouse and human immunology. The Journal of Immunology, 172(5), 2731-2738.

Mogensen T. H. (2009). Pathogen recognition and inflammatory signaling in innate immune defenses. Clinical Microbiology Reviews, 22(2), 240-273.

Mohan H. (2015). Characterization of Endogenous Nucleobindin-1/Nesfatin-1 in Rodents. University of Saskatchewan.

Mohan H., Ramesh N., Mortazavi S., Le A., Iwakura H., & Unniappan S. (2014). Nutrients differentially regulate nucleobindin-2/nesfatin-1 in vitro in cultured stomach ghrelinoma (MGN3-1) cells and in vivo in male mice. PLoS ONE, 9(12), e115102.

Murphy H. S. (2008). Chapter 2: Inflammation. In Rubin R. & Strayer D. S. (Eds.), Rubin's Pathology: Clinicopathologic Foundations of Medicine 5th Edition (5th ed.).

Muzio M., Bosisio D., Polentarutti N., D'amico G., Stoppacciaro A., Mancinelli R., . . . Mantovani A. (2000). Differential expression and regulation of toll-like receptors (TLR) in human leukocytes: selective expression of TLR3 in dendritic cells. Journal of Immunology, 164(11), 5998-6004.

Myers Lab. (2014). Myers Lab ChIP-seq Protocol v011014. Retrieved from https://www.encodeproject.org/documents/6ecd8240-a351-479b-9de6-f09ca3702ac3/@@download/attachment/ChIP-seq_Protocol_v011014.pdf

Nelson S. (1994). Role of granulocyte colony-stimulating factor in the immune response to acute bacterial infection in the nonneutropenic host: an overview. Clinical Infectious Diseases, 18, S197-S204.

Nuovo A. J., Garofalo M., Mikhail A., Nicol A. F., Vianna-Andrade C., & Nuovo G. J. (2013). The effect of aging of formalin-fixed paraffin-embedded tissues on the in situ hybridization and immunohistochemistry signals in cervical lesions. Diagnostic Molecular Pathology: The American Journal of Surgical Pathology, Part B, 22(3), 164-173.

O'Grady N. P., Preas H. L., Pugin J., Fiuza C., Tropea M., Reda D., . . . Suffredini A. F. (2001). Local inflammatory responses following bronchial endotoxin instillation in humans. American Journal of Respiratory and Critical Care Medicine, 163(7), 1591-1598.

O'Grady N. P., Tropea M., Preas II H. L., Reda D., Vandivier R. W., Banks S. M., & Suffredini A. F. (1999). Detection of macrophage inflammatory protein (MIP)-1α and MIP-β during experimental endotoxemia and human sepsis. The Journal of Infectious Diseases, 179(1), 136-141.

Oh-I, S., Shimizu, H., Satoh, T., Okada, S., Adachi, S., Inoue, K., . . . Mori, M. (2006). Identification of nesfatin-1 as a satiety molecule in the hypothalamus. Nature, 443(7112), 709-712.

Ozsavci D., Ersahin M., Sener A., Ozakpinar O. B., Toklu H. Z., Akakin D., . . . Yegen B. C. (2011). The novel function of nesfatin-1 as an anti-inflammatory and antiapoptotic peptide in subarachnoid hemorrhage-induced oxidative brain damage in rats. Neurosurgery, 68(6), 1699-1708.

Park W. Y., Goodman R. B., Steinberg K. P., Ruzinski J. T., Radella F., Park D. R., . . . Martin T. R. (2001). Cytokine balance in the lungs of patients with acute respiratory distress syndrome. American Journal of Respiratory and Critical Care Medicine, 164, 1896-1903.

Parsons P. E., Eisner M. D., Thompson B. T., Matthay M. A., Ancukiewicz M., Bernard G. R., . . . NHLBI Acute Respiratory Distress Syndrome Clinical Trials Network. (2005). Lower tidal volume ventilation and plasma cytokine markers of inflammation in patients with acute lung injury. Critical Care Medicine, 33(1), 1-6; discussion 230-232.

Pilette C., Colinet B., Kiss R., Andre S., Kaltner H., Gabius H. J., . . . Sibelle Y. (2007). Increased galectin 3 expression and intra-epithelial neutrophils in small airways in severe chronic obstructive pulmonary disease. The European Respiratory Journal, 29(5), 914-922.

Price T. H., Chatta G. S., & Dale D.C. (1996). Effect of recombinant granulocyte colony-stimulating factor on neutrophil kinetics in normal young and elderly humans. Blood, 88(1), 335-340.

Prinz P., Goebel-Stengel M., Teuffel P., Rose M., Klapp B. F., & Stengel A. (2016). Peripheral and central localization of the nesfatin-1 receptor using autoradiography in rats. Biochemical and Biophysical Research Communications, 470(3), 521-527.

Ramanjaneya M., Chen J., Brown J. E., Tripathi G., Hallschmid M., Patel S., . . . Randeva H. S. (2010). Identification of nesfatin-1 in human and mouse adipose tissue: A novel depot-specific adipokine with increased levels in obesity. Endocrinology, 151(7), 3169-3180.

Ravussin A. (2016). Nucleobindin-2: A novel regulator of immune-metabolic interactions. (Doctor of Philosophy), Louisiana State College.

Rice L., & Teruya M. (2016). Neutrophil production and kinetics: neutropenia and neutrophilia. In J. M. T. L. Simon, E. L. Snyder, B. G. Solheim, R. G. Strauss (Ed.), Rossi's Principles of Transfusion Medicine (5th Edition ed., pp. 265-270): John Wiley & Sons, Ltd.

Rubenfeld G. D., Caldwell E., Peabody E., Weaver J., Martin D. P., Neff M., . . . Hudson L. D. (2005). Incidence and outcomes of acute lung injury. The New England Journal of Medicine, 353, 1685-1693.

Rydell-Tormanen K., Uller L., & Erjefait J. S. (2006). Direct evidence of secondary necrosis of neutrophils during intense lung inflammation. The European Respiratory Journal, 28(2), 268-274.

Saito, T., Yamamoto, T., Kazawa, T., Gejyo, H., & Naito, M. (2005). Expression of toll-like receptor 2 and 4 in lipopolysaccharide-induced lung injury in mouse. Cell and Tissue Research, 321(1), 75-88.

Sapey E., & Stockley R. A. (2009). The neutrophil and its special role in chronic obstructive pulmonary disease. In Barnes P. J., Drazen J., Rennard S. I., & Thomson N. C. (Eds.), Asthma and COPD: Basic Mechanisms and Clinical Management: Elsevier Ltd.

Scotece M., Conde J., Abella V., Lopez V., Lago F., Pino J., . . . Gualillo O. (2014). NUCB2/nesfatin-1: A new adipokine expressed in human and murine chondrocytes with pro-inflammatory properties, an in vitro study. Journal of Orthopaedic Research, 32, 653-660.

Selby C., Drost E., Lannan S., Wraith P. K., & MacNee W. (1991). Neutrophil retention in the lungs of patients with chronic obstructive pulmonary disease. The American Review of Respiratory Disease, 143(6), 1359-1364.

Stengel, A., Goebel, M., Wang, L., Rivier, J., Kobelt, P., Mönnikes, H., . . . Taché, Y. (2009). Central Nesfatin-1 Reduces Dark-Phase Food Intake and Gastric Emptying in Rats: Differential Role of Corticotropin-Releasing Factor2 Receptor. Endocrinology, 150(11), 4911-4919.

Stengel A., Goebel-Stengel M., Jawien J., Kobelt P., Tache Y., & Lambrecht N. W. (2011). Lipopolysaccharide increases gastric and circulating NUCB2/nesfatin-1 concentration in rats. Peptides, 32(9), 1942-1947.

Stengel A., Hofmann T., Goebel-Stengel M., Lembke V., Ahnis A., Elbelt U., . . . Kobelt P. (2013). Ghrelin and NUCB/nesfatin-1 are expressed in the same gastric cell and differentially correlated with body mass index in obese subjects. Histochemistry and Cell Biology, 139(6), 909-918.

Summers C., Rankin S. M., Condliffe A. M., Singh N., Peters A. M., & Chilvers E. R. (2010). Neutrophil kinetics in health and disease. Trends in Immunology, 31(318-324).

Suratt B. T., Young S. K., Lieber J., Nick J. A., Henson P. M., & Worthen G. S. (2001). Neutrophil maturation and activation determine anatomic site of clearance from circulation. American Journal of Physiology - Lung Cellular and Molecular Physiology, 281(4), L913-L921.

Tang C. H., Fu X. J., Xu X. L., Wei X. J., & Pan H. S. (2012). The anti-inflammatory and anti-apoptotic effects of nesfatin-1 in the traumatic rat brain. Peptides, 36(1), 39-45.

The Jackson Laboratory. (2015). Life span as a biomarker. Retrieved from https://www.jax.org/research-and-faculty/research-labs/the-harrison-lab/gerontology/life-span-as-a-biomarker

Tumpey T. M., Fenton R., Molesworth-Kenyon S., Oakes J. E., & Lausch R. N. (2002). Role of macrophage inflammatory protein 2 (MIP-2), MIP-1alpha, and interleukin-1alpha in the delayed-type hypersensitivity response to viral antigen. Journal of Virology, 76(16), 8050-8057.

Walker F., Zhang H. H., Matthews V., Weinstock J., Nice E. C., Ernst M., . . . Burgess A. W. (2008). IL6/sIL6R complex contributes to emergency granulopoietic responses in C-CSF- and GM-CSF-deficient mice. Blood, 111(8), 3978-3985.

World Health Organization. (2017). The top 10 causes of death. Retrieved from http://www.who.int/mediacentre/factsheets/fs310/en/

Wright H. L., Cross A. L., Edwards S. W., & Moots R. J. (2014). Effects of IL-6 and IL-6 blockade on neutrophil function in vitro and in vivo. Rheumatology (Oxford), 53(7), 1321-1331.

Wurfel M. M., Park W. Y., Radella F., Ruzinski J., Sandstrom A., Strout J., . . . Martin T. R. (2005). Identification of high and low responders to lipopolysaccharide in normal subjects: an unbiased approach to identify modulators of innate immunity. Journal of Immunology, 175, 2570-2578.

Xu S., Hoglund M., Hakansson L., & Venge P. (2000). Granulocyte colony-stimulating factor (G-CSF) induces the production of cytokines in vivo. British Journal of Haematology, 108(4), 848-853.

Xu S., Hoglund M., & Venge P. (1996). The effect of granulocyte colony-stimulating factor (G-CSF) on the degranulation of secondary granule proteins from human neutrophils in vivo may be indirect. British Journal of Haematology, 93, 558-568.

Xu Y. -Y., Ge J. -F., Qin G., Peng Y. -N., Zhang C. -F., Liu X. -R., . . . Li J. (2015). Acute, but not chronic, stress increased the plasma concentration and hypothalamic mRNA expression of NUCB2/nesfatin-1 in rats. Neuropeptides, 54, 47-53.

Yipp B. G., Kim J. H., Lima R., Zbytnuik L. D., Petri B., Swanlund N., . . . Kubes P. (2017). The lung is a host defense niche for immediate neutrophil-mediated vascular protection. Science Immunology, 2(10).

Yipp B. G., Petri B., Salina D., Jenne C. N., Scott B. N.V., Zbytnuik L. D., . . . Kubes P. (2012). Dynamic NETosis is carried out by live neutrophils in human and mouse bacterial abscesses and during severe gram-positive infection. Nature Medicine, 18(9), 1386-1393.

Yosten G. L., & Samson W. K. (2009). Nesfatin-1 exerts cardiovascular actions in brain: possible interaction with the central melanocortin system. American Journal of Physiology - Regulatory, Integrative and Comparative Physiology, 297(2), R330-R336.

Zarbock A., & Ley K. (2009). New insights into leukocyte recruitment by intravital microscopy. Current Topics in Microbiology and Immunology, 334, 129-152s.

Zemans R. L., Colgan S. P., & Downey G. P. (2009). Transepithelial migration of neutrophils: mechanisms and implications for acute lung injury. American Journal of Respiratory Cell and Molecular Biology, 40, 519-535.